SURFACE CHEMISTRY STUDIES OF CARBON DIOXIDE WITH MAGNESIUM OXIDE AND TITANIUM DIOXIDE

A Dissertation

presented to

the Faculty of the Graduate School

at the University of Missouri-Columbia

In Partial Fulfillment

of the Requirements for the Degree

Doctor of Philosophy

---

by

JUAN WANG

Dr. C. Michael Greenlief, Dissertation Supervisor

MAY 2016

The undersigned, appointed by the dean of the Graduate School, have examined the dissertation entitled

SURFACE CHEMISTRY STUDIES OF CARBON DIOXIDE WITH MAGNESIUM OXIDE AND TITANIUM DIOXIDE

presented by Juan Wang,

a candidate for the degree of doctor of philosophy

and hereby certify that, in their opinion, it is worthy of acceptance.

Professor C. Michael Greenlief

Professor Timothy E. Glass

Professor Renee D. Jiji

Professor Gavin M. King

Acknowledgement

I would like to express my deepest appreciation to my academic advisor Dr. C. Michael Greenlief. I am so grateful for his acceptance to his research group, academic guidance and great advice on research projects through these years. Dr. Greenlief has always been a role model to me. His mentor is like a candle in the darkness for me to see the right direction. Dr. Greenlief is an excellent professor with stringent academic attitude, critical thinking ability, and perfect time management. His kindness and patience to students deeply sink to my mind and will benefit my future life and career.

I would also want to thank all of my committee members: Dr. Timothy E. Glass, Dr. Renee D. Jiji and Dr. Gavin M. King for their precious knowledge, advice, and guidance in my academic research and preparation of this dissertation. Their suggestion and unique ideas of my research broaden my insight and help me prepare my dissertation much better.

I would like to acknowledge Dr. Thomas R. Marrero for his encouragement and guidance in the research of CO_2 with MgO (100) single crystal surfaces. His enthusiasm to his work, patience to his students and me all impressed me deeply. And his approval of my work give me confidence to endeavor to my research.

I would also like to express my gratitude to all former and current members in Dr. Greenlief's research group. Their support and friendship make my doctoral life much easier and more enjoyable in these years. Many thanks to all faculty and staff members of Department of Chemistry in University of Missouri-Columbia. They are very nice and willing to offer help when needed. All of these made a wonderful memory for me at

University of Missouri. I am also grateful to University of Missouri Research Board for their financial support of this research and great facilities to use.

Finally, I am highly indebted to my friends and family. Especially my parents. I left home six years to study in U.S.A. I would not be able to accomplish this Doctoral Degree smoothly without their understanding and support.

Table of Contents

List of Figures

List of Tables

SURFACE CHEMISTRY STUDIES OF CARBON DIOXIDE WITH MAGNESIUM OXIDE AND TITANIUM DIOXIDE

JUAN WANG

Dr. C. Michael Greenlief, Dissertation Supervisor

ABSTRACT

There is significant interest in methods to aid in the removal of carbon dioxide from our environment. The methods range from sequestration to catalytic transformations. In sequestration, CO_2 is collected from emission sources, and may be stored in a variety of materials including geological formations. Catalytic research often involves the transformation of CO_2 to another compound such as methane. The majority of these latter studies focus on the use of photocatalysis for the conversion of CO_2. An alternative method, discussed in this dissertation, is to examine the surface chemistry for the adsorption and thermal reduction of carbon dioxide with magnesium oxide and titanium oxide surfaces. We are also interested in gaining a better understanding of the refractory nature of CO_2.

The overall goal of these studies is to elucidate the surface reaction mechanism for the reaction of carbon dioxide on metal oxide surfaces with and without UV light. We combine the use of X-ray photoelectron and Auger electron spectroscopies to examine the surface chemistry of CO_2. First, carbon dioxide is exposed to the heated metal oxide

surface and the surface atomic concentrations are measured after reaction. The substrate temperature and CO_2 exposure are varied in the experiment. Similar studies are also performed in the presence of UV light to gain a better understanding of photocatalysis. The results from these experiments will be discussed, as well as, the direction of future studies.

Chapter 1 Introduction

1.1 CO_2 Utilization

1.1.1 Overview of greenhouse gases and global warming

Global warming is becoming a severe problem because of human activities. There are many different kinds of greenhouse gasses (GHGs) such as CO_2, CH_4 and N_2O[1]. Some of these GHOs are listed in Table 1.1 with their contribution to the global warming. Among them, CO_2 plays a key role. Due vast amounts of fossil fuels combusted and the rapid transformation of forest ecosystems, the average atmospheric concentration of CO_2 had increased from 280 ppmV to 387 ppmV in 2009[2]. Studies by the IPCC (Intergovernmental Panel on Climate Change) pointed out that if the CO_2 concentration is higher than 500 ppmV, the environment would be deeply affected [3]. At the same time, increasing amounts of CO_2 released into atmosphere has caused the global mean temperature to rise by 0.5 °C since 1970[4]. Therefore, reducing the amount of CO_2 in the atmosphere becomes an important research topic.

Table 1. 1. Relative emission of GHGs

Compound	Formula	Contribution (%)
Carbon dioxide	CO_2	79.9%
Methane	CH_4	9.5%
Nitrous oxide	N_2O	5.8%

1.1.2 Industrial applications of CO_2

Although the increased amount of CO_2 released in the atmosphere has resulted in an increase of global temperature, it is also potentially a huge source of carbon. Compared to other materials, like phosgene that is traditionally used to produce polycarbonate by the "phosgene process", CO_2 is a nontoxic, low cost, and reproducible material. Currently, it is used as a starting material in several industrial processes as follows[5]:

1) Reacting with ammonia to produce urea;
2) Reacting with sodium phenolate to synthesize salicylic acid which is used for the production of pharmaceuticals and pesticides;
3) Polycarbonates synthesized from CO_2;
4) Reforming of methanol can be achieved through the water gas-shift reaction, and this technique also led to recent interest in CO_2 surface chemistry.

The utilization of CO_2 could not only reduce the emission of carbon dioxide into the air, but also bring economic benefit. Thus, there is significant interest in methods that

aid in utilizing CO_2 and to achieve the final goal of removal of carbon dioxide from our environment.

1.1.3 Strategies for managing atmospheric CO_2

In order to reduce the emission of carbon dioxide into the atmosphere, there are two strategies that can be used, adaptive options and mitigative options. Adaptive options include modification of human behavior for the use of land in both the terrestrial and aquatic biosphere like our forests, deserts, wetlands, and methods of cultivation. We cannot trade the ecosystem for profits. Mitigation options include two approaches: reducing and sequestering emissions. Reducing emissions could be realized by enhancing energy use efficiency such as improving energy management, modifying the source energy; altering people's life style; choosing low-C, or no-C fuels as a clean energy source, e.g. wind, water, solar, H_2 and so forth. In sequestration, CO_2 is collected from emission sources, and may be stored in a variety of materials including biotic, geological formations, oceanic, and chemical sequestrations[6-7]. Figure 1.1 shows the strategies of managing atmospheric CO_2 enrichment.

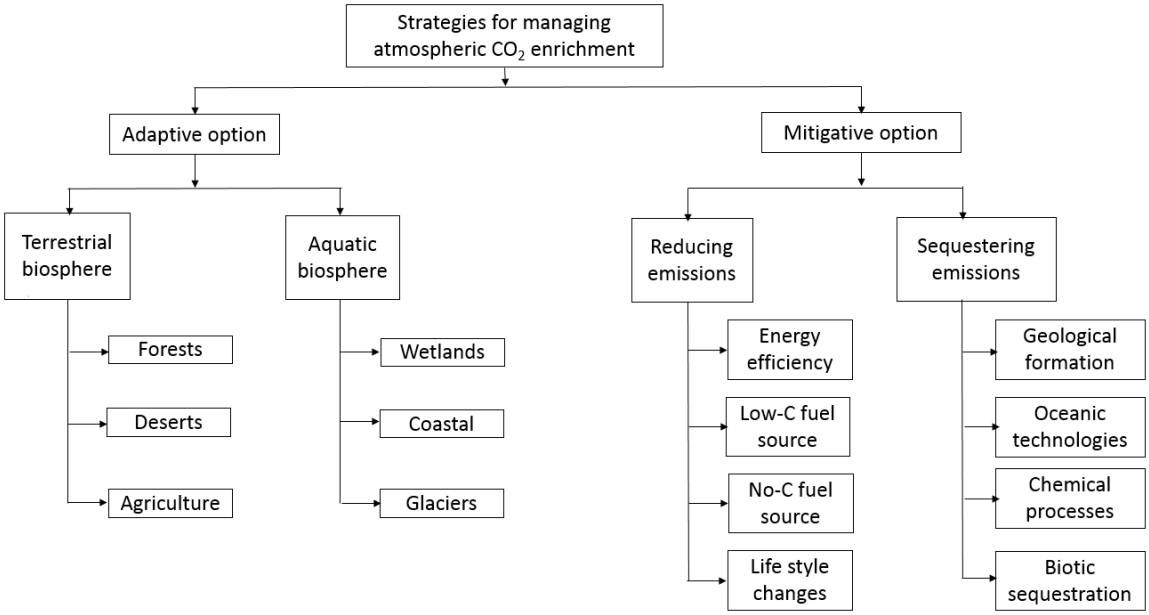

Figure 1. 1. Strategies for managing atmospheric CO_2 enrichment.

Sequestration includes carbon capture, separation, transportation, storage and utilization. Among them, carbon capture is the key point. There are two methods: physical methods include physical adsorption, cryogenic separation and membrane separation. The second method is chemical adsorption which is becoming the most widely used method. It is often carried out using basic solutions containing an ammine to form chemical bonds with CO_2.

The rate of using carbon dioxide as a starting material is far behind the rate of CO_2 released into the atmosphere. Therefore, how to efficiently recycle carbon dioxide becomes a serious question. Because of its thermodynamic stability, carbon dioxide is the final product of complete combustion reaction. Most reactions using carbon dioxide as the starting material require a catalyst to help convert carbon dioxide into carbon monoxide or a hydrocarbon, such as methane, or methanol. A growing number of

scientists and research groups had tried to react CO_2 with various metal oxides (e.g. ZnO, WO_3, TiO_2, MgO). Recent advances in this area are summarized in a review by Wei-Ning Wang et al[8] in 2014. Several metal oxide, or modified metal oxide systems are covered in the review, including TiO_2. Most of the photocatalytic studies use UV light as an excitation source. The band gap of TiO_2 is small enough that UV photons can be used to initiate electronic transitions within the oxide. Compared to titanium dioxide's narrow band gap (~3.05 eV), magnesium oxide has a wider band gap (~7.7eV). The difference between these two metal oxides can give an idea of the function of UV light in the photocatalytic reduction of CO_2. Therefore, more details of these two different oxide surfaces will be addressed in section 1.2-1.4.

1.2 Metal oxide surfaces: MgO (100) and TiO_2 (110) single crystal surfaces

While the conversions of CO_2 to methane and methanol have received attention, it is also highly desirable to directly decompose CO_2 to oxygen and carbon. Such a process could provide respirable oxygen useful in isolated habitats. The direct reduction of CO_2 was originally proposed by Sabatier [9]. In this reaction, CO_2 is reacted over Ni or Co metal catalysts at 400-500ºC, some carbon deposition was obtained indicating the complete decomposition of CO_2 to carbon and oxygen. However, the reaction had been shown to be incomplete over these metal catalysts, and it requires the addition of hydrogen or steam. The Sabatier reaction today involves the mixture of CO_2 and H_2 to produce CH_4 and H_2O[10] as shown in equation 1.1.

$$CO_2 + 4H_2 \underset{400\sim500°C}{\overset{\text{Ni or Co}}{\rightleftharpoons}} 2H_2O + CH_4 \quad (\Delta H = -167 \text{ kJ/mol}) \qquad (1.1)$$

In this dissertation, a series of experiments to explore the interactions of CO_2 with the MgO and TiO_2 surfaces wild be described. The final goal is to understand the thermal decomposition of CO_2 on MgO crystal surfaces and try to elucidate the mechanism of CO_2 photocatalytic reduction on TiO_2 single crystal surfaces.

1.3 MgO (100) single crystal surfaces

Magnesium oxide is considered a CO_2 sorbent[11] and is widely used to capture CO_2 due to its wide availability in nature, easy regeneration in bulk amount, and low cost. On the other hand, carbon dioxide is used as a probe molecule in many different kinds of investigations of the basic properties of oxide surface. For instance, CO_2 interactions have been followed by the Fourier Transform Infrared Spectroscopy (FTIR), Temperature-Programmed Desorption (TPD), and Cluster-Model computational studies [12].

MgO (100) is a refractory metal oxide with a NaCl crystal structure. The (100) plane is presented as the top layer in Figure 1.2. This surface plane contains an equal number of Mg and O atoms. MgO is the starting surface and there are many different types of adsorption sites, including magnesium atoms, oxygen atoms, and step sites. The oxide surface might be altered by UV light or CO_2 (or reaction products). For instance, the UV light might stimulate the desorption of oxygen and create a Mg-rich surface.

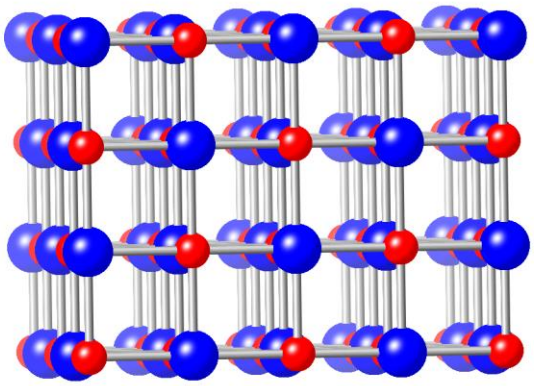

Figure 1. 2. Ball and stick model of the MgO (100) surface. The red spheres represent magnesium atoms and the blue spheres represent oxygen atoms.

1.3.1 Thermal interaction of CO_2 with magnesium oxide surfaces

The adsorption of CO_2 on MgO (100) surfaces has been studied by several research groups [13-18]. These studies examined the low temperature adsorption products and their structures. CO_2 was determined to physisorb at low temperature through a precursor state with little mobility. Due to different adsorption conditions and surface structures, a variety of weakly bond carbonate-like intermediates formed, such as unidentate carbonates, bidentate carbonates, carbonate ions and hydrogen-carbonates[19]. Five possible adsorption structures of CO_2 on MgO surface at room or lower than room temperature are shown in Figure 1.3.

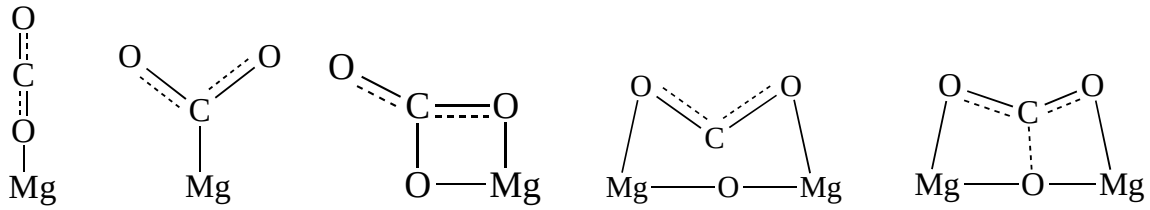

a b c d e

Figure 1. 3. Possible adsorption structures of CO_2 on MgO surface. a. Linear, b. Unidentate, c. Bidentate, d. & e. Bridged.

Unidentate and bidentate carbonate-like structures are the two most common structures on a well degassed MgO surface. Fukuda and Tanabe[20-21] indicated that with a high coverage of adsorbed CO_2, unidentate carbonates are predominant, while at a lower coverage, bidentate carbonates become the major surface species.

Pacchioni[17] investigated the interaction of CO_2 at the surface and at step sites on the MgO (100) surface using an ab initio cluster model and correlated calculations. He concluded that CO_2 physisorbs molecularly at the Mg^{2+} surface and step sites with an end-on linear complex; however, at 0 K, CO_2 could chemisorb on a four-coordinated step O^{2-} sites and form a stable monodentate carbonate.

When CO_2 was adsorbed on the MgO surface, there can also be an oxygen exchange between magnesium oxide surface and carbon dioxide. In Yanagisawa et al[12]'s research, they used three methods, including Temperature-Programmed Desorption (TPD), Fourier Transform Infrared Spectroscopy (FTIR), and ab initio molecular orbital calculations to examine the sties on MgO surface for CO_2 adsorption. They reported that there are two types of carbonate species, Type 1 and Type 2. For Type 2, it is a monodentate carbonate, however, Type 1 is from a monodentate model with partly

"bidentate" and "tridentate" characters. In Tsuji's study[22], they delivered a more detailed TPD study of the MgO surface interaction with $C^{18}O_2$ and an IR study of the adsorbed CO_2. They concluded that the oxygen exchange happens at room temperature and at not only O^{2-} basic sites but Mg^{2+} acidic sites are also involved in CO_2 adsorption. A complete detailed picture of CO_2 adsorption on MgO surface is still unclear and further study is needed.

1.3.2 Photocatalysis of CO_2 on MgO (100) surfaces

Magnesium oxide has a 7.7 eV wide band gap, compared to the lower band gap of titanium dioxide (3.0eV-3.2 eV). UV light (defined as a wavelength lower than 290 nm and higher than 161 nm) will not have sufficient energy to photo-excite electrons across the band gap in MgO. This property offers the potential to separate and understand the role of light in the surface reaction of CO_2. However, when MgO surface is exposed to UV light, it might lead to the creation of active sites as we discussed in section 1.3. Therefore, this study will supply more comprehensive knowledge of the surface studies.

1.4 TiO_2 (110) single crystal surfaces

The surface science of metal oxides is a new and young research area. "The Surface Science of Metal Oxides"[23] book which was published in 1994 reviewed single-crystalline metal oxide surfaces in detail. This book is a classic in surface science. In this book, the author mentioned that the number of papers published about metal oxides has increased since 1975 and in 1991 about 100 articles per year are published, the last year they reviewed. Another similar analysis shows that the number of studies of TiO_2 (110) surfaces has increased since 1990 with more than 70 papers published in 2000 [24].

1.4.1 Applications of titanium dioxide

The reason that the study of titanium dioxide is so popular is its wide range of applications and special properties. Generally, TiO_2 is a metal oxide that is thermally stable, non-flammable, and non-toxic. Meanwhile, TiO_2 is a very good semiconductor with high catalytic activities. Polished crystals with highly good surface quality can be purchased from various commercial companies. These advantages make titanium dioxide competitive for applications in both energy utilization and environmental areas.

Titanium dioxide has long been used as a white pigment because of its high refractive index (3.87). Ultrafine forms of TiO_2 can be applied in cosmetics (e.g. make-up products and sunscreens) owing to its good transparency and UV absorbance. TiO_2 nanomaterials, as an n-type semiconductor with small particle sizes and higher surface area, have been developed as a high quality material. In titanium dioxide, its valance band can create electron-hole (e^--h^+) pairs when irradiated with UV light with wavelength is lower than 387.5 nm. These pairs might migrate to oxide surface and perform redox

reactions with other materials (e.g. O_2, H_2O) to generate radical species (e.g. O_2^- and ·OH). These radicals might be able to react with organic molecules and decompose into carbon dioxide and H_2O. This application can be used in vast applications like sterilization[25] (e.g. in operation rooms in hospital); purification of wastewaters[26]; self-cleaning coatings on car windshields[27]; and protective coatings of marble. The photoelectric and photocatalytic properties of titanium dioxide drive people to explore TiO_2 surfaces in greater detail.

In 1972, Fujishima and Honda[28] first indicated that water could be decomposed into H_2 and O_2 by TiO_2 electrodes without an external bias but under light irradiation when the wavelength was shorter than 415 nm (~3eV). Since then, people have actively studied photocatalysis on TiO_2. In 1977, Frank and Bard[29] reported that by using TiO_2 as the photocatalyst, they could decompose cyanide (CN^-) to cyante (CNO^-). In 1979, Inoue et al[30] published a paper in Nature about the photoelectrocatalytic reduction of carbon dioxide in aqueous suspensions of semiconductor powders. Choosing WO_3, TiO_2, ZnO, CdS, GaP and SiC semiconductors as the photocatalysts, H_2O and CO_2 under the irradiation of Xe or Hg lamp resulted in a redox reaction to yield HCOOH, CH_3OH, CH_3O and a very little amout of CH_4. The photocatalytic reduction of CO_2 with TiO_2 has the potential to contribute to the environmental protection and energy saving. The photocatalytic reduction of CO_2 with TiO_2 is a main part to discuss in this dissertation and the overview about the machanism of titanium dioxide photocatalysis reaction is addressed in section 1.4.7.

1.4.2 The structure of TiO_2 surfaces

Despite the wide range applications of TiO_2, there is still a lacking of a complete understanding of the surface science of TiO_2. Several outstanding reviews about the single-crystalline metal oxide surfaces were published recently and TiO_2 surfaces studies constitute a good portion of the reviews. Therefore, it is very necessary to have a general picture of titanium dioxide surfaces by introducing its structure first and this is explained in detail in this section. The ball and stick model of the perfect (110) plane is presented in Figure 1.4. There are many different types of adsorption sites, including titanium atoms that are drawn as red spheres, oxygen atoms that are shown as blue spheres and step sites.

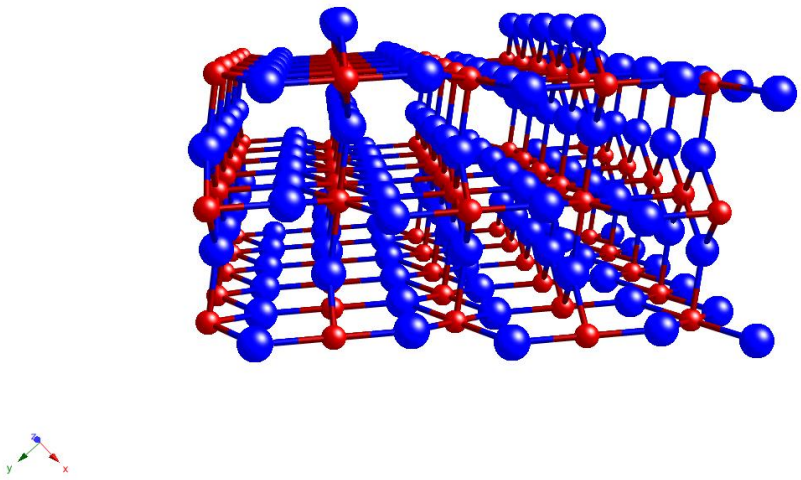

Figure 1. 4. Ball and stick model of the TiO_2 (110) surface. The red spheres represent Ti atoms and the blues spheres represent oxygen atoms.

1.4.3 Bulk structure

There are three major titanium dioxide structures: rutile (tetragonal, D_{4h}^{19} – $I4_2/mnm$, a = b = 4.854 Å, c = 2.953 Å[31]), anatase (tetragonal, D_{4h}^{19}-$I4_1$ /amd, a = b = 3.782 Å, c= 9.502 Å) and brookite (rhombohedrical, D_{2h}^{15}-Pbca, a = 5.436 Å, b = 9.166 Å, c = 5.135 Å)[32]. There are some other TiO_2 structures, for example, cotunnite TiO_2 that is one of the hardest polycrystalline materials known and must be synthesized at high temperature [33]. Rutile and anatase play the main roles in surface science studies because of their high catalytic reactivity. Anatase has the best photocatalytic reactivity, while rutile is the most stable structure. Usually, in the lab we can make the amorphous titanium dioxide and after calcination (T>700K-800K) it would be transformed into anatase, and becomes rutile. Surface science studies of anatase single crystals begun in year 2000[34-42]. However, the rutile surfaces have been examined more extensively[43-47]. By using controlled conditions, people can generate rutile, anatase and brookite easily. For both rutile and anatase, the basic building block includes a titanium atom, surrounded by six atoms, in a slightly distorted octahedral configuration. The only difference between rutile and anatase is the distortion and the connection between the octahedrons. There are two different connections between octahedrons shown in Figure 1.5, sharing corners and sharing edges.

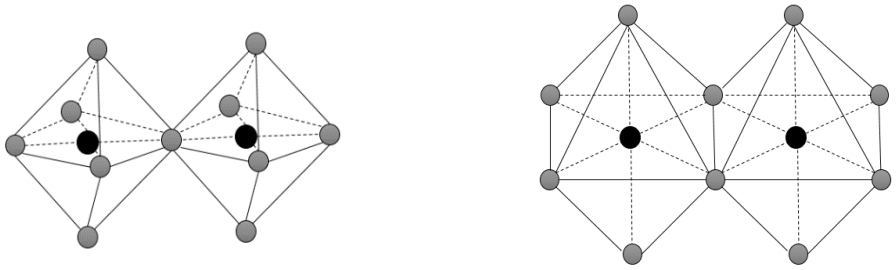

a b

Figure 1. 5. Two different connections between octahedrons. a) Sharing corners; b) Sharing edges. The black dots represent titanium atoms and the grey dots represent oxygen atoms.

The bulk structures of rutile and anatase are shown in Figure 1.6. In the rutile structure, every octahedron is connected with 10 other octahedrons, two share edges and the other 8 share corners along (110) direction. Two titanium dioxide molecules compromise a crystal unit, and the distortion of the octahedral is less than that of anatase. The length of the Ti-Ti band is shorter than that of anatase, however, the length of Ti-O band is longer than that of anatase. As to anatase, each crystal unit has four TiO_2 molecules and every octahedron is connected with eight octahedrons, four share the corners and the other four share the edges along (001) direction. Brookite is a rhombohedrical which is not shown in Figure 1.6, and each crystal unit consists six titanium dioxide molecules. All of stacking of the octahedrons in the three different titanium dioxide structures results in threefold coordinated oxygen atoms.

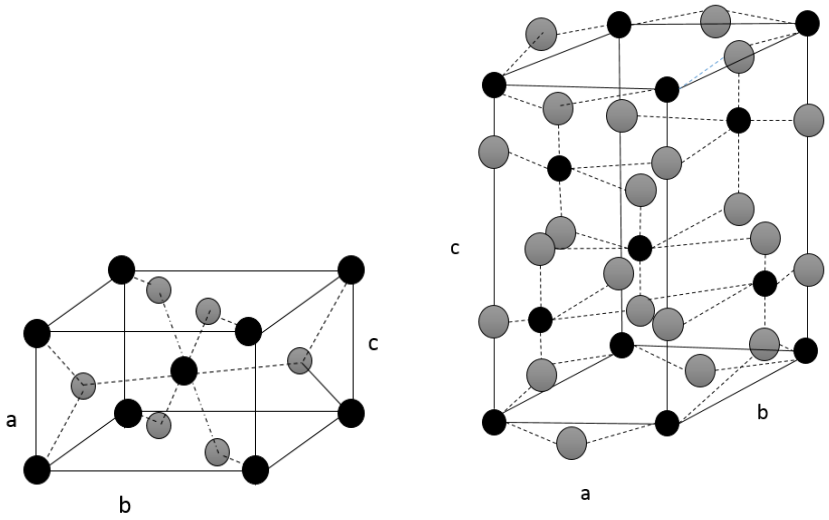

Rutile Anatase

Figure 1. 6. Bulk structures of rutile and anatase. The tetragonal bulk unit cell of rutile has the dimensions, a = b =4.584 Å, c=2.953 Å; and the one of anatase a = b=3.782 Å, c=9.502 Å). The black spheres are titanium atoms, the grey spheres are oxygen atoms.

There are several stable low-index planes of titanium dioxide as shown in Figure 1.7. Ramamoorthy and Vanderbilt[48] used a Wulff construction[49] to illustrate the equilibrium crystal shape of a macroscopic crystal to calculate the total energy of periodic titanium dioxide slabs by employing a self-consistent ab initio method. Their calculations showed that the (110) surface has the lowest surface energy while (001) surface has the highest. As to the (100) and (011) surfaces, their surface energies were lying between these two extremes. For rutile, (110) surfaces are the most stable compare

to the (011) and (100) surfaces. More details about the (110) surface will be addressed in section 1.4.4 below.

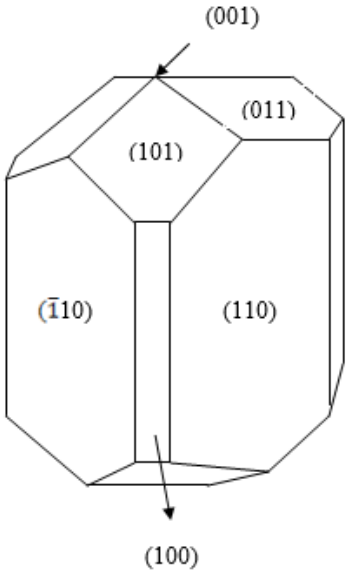

Figure 1. 7. The equilibrium shape of a macroscopic TiO_2 crystal.

1.4.4 The structure of the rutile TiO_2 (110) surfaces

As discussed above, the rutile (110) surface has the lowest surface energy and is the most stable crystal surface. When we prepare the surfaces, by cutting or cleaving, it will create different kinds of titanium atoms or oxygen atoms which play very important roles in surface reactions. According to Tasker's[50] discussion about the stability of ionic surfaces and LaFemina's[51] total energy computations of oxide surface reconstructions, we are able to create a stable (110) surface. On this surface, there are two different types of titanium atoms. The Ti labeled number 1 in Figure 1.8A is a sixfold coordinated Ti

atom in the bulk structure becomes a fivefold coordinated Ti atoms with one dangling bond perpendicular to the surface (Figure 1.8B). At the same time, bridging oxygen atoms (labeled number 3 in Figure 1.8A) are also present. They are altered from the threefold coordination observed in the bulk to twofold coordinated oxygen.

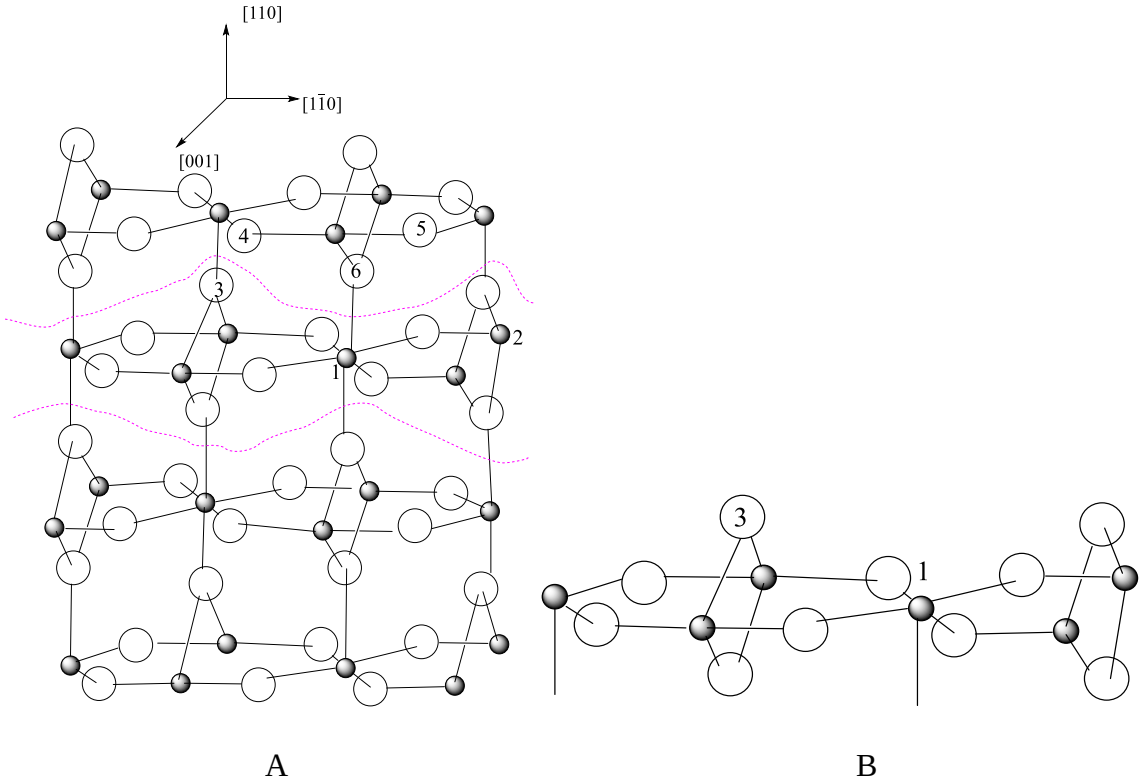

Figure 1. 8. Model of the TiO_2 (110)-(1×1) surface. A. bulk structure. B. The crystal is 'cut' along pink line. The same number of Ti→O and O→Ti bonds are broken, and the surface is autocompensated.

1.4.5 Surface defects

Titanium dioxide surfaces can also have a number of surface defects that can change its electronic structure and this leads to an active photocatalyst. In this section, the step edges, and oxygen vacancies which are produced by sputtering, thermal annealing and electron bombardment in UHV are discussed.

i. Step edges

Sputtering and annealing (T~1000K) in UHV is the common method of generating a clean and flat surface. Fisher et al.[52] had shown that when annealing sputter-damaged surfaces, the terrace size increases with the annealing temperature. Owing to the step geometries, the coordination number of atoms (e.g. Ti, O) at step edges and kink sites is altered. For example, the threefold O atoms in the bulk along the $<1\bar{1}1>$ step edge in Figure 1.8 will change to twofold coordination; meanwhile, the formation of step edges change six-fold Ti atoms in the bulk to five-fold coordination Ti atoms. The decrease in coordination number of the atoms often correlate with an increase in chemical reactivity. S. Suzuki[53] reported that pyridine molecules preferred to adsorb at the fourfold coordinated Ti atoms located at step sites rather than the fivefold coordinated sites.

ii. Oxygen vacancies

There is overwhelming spectroscopic and chemical evidence showing that oxygen vacancies of titanium dioxide can be created by annealing in UHV, bombardment with electrons, and irradiation by UV light at the surface[54]. Figure 1.9a shows the ball and stick models of vacancy free titanium dioxide surface. Bridging oxygen vacancies along the [001] direction of titanium dioxide surface as shown in Figure 1.9b. Exposure of

molecular oxygen to the surface at room temperature will cause the defect state disappear.

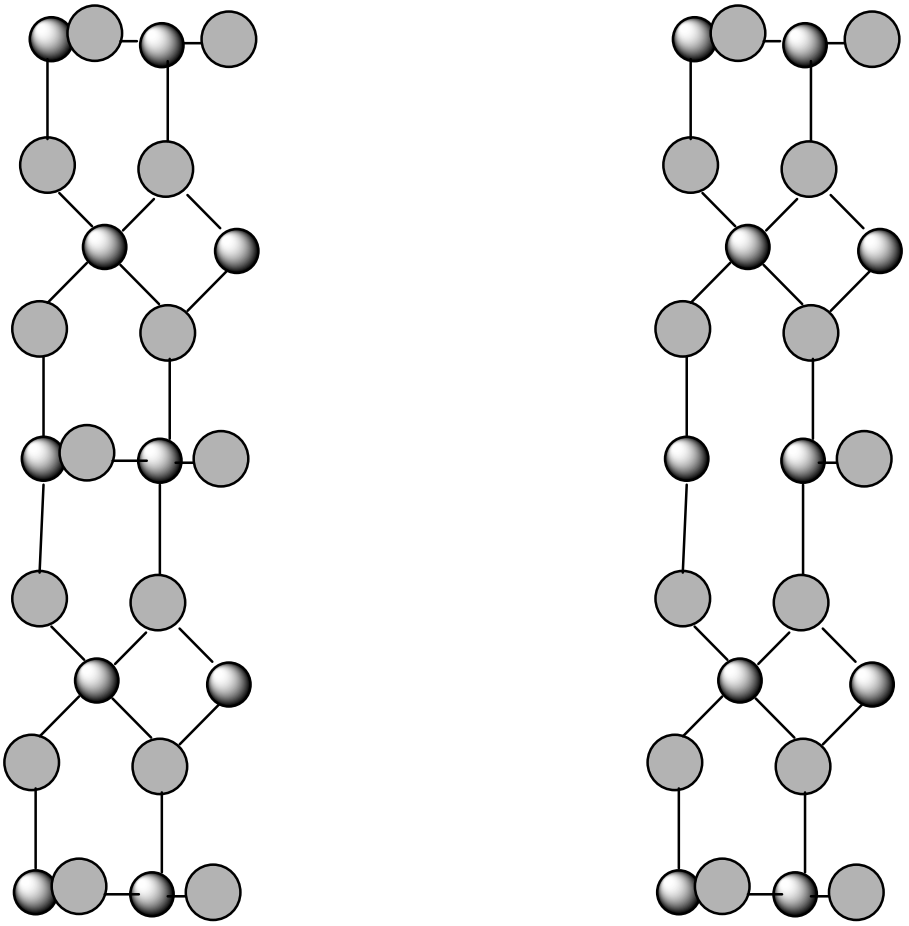

(a) (b)

Figure 1. 9. Ball-and-stick model of TiO_2. The small black spheres represent titanium atoms and the large grey spheres represent oxygen atoms: (a) vacancy-free surface, (b) bridging oxygen vacancy

1.4.6 Band bending

For a stoichiometric (clean) TiO_2 surface, the conduction and valence band are flat[55]. Reduced titanium dioxide is an n-type semiconductor and contains a number of defects, such as oxygen vacancies, O_v. The extra electrons which are initially located in O (2p) orbitals and are then transferred into the conduction band and create an accumulation layer in the near-surface region. This results in downward band bending as shown in Figure 1.10.

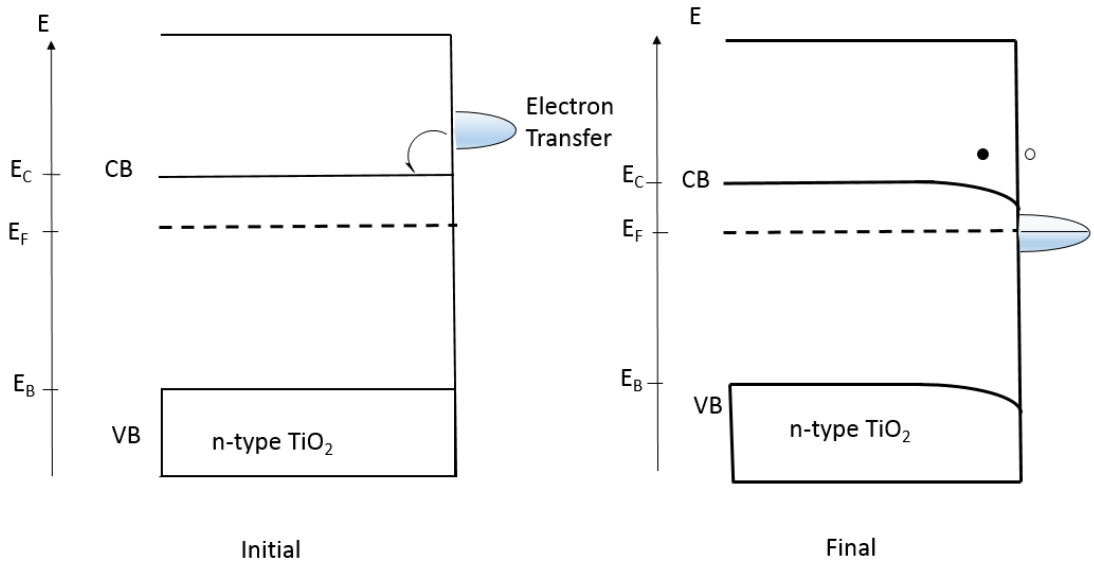

Figure 1. 10. Schematic diagram of the surface band-bending of a clean n-type TiO_2 in a vacuum due to the presence of surface defect states (black dot, electron; circle dot, hole. Another energy diagram of clean n-type TiO_2 has been discussed by Diebold[24].)

1.4.7 Overview of photocatalytic reaction of CO_2

In 1978, Halmann et al.[56] used a p-type gallium phosphide crystal under UV light irradiation in an electrochemical all and followed the photoelectrochemical reduction of aqueous carbon dioxide to yield HCOOH, CH_3O and CH_3OH. This was the earliest study of the photoelectrochemical reduction of carbon dioxide. Since then, researchers have tried different semi-conductors in order to find a better photocatalyst for the reduction of carbon dioxide. TiO_2 is one of the most studied semiconductors in heterogeneous photocatalysts.

1.4.8 Single crystal TiO_2 catalyst and mechanism of TiO_2 photocatalysis

Anpo[57] examined the photocatalytic reduction of carbon dioxide with water on various TiO_2 catalysts and found that anatase crystals have a larger surface area and higher quantum efficiency. Therefore, its photocatalytic activity was better than rutile. The results are shown in Table 1.2.

Table 1. 2. Physical properties and photocatalytic activity of TiO_2 catalysts

Catalyst	Surface area / ($m^2 \cdot g^{-1}$)	CO_2 absorbed /($\mu mol \cdot g^{-1}$)	Reduction of CO_2 / ($\mu mol \cdot g^{-1}$)
Anatase 1	16	1	0.03
Anatase 2	49	10	0.17
Rutile 1	51	17	0.02
Rutile 2	3	0.4	0.04

Saji[58-59] and Tan[60] found that TiO_2 with UV light irradiation, could reduce CO_2 to different fuels (e. g. methane, methanol, and ethanol). Using CO_2 photocatalytic reduction on TiO_2 with H_2O as an example, an explanation of the possible mechanism is shown as equation 1.2.

Table 1.3 shows the band gap energies for three different phases of TiO_2 nanoparticles[61]. The band gap of TiO_2 is 3.0~3.2 eV which means the electrons in valence band of titanium can be irradiated by UV light with enough (greater than the band gap) energy and the excited electrons in valence band will be able to transfer to the conduction band and create electron-hole pairs (e^--h^+) as shown in Eq. 1.2a. These electron-hole pairs can migrate to the surface of titanium and lead to desirable reduction and oxidation reactions when there are acceptors and donors at the surface. Figure 1.11 is a schematic of the photoexcitation of titanium dioxide with CO_2 and H_2O[62]. H_2O can initiate an oxidation reaction by combining the photo-generated valance band hole and yield H^+ and ·OH radical as shown in Eq. 1.2b. $OH^{\bullet}$ is a very strong oxidant and usually used to kill the bacteria in real life. At the same time, CO_2 would accept the electrons which are trapped in the conduction band and be reduced to $CO_2^{\cdot-}$ radicals as shown in Eq. 1.2c.

$$TiO_2 \xrightarrow{hv} e^- + h^+ \qquad (1.2a)$$

$$h^+ + H_2O \longrightarrow OH\cdot + H^+ \qquad (1.2b)$$

$$e^- + CO_2 \longrightarrow CO_2^{\bullet-} \qquad (1.2c)$$

Table 1. 3. Band gap energies of three different phase-pure TiO_2 nanoparticles

Phase-pure TiO_2	Bandgap energy/ eV
Rutile	3.0
Brookite	3.13
Anatase	3.21

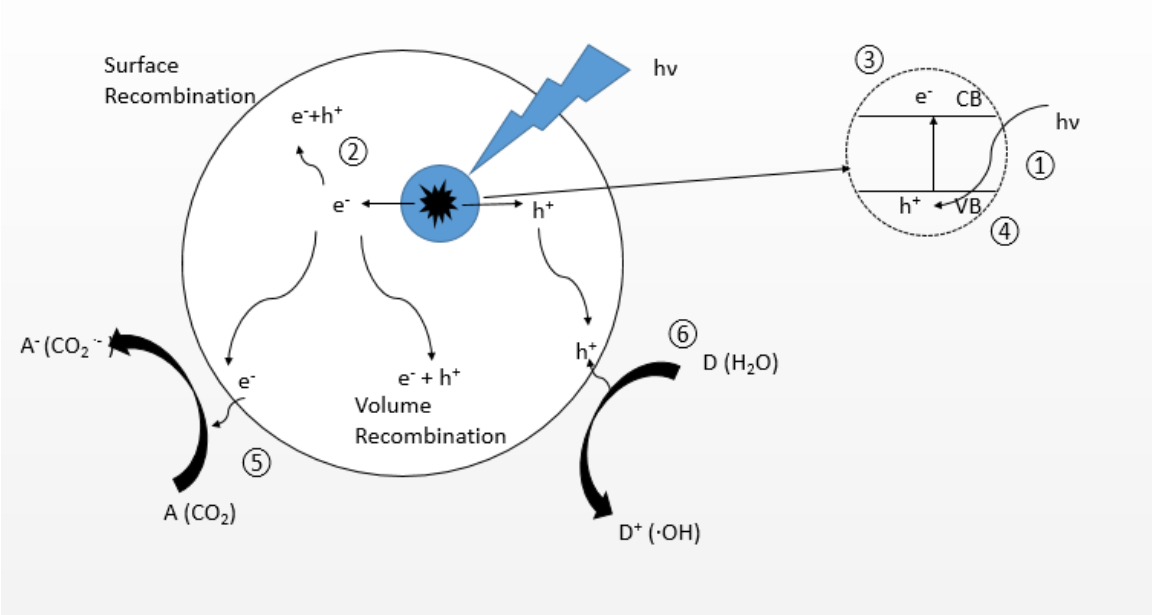

Figure 1. 11. Primary steps in photocatalytic mechanism on TiO_2 and later events. ① formation of charge species electron (e^-) and hole (h^+) by a photon, ② recombination of e^- and h^+, ③trapping of a conduction band electron, ④trapping of a valence band hole, ⑤initiation of reduction reaction by photo-generated conduction band electron, i.e. $CO_2^{\cdot -}$ radical, ⑥ initiation of oxidative pathway by photo-generated valence band hole, i.e. formation of surface adsorbed $OH^{\bullet}$ radical in aqueous system.

1.4.9 The modification of TiO_2

Because of the band gap of TiO_2 is relatively small (3.0 eV-3.2 eV), light with a wavelength lower than 387 nm for anatse and smaller than 413 nm for rutile can be used to irradiate the surface with enough energy to photo-excite electrons. In order to enhance the utilization of solar energy, people tried many methods to modify titanium dioxide by metal doping (e.g. Ru [63], Cu[64]), metal oxide doping (e. g. CuO, ZnO, Li_2O[65]) and non-metal doping(e. g. N[66]). The goal of doping efforts is mostly to shift the wavelength of light more to the visible region, while retaining catalytic activity.

There are several drawbacks to these methods. First, the utilization rate of solar energy is low. Because of the properties of titanium dioxide, the photocatalysts can only absorb the UV portion of the solar spectrum. Secondly, the high rate of recombination of photoexcited electron-hole pairs leads to a lower quantum efficiency. Although many methods are used to suppress these combinations, further development is needed. Lately, the recycle efficiency of the photocatalysts is not good. As the number of times that a catalyst cycled, their catalytic activity becomes poorer. Because of the drawbacks mentioned, there is still significant effort focused trying to understand the mechanism of CO_2 reduction and in the development of better catalysts.

1.5 Overview of surface analytical techniques

For the experiments described in this dissertation, the approach is to use ultra-high vacuum (UHV) based surface chemical studies with single crystals. In the UHV-based studies, X-ray photoelectron and Auger electron spectroscopies are used to examine the surface chemistry occurring upon adsorption and reaction of CO_2 as a function of different surface temperatures and pressures. All of these analytical techniques will be introduced in this section.

1.5.1 Mechanism of Auger electron spectroscopy (AES)

Auger electron spectroscopy is one of the most useful surface analytical analysis method. It can provide elemental information about a material from the first 2-10 outermost atomic layers. Figure 1.12 shows schematically the Auger process. In the first step of the Auger process, a high energy particle (an electron beam in our case) creates a core hole in the K shell of an atom. An electron from an outer electron orbital level such as L_1 in Figure 1.12 that is closer the Fermi level (zero atomic energy level for binding energies of electrons) fills in the K hole. During this transition, there is a transfer of energy which will result in a third electron being ejected (L_2 in Figure 1.12). In the final state, there are two electron holes in the atom, one in the L_1 orbital and the other in the L_2 orbital. We can estimate the kinetic energy of an Auger electron from an element with atomic number Z ($Z \geq 3$) using equation 1.3. The Auger transition energy involves all three electronic orbital energies within the atom. Using the orbitals from Figure 1.12, the energy is:

$$E = E_K - E_{L1} - E_{L2} - \Phi_A \quad (1.3)$$

Where Φ_A is the work function of the analyzer and K, L_1, and L_2 are the three energy levels involved in the Auger process.

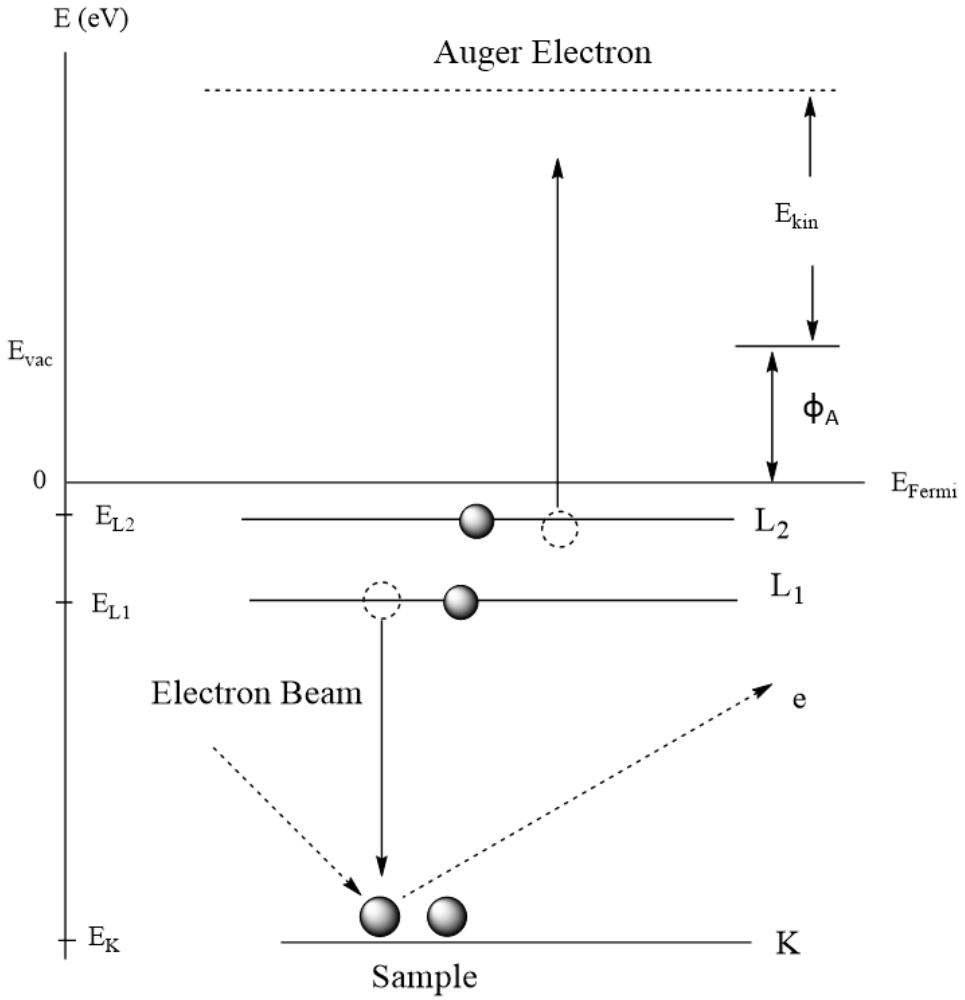

Figure 1. 12. Overview of the Auger process.

1.5.2 Mechanism of X-ray photoelectron spectroscopy (XPS)

X-ray photoelectron spectroscopy (XPS) is another important qualitative and quantitative surface analysis technique. It is performed under ultra-high vacuum (UHV) condition by irradiating the sample with a beam of X-rays and the kinetic energy of the emitted electrons is measured to obtain a spectrum.

Figure 1.14 illustrates the process of X-ray photoelectron spectroscopy. The sample surface to be analyzed is placed in the ultra-high vacuum chamber, and then irradiated with X-ray photons. The kinetic energy and number of the emitted electrons are measured with an electron energy analyzer. Because the energy of an X-ray with particular source is known, the binding energy of each emitted electron can be determined by using equation 1.4:

$$E_{binding} = E_{photon} - (E_{kinetic} + \phi) \qquad (1.4)$$

where $E_{binding}$ is the binding energy (BE) of the photoelectron, E_{photon} is the energy of the X-ray photons being used, $E_{kinetic}$ is the kinetic energy of the photoelectron as measured by the electron energy analyzer and φ is the work function of the spectrometer (not the material).

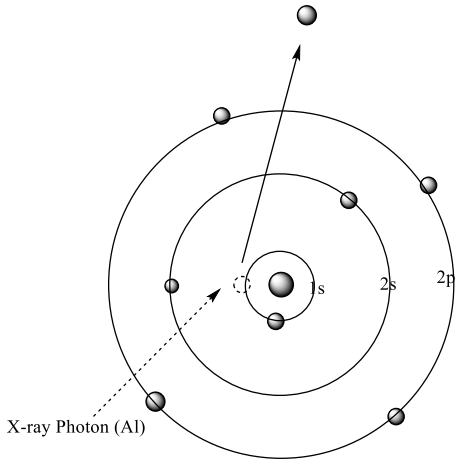

Figure 1. 13. Process of XPS in UHV.

1.6 References

1. www.climatetechnology.gov.
2. Nishimura, A.; Mitsui, G.; Nakamura, K.; Hirota, M.; Hu, E., CO_2 Reforming Characteristics under Visible Light Response of Cr- or Ag-Doped TiO_2 Prepared by Sol-Gel and Dip-Coating Process. International Journal of Photoenergy. **2012,** 2012, 1-12.
3. Metz, B.; Intergovernmental Panel on Climate Change. Working, G., III, IPCC special report on carbon dioxide capture and storage. Cambridge University Press for the Intergovernmental Panel on Climate Change: Cambridge, 2005.
4. Allen, C. D.; Hogg, E. H.; Gonzalez, P.; Fensham, R.; Zhang, Z.; Castro, J.; Demidova, N.; Lim, J.-H.; Allard, G.; Running, S. W.; Semerci, A.; Macalady, A. K.; Cobb, N.; Chenchouni, H.; Bachelet, D.; McDowell, N.; Vennetier, M.; Kitzberger, T.; Rigling, A.; Breshears, D. D., A global overview of drought and heat-induced tree mortality reveals emerging climate change risks for forests. Forest Ecology and Management **2010,** 259 (4), 660-684.
5. Freund, H. J.; Roberts, M. W., Surface chemistry of carbon dioxide. Surface Science Reports **1996,** 25 (8), 225-273.
6. Rattan, L., Carbon sequestration. Philosophical Transactions of the Royal Society B: Biological Sciences **2008,** 363 (1492), 815-830.
7. Lal, R., Sequestration of atmospheric CO_2 in global carbon pools. Energy & Environmental Science **2008,** 1 (1), 86-100.
8. Wang, W. N.; Soulis, J.; Yang, Y. J.; Biswas, P., Comparison of CO2 Photoreduction Systems: A Review. Aerosol And Air Quality Research **2014,** 14 (2), 533-549.
9. Armstrong, E. F.; Hilditch, T. P., A Study of Catalytic Actions at Solid Surfaces. X. The Interaction of Carbon Monoxide and Hydrogen as Conditioned by Nickel at Relatively Low Temperatures. A Practical Synthesis of Methane. Proceedings of the Royal Society of London. Series A, Containing Papers of a Mathematical and Physical Character **1923,** 103 (720), 25-34.
10. K. Ravindranathan Thampi, J. K. M. G., Methanation and photo-methanation of carbon dioxide at room temperature and atmospheric pressure. Nature **1987,** 327 (6122), 506-508.
11. Wang, S.; Yan, S.; Ma, X.; Gong, J., Recent advances in capture of carbon dioxide using alkali-metal-based oxides. Energy & Environmental Science **2011,** 4 (10), 3805-3819.
12. Yanagisawa, Y.; Takaoka, K.; Yamabe, S., Interaction of CO_2 with magnesium oxide surfaces. A TPD, FTIR, and cluster-model calculation study. Journal of physical chemistry **1995,** 99 (11), 3704-3710.
13. Pacchioni, G.; Ricart, J. M.; Illas, F., Ab Initio Cluster Model Calculations on the Chemisorption of CO_2 and SO_2 Probe Molecules on MgO and CaO (100) Surfaces. A Theoretical Measure of Oxide Basicity. Journal of the American Chemical Society **1994,** 116 (22), 10152-10158.
14. Heidberg, J.; Meine, D., Polarized infrared spectra of CO_2 adsorbed on the MgO(100) single crystal surface. Surface Science **1992,** 279 (1–2), L175-L179.
15. Meixner, D. L.; Arthur, D. A.; George, S. M., Kinetics of desorption, adsorption, and surface diffusion of CO_2 on MgO(100). Surface Science **1992,** 261 (1–3), 141-154.

16. Heidberg, J.; Meine, D.; Redlich, B., CO_2 adsorption on the MgO (100) single crystal surface detected by polarization FTIR spectroscopy and SPA-LEED. Journal of Electron Spectroscopy and Related Phenomena **1993,** 64–65 (0), 599-608.
17. Pacchioni, G., Physisorbed and chemisorbed CO_2 at surface and step sites of the MgO (100) surface. Surface Science **1993,** 281 (1–2), 207-219.
18. Suzanne, J.; Panella, V.; Ferry, D.; Sidoumou, M., The structure of CO_2 monolayers on MgO (100) single crystal surfaces. Surface Science Letters **1993,** 293 (3), L912-L916.
19. Little, L. H., Infrared spectra of adsorbed species. Academic Press: 1966.
20. Gregg, S. J.; Ramsay, J. D., Adsorption of carbon dioxide by magnesia studied by use of infrared and isotherm measurements. Journal of the Chemical Society A: Inorganic, Physical, and Theoretical Chemistry **1970**, 2784-2787.
21. Fukuda, Y.; Tanabe, K., Infrare Study of Carbon Dioxide Adsorbed On Magnesium and Calcium Oxides. Bullentin Of The Chemical Society Of Japan **1973,** 46 (6), 1616-1619.
22. Tsuji, H.; Shishido, T.; Okamura, A.; Gao, Y.; Hattori, H.; Kita, H., Oxygen exchange between magnesium oxide surface and carbon dioxide. Journal of the Chemical Society, Faraday Transactions **1994,** 90 (5), 803-807.
23. Henrich, V. E.; Cox, P. A., The surface science of metal oxides. Cambridge University Press: Cambridge, 1994.
24. Diebold, U., The surface science of titanium dioxide. Surface Science Reports **2003,** 48 (5), 53-229.
25. Pin-Ching, M.; Sharon, S.; Daniel, M. B.; Zheng, H.; Edward, J. W.; William, A. J., Bactericidal Activity of Photocatalytic TiO_2 Reaction: toward an Understanding of Its Killing Mechanism. Applied and Environmental Microbiology **1999,** 65 (9), 4094-4098.
26. Mills, A.; Davies, R. H.; Worsley, D., Water purification by semiconductor photocatalysis. Chemical Society Reviews **1993,** 22 (6), 417-425.
27. Paz, Y.; Luo, Z.; Rabenberg, L.; Heller, A., Photooxidative self-cleaning transparent titanium dioxide films on glass. Journal of Materials Research **1995,** 10 (11), 2842-2848.
28. A. Fujishima, K. H., Electrochemical Photolysis of Water at a Semiconductor Electrode. Nature **1972,** 238 (5358), 37-38.
29. Frank, S. N.; Bard, A. J., Heterogeneous photocatalytic oxidation of cyanide ion in aqueous solutions at TiO_2 powder Journal of the American Chemical Society **1977,** 99 (1), 303-304.
30. Tooru Inoue, A. F., Satoshi Konishi, Kenichi Honda, Photoelectrocatalytic reduction of carbon dioxide in aqueous suspensions of semiconductor powders. Nature **1979,** 277 (5698), 637-638.
31. Grant, F. A., Properties of rutile (titanium dioxide). Reviews of Modern Physics **1959,** 31 (3), 646-674.
32. Samsonov, G. V., The Oxide handbook. IFI/Plenum: New York, 1982.
33. Dubrovinsky, L. S.; Dubrovinskaia, N. A.; Swamy, V.; Muscat, J.; Harrison, N. M.; Ahuja, R.; Holm, B.; Johansson, B., The hardest known oxide. Nature **2001,** 410 (6829), 653-654.
34. Gong, X.-Q.; Selloni, A.; Batzill, M.; Diebold, U., Steps on anatase TiO_2 (101). Nat Mater **2006,** 5 (8), 665-670.

35. Gong, X.-Q.; Selloni, A.; Vittadini, A., Density Functional Theory Study of Formic Acid Adsorption on Anatase TiO_2 (001): Geometries, Energetics, and Effects of Coverage, Hydration, and Reconstruction. The Journal of Physical Chemistry B **2006,** 110 (6), 2804-2811.
36. Gong, X.-Q.; Selloni, A., Reactivity of Anatase TiO_2 Nanoparticles: The Role of the Minority (001) Surface. The Journal of Physical Chemistry B **2005,** 109 (42), 19560-19562.
37. Gong, X.-Q.; Selloni, A.; Dulub, O.; Jacobson, P.; Diebold, U., Small Au and Pt Clusters at the Anatase TiO_2 (101) Surface: Behavior at Terraces, Steps, and Surface Oxygen Vacancies. Journal of the American Chemical Society **2008,** 130 (1), 370-381.
38. Diebold, U.; Ruzycki, N.; Herman, G. S.; Selloni, A., One step towards bridging the materials gap: surface studies of TiO_2 anatase. Catalysis Today **2003,** 85 (2–4), 93-100.
39. Ruzycki, N.; Herman, G. S.; Boatner, L. A.; Diebold, U., Scanning tunneling microscopy study of the anatase (1 0 0) surface. Surface Science **2003,** 529 (1–2), L239-L244.
40. Lazzeri, M.; Selloni, A., Stress-Driven Reconstruction of an Oxide Surface: The Anatase TiO_2(101) and (001) surfaces. Physical Review Letters **2001,** 87 (26), 266105.
41. Liang, Y.; Gan, S.; Chambers, S. A.; Altman, E. I., Surface structure of anatase TiO_2 (001): Reconstruction, atomic steps, and domains. Physical Review B **2001,** 63 (23), 235402.
42. Hengerer, R.; Bolliger, B.; Erbudak, M.; Grätzel, M., Structure and stability of the anatase TiO_2 (101) and (001) surfaces. Surface Science **2000,** 460 (1–3), 162-169.
43. Göpel, W.; Rocker, G.; Feierabend, R., Intrinsic defects of TiO_2 (110): Interaction with chemisorbed O_2, H_2, CO, and CO_2. Physical Review B **1983,** 28 (6), 3427-3438.
44. Nerlov, J.; Christensen, S. V.; Weichel, S.; Pedersen, E. H.; Møller, P. J., A photoemission study of the coadsorption of CO_2 and Na on TiO_2(110)-(1 × 1) and -(1 × 2) surfaces: adsorption geometry and reactivity. Surface Science **1997,** 371 (2–3), 321-336.
45. Gutiérrez-Sosa, A.; Walsh, J. F.; Lindsay, R.; Wincott, P. L.; Thornton, G., Carbonate co-adsorption geometry on TiO_2(110)1×1-Na. Surface Science **1999,** 433–435, 538-542.
46. Krischok, S.; Höfft, O.; Kempter, V., The chemisorption of H2O and CO2 on TiO2 surfaces: studies with MIES and UPS (HeI/II). Surface Science **2002,** 507–510, 69-73.
47. Brause, M.; Kempter, V., CO_2 chemisorption on alkalated TiO_2(1 0 0)-(1×3) studied with MIES and UPS(HeI). Surface Science **2001,** 476 (1–2), 78-84.
48. Ramamoorthy, M.; Vanderbilt, D.; King-Smith, R. D., First-principles calculations of the energetics of stoichiometric TiO_2 surfaces. Physical Review B **1994,** 49 (23), 16721-16727.
49. Zangwill, A., Physics at surfaces. Cambridge University Press: Cambridge [Cambridgeshire], 1988.
50. Tasker, P. W., The stability of ionic crystal surfaces. Journal of Physics C: Solid State Physics **1979,** 12 (22), 4977-4984.
51. LaFemina, J., Total energy computations of oxide surface reconstructions. Crit. Rev. Surf. Chem **1994,** 3 (3/4), 297-386.

52. Fischer, S.; Munz, A. W.; Schierbaum, K.-D.; Göpel, W., The geometric structure of intrinsic defects at TiO_2(110) surfaces: an STM study. Surface Science **1995,** 337 (1–2), 17-30.
53. Suzuki, S.; Yamaguchi, Y.; Onishi, H.; Sasaki, T.; Fukui, K.-i.; Yasuhiro Iwasawa, a., Study of pyridine and its derivatives adsorbed on a TiO_2(110)-(1×1)surface by means of STM, TDS, XPS and MD calculation in relation to surface acid[ndash]base interaction. Journal of the Chemical Society, Faraday Transactions **1998,** 94 (1), 161-166.
54. Diebold, U.; Lehman, J.; Mahmoud, T.; Kuhn, M.; Leonardelli, G.; Hebenstreit, W.; Schmid, M.; Varga, P., Intrinsic defects on a TiO_2 (110)(1 × 1) surface and their reaction with oxygen: A scanning tunneling microscopy study. Surface Science **1998,** 411 (1-2), 137-153.
55. Hardman, P.; Raikar, G.; Muryn, C.; van der Laan, G.; Wincott, P.; Thornton, G.; Bullett, D.; Dale, P., Valence-band structure of TiO_2 along the Γ-Δ-X and Γ-Σ-M directions. Physical Review B **1994,** 49 (11), 7170-7177.
56. Halmann, M., Photoelectrochemical reduction of aqueous carbon dioxide on p-type gallium phosphide in liquid junction solar cells. Nature **1978,** 275 (5676), 115-116.
57. Anpo, M.; Yamashita, H.; Ichihashi, Y.; Ehara, S., Photocatalytic reduction of CO_2 with H_2O on various titanium oxide catalysts. Journal of Electroanalytical Chemistry **1995,** 396 (1–2), 21-26.
58. Mizuno, T.; Adachi, K.; Ohta, K.; Saji, A., Effect of CO_2 pressure on photocatalytic reduction of CO_2 using TiO_2 in aqueous solutions. Journal of Photochemistry and Photobiology A: Chemistry **1996,** 98 (1–2), 87-90.
59. Kaneco, S.; Kurimoto, H.; Ohta, K.; Mizuno, T.; Saji, A., Photocatalytic reduction of CO_2 using TiO_2 powders in liquid CO_2 medium. Journal of Photochemistry and Photobiology A: Chemistry **1997,** 109 (1), 59-63.
60. Tan, S. S.; Zou, L.; Hu, E., Photocatalytic reduction of carbon dioxide into gaseous hydrocarbon using TiO_2 pellets. Catalysis Today **2006,** 115 (1–4), 269-273.
61. Reyes-Coronado, D.; Rodríguez-Gattorno, G.; Espinosa-Pesqueira, M. E.; Cab, C.; de Coss, R.; Oskam, G., Phase-pure TiO_2 nanoparticles: anatase, brookite and rutile. Nanotechnology **2008,** 19 (14), 145605-145605 (10).
62. Yates Jr, J. T., Photochemistry on TiO_2: Mechanisms behind the surface chemistry. Surface Science **2009,** 603 (10-12), 1605-1612.
63. Sasirekha, N.; Basha, S. J. S.; Shanthi, K., Photocatalytic performance of Ru doped anatase mounted on silica for reduction of carbon dioxide. Applied Catalysis B, Environmental **2006,** 62 (1), 169-180.
64. Li, Y.; Wang, W.-N.; Zhan, Z.; Woo, M.-H.; Wu, C.-Y.; Biswas, P., Photocatalytic reduction of CO_2 with H_2O on mesoporous silica supported Cu/TiO_2 catalysts. Applied Catalysis B: Environmental **2010,** 100 (1-2), 386-392.
65. Subrahmanyam, M.; Kaneco, S.; Alonso-Vante, N., A screening for the photo reduction of carbon dioxide supported on metal oxide catalysts for C_1–C_3 selectivity. Applied Catalysis B: Environmental **1999,** 23 (2–3), 169-174.
66. Varghese, O. K.; Paulose, M.; LaTempa, T. J.; Grimes, C. A., High-Rate Solar Photocatalytic Conversion of CO_2 and Water Vapor to Hydrocarbon Fuels. Nano Letters **2009,** 9 (2), 731-737.

Chapter 2 Experimental Methods

2.1 Instrumentation and calibration

All experiments were performed in an ultra-high vacuum (UHV) system which is equipped with an ion and turbomolecular pump. The base pressure of the system used in this study was 2×10^{-10} torr. The UHV chamber is equipped with facilities for XPS and AES. XPS measurements are performed using a twin anode (Mg/Al) X-ray source (VSW TA-10). The Mg (K_α) anode is operated at 15 kV and 20 mA (300 Watts) and the Al (K_α) anode is operated at 15 kV and 30 mA (450 Watts). A double-pass cylindrical mirror analyzer (CMA) is operated in the fixed pass energy mode for XPS to measure the kinetic energy of the emitted electrons. A pass energy of 50 eV was used for high-resolution scans. A clean Au sample was used to calibrate the spectrometer. The following gold transitions were used for the calibration: Au $4f_{7/2}$ (84.0 eV), Au $4d_{5/2}$ (335.0 eV), and Au $4p_{3/2}$ (546.0 eV). The Mg ($2p_{3/2}$) XPS transition for the clean surface was recorded and the spectrum was corrected to a binding energy of 51.7 eV, using the Au calibration.

In photochemical experiments, a Hg UV light source lamp (100 watt) was used for the irradiation of the MgO and TiO_2 single crystal surfaces. The UV lamp was oriented along the sample surface normal. The sample surfaces were irradiated by the light through a sapphire window mounted on the UHV chamber.

2.2 Materials

2.2.1 Preparation of MgO (100) single crystal surfaces

MgO(100) single crystal substrates (Sigma-Aldrich, 10×10×0.5 mm, >99.9% purity, trace metal basis) were cleaned by cycles of exposing the crystal to oxygen (Linde, research grade, >99.998% purity) for ~30 minutes at a pressure of 4×10^{-7} torr while maintaining a surface temperature of ~700ºC. Surface cleanliness was measured by Auger electron spectroscopy (AES). A surface was considered clean when the measured carbon atomic concentration was less than one percent. Figure 2.1 is Auger spectra of the MgO (100) single crystal surface. The green line is MgO surface before cleaning. The atomic percentage of carbon which located at the peak position 272 eV is 12.3 %. The red line is the AES spectrum taken after cycles of O_2 cleaning. The carbon contamination is gone and the percentage of carbon decreased to 0%. The O peak is measured at 503 eV and the Mg peak is measured at 1174 eV.

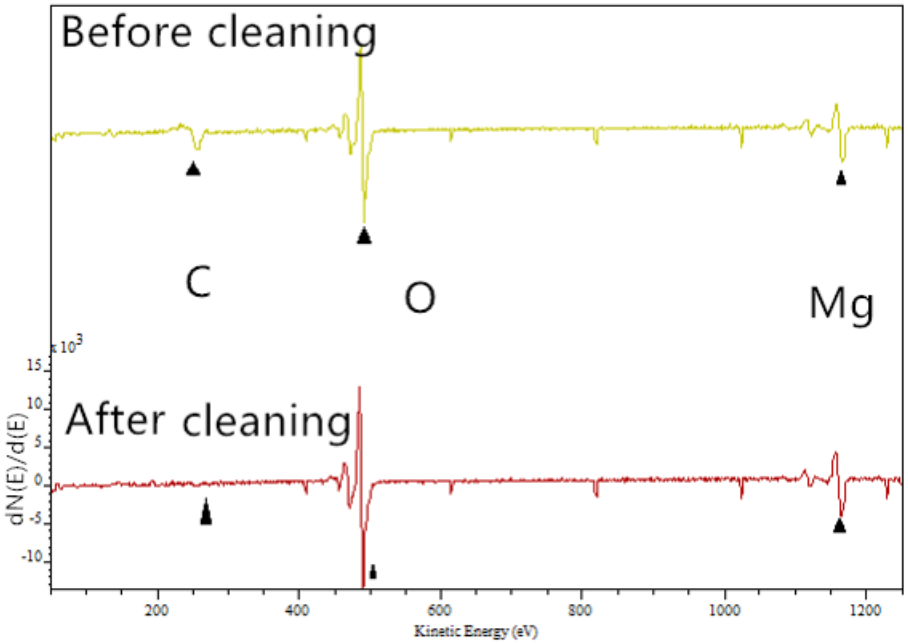

Figure 2. 1. AES spectra of a MgO (100) single crystal surface before and after cleaning.

2.2.2 Preparation of TiO_2 (110) single crystal surfaces

TiO_2 (110) single crystal substrates (Sigma-Aldrich, 10×10×0.5 mm, >99.9% purity, trace metal basis) were cleaned by a combination of sputtering and annealing at 950K for 5 min until a clean and ordered TiO_2 (110) surface was obtained by AES. For sputtering, a 1.5 keV Ar^+ beam was used, with a total current collected on the sample holder of 0.2 μA. To maintain the clean surface, a brief 10 min sputtering at 300K followed by 5 min annealing at 950 K was used on a daily basis.

A surface is considered be as clean when the carbon atomic percentage is lower than 1%. Figure 2.2 shows the AES spectra of TiO_2 (110) single crystal surface before and after cleaning. The green line is before cleaning and the atomic percentage of carbon

is 9.5%. After cycles of sputtering and annealing, the atomic percentage of carbon is reduced to 0%.

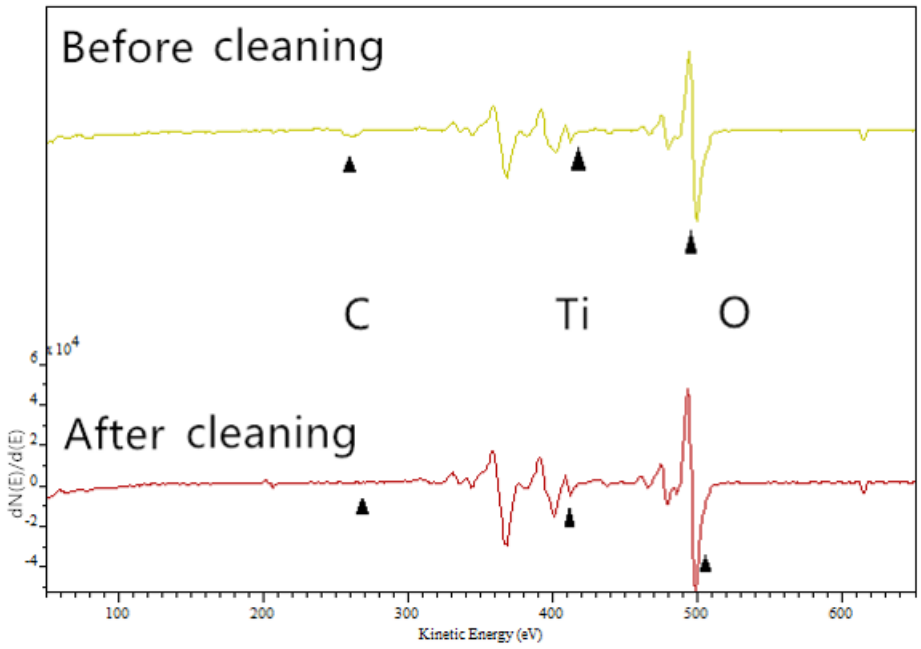

Figure 2. 2. Auger spectra of a TiO_2 (110) single crystal surface before and after cleaning.

2.2.3 CO_2 exposures

Carbon dioxide (Lindweld, research grade – bone dry, >99.995% purity) was used as received and the purity of the gas was checked in-situ by mass spectrometry. The reagent gas is admitted to the chamber through an effusive doser directed onto the front face of the crystal for various periods of time. The actual pressure at the sample is higher than the chamber pressure as measured by the ion gauge and since these pressures should be proportional to one another, the chamber pressure is used as a measure of the overall sample exposure. The exposures (uncorrected for ion gauge sensitivity for carbon

dioxide) are reported in Langmuir (1 L = 10^{-6} torr· sec). The details of exposures will be discussed in Section 2.3.

2.3 Thermal surface reactions of CO_2 with oxide surfaces

2.3.1 Experimental setup

A MgO (100) single crystal or TiO_2 (110) single crystal was mounted onto a Ta support plate (1mm thickness and of the same dimensions as the crystal). The Ta support was cooled and resistively heated by two Ta wires spot-welded to its backside. The sample temperature could be controlled between 77 and 1073 K and was measured by a chromel-alumel thermocouple spot-welded to the back of the sample plate. Figure 2.3 is the top view of UHV chamber. Prior to experiments, after MgO or TiO_2 single crystals surfaces mounted to the Ta plate, the UHV chamber was thoroughly degassed by pumping at a temperature of 160 °C for 72-96 hrs.

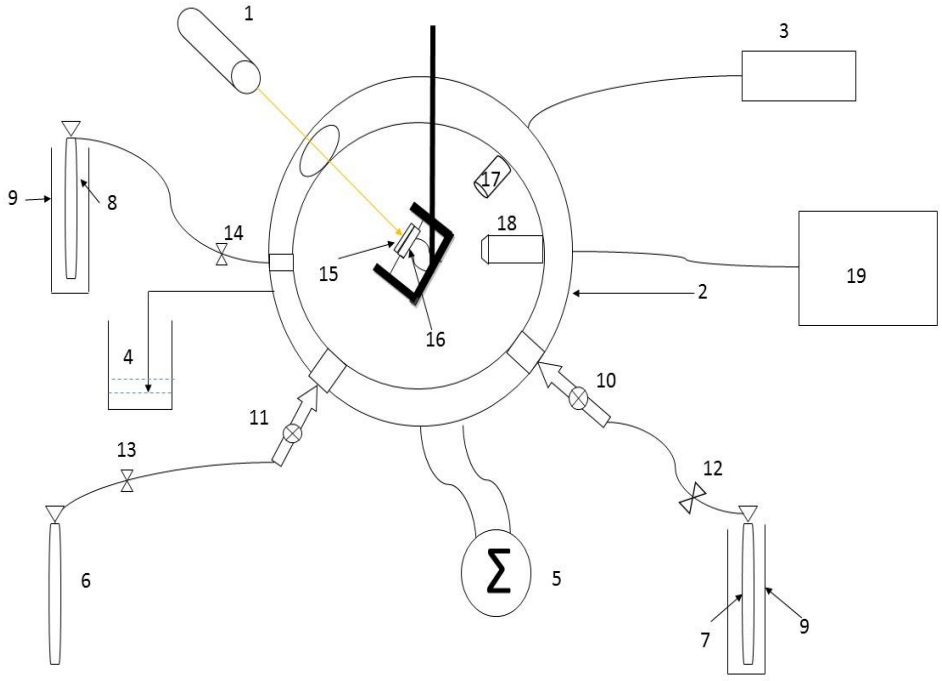

Figure 2. 3. Schematic drawing of UHV chamber setup (top view). (1) Hg UV light; (2) stainless steel chamber; (3) pump; (4) water cooling system; (5) heater w/temp. control; (6) CO_2 gas cylinder; (7) O_2 gas cylinder; (8) Ar gas cylinder; (9) liquid N_2 cooling tank ; (10)-(14) valves; (15) sample; (16) Ta holder; (17) X-ray source (18) electron energy analyzer; (19) computer.

All the reactions of CO_2 on both MgO and TiO_2 single crystal surfaces were performed in the ultra-high vacuum chamber, and AES and XPS were used to examine the surface chemistry.

2.3.2 Thermal reactions of CO_2 with MgO (100) and TiO_2 (110) single crystal surfaces

2.3.2.1 CO_2 reactions with MgO (100) single crystal surfaces

AES and XPS scans of the MgO (100) single crystal clean surface were taken and then the surface was exposed to different exposures of CO_2 (500-5000 Langmuir). The CO_2 was introduced into the chamber via a leak valve connected to a high purity CO_2 cylinder. The temperature of the sample was held constant during the exposure (550-650 °C). After each exposure at a given temperature, AES and XPS spectra were obtained from the surface at room temperature. A schematic of CO_2 reacting with MgO is shown in Figure 2.4.

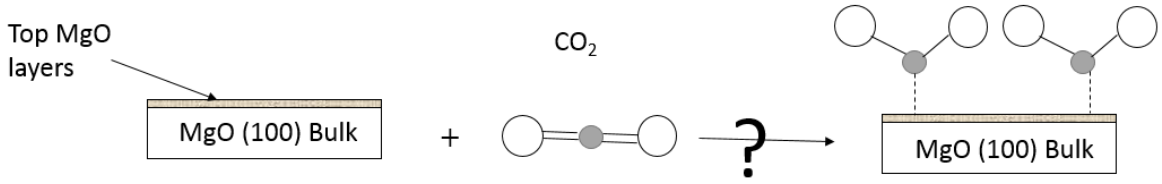

Figure 2. 4. Schematic reaction of CO_2 with a MgO (100) single crystal surface.

2.3.2.2 CO_2 reactions with TiO_2 (110) single crystal surfaces

AES and XPS scans were taken of the TiO_2 (110) surface after cleaning and then exposed to different exposures (500-5000 Langmuir) of CO_2. The temperature of the sample was held constant during the exposure (200-700 °C). After each exposure at a

given temperature, AES and XPS spectra were taken from the surface at room temperature. Figure 2.5 shows the schematic of this reaction.

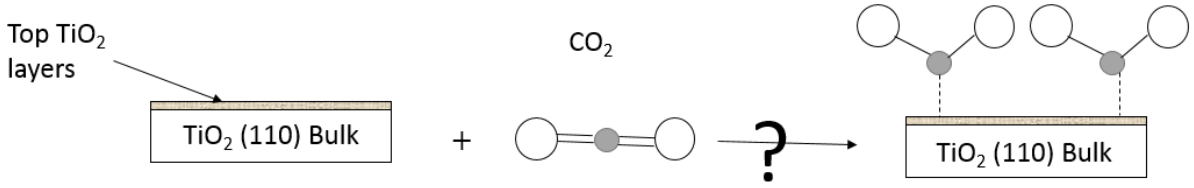

Figure 2. 5. Schematic reaction of CO_2 with a TiO_2 (110) single crystal surface.

2.4 Photocatalytic reactions of CO_2 with MgO (100) and TiO_2 (110) single crystal surfaces

The photocatalytic surface reactions of CO_2 with MgO and TiO_2 were compared with thermally induced surface reactions. The differences and surface species were spectroscopically identified by using XPS and AES techniques. Examination of the surfaces after UV light irradiation could demonstrate the role it played in surface chemical reactions.

2.4.1 Setup of instrumentation

The UV lamp was warmed up about 10 mins before using it. The schematic setup of the apparatus has been shown in Figure 2.3. The UV lamp source was set along the sample surface normal, and the sample surface was irradiated by UV light through a sapphire window mounted on the UHV chamber.

2.4.2 Photocatalysis of CO_2 on MgO (100) and TiO_2 (110) single crystal surfaces

2.4.2.1 Photocatalytic reaction of CO_2 on MgO (100) single crystal surface

The clean surface of MgO (100) surface was first prepared and then exposed to different exposures of CO_2 (500-5000 Langmuir) at room temperature. After the exposure, an AES spectrum and set of XPS scans were obtained. After the measurements, the sample was exposed UV irradiation for 10 minutes and AES and XPS scans were taken again. Figure 2.6 shows the schematic of this reaction process.

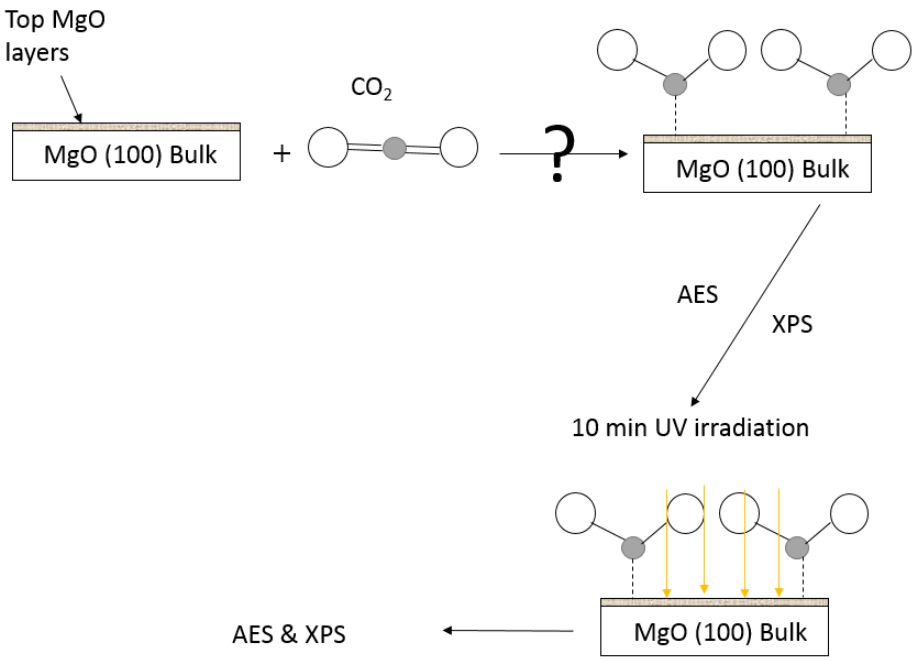

Figure 2. 6. Schematic of photocatalytic reactions of CO_2 with MgO (100) single crystal surfaces.

2.4.2.2 Photocatalytic reaction of CO_2 on TiO_2 (110) single crystal surfaces

The TiO_2 (110) single crystal was cleaned and then exposed to different amounts of CO_2 (500-5000 Langmuir) at room temperature. After the exposure, the sample was exposed under 10 or 20 min UV light irradiation. AES and XPS scans of the surface were made after the irradiation. Figure 2.7 shows the schematic of the reactions.

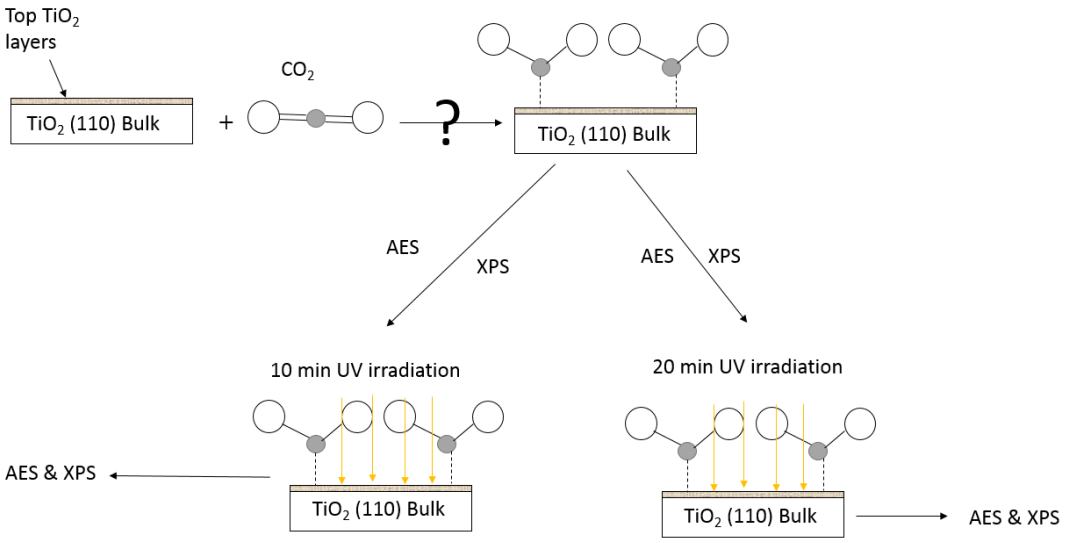

Figure 2. 7. Schematic of photocatalytic reactions CO_2 with TiO_2 (110) with UV irradiation.

In another set of experiments, the clean surface of TiO_2 (110) was exposed UV irradiation during the CO_2 exposure (500-5000 Langmuir) at room temperature. After the lamp and CO_2 were turned off, AES and XPS scans were taken. Figure 2.8 shows the schematic of this reaction.

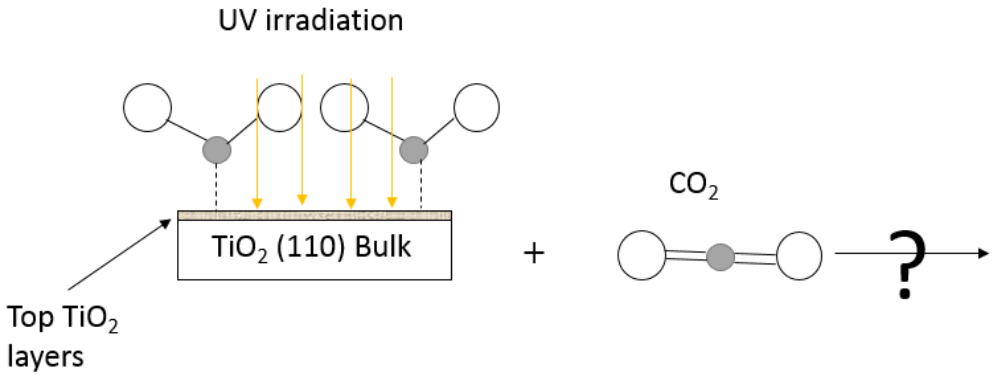

Figure 2. 8. Schematic of photocatalytic reaction CO_2 with TiO_2 (110) during UV irradiation.

2.5 Characterization of samples

Before each experiment, the MgO (100) and TiO_2 (110) single crystal were cleaned and surface cleanness was verified by Auger electron spectroscopy (AES) and X-ray photoelectron spectroscopy (XPS). Then after each experiment involving CO_2 exposure and/or UV irradiation of the surfaces, AES and XPS scans were taken. By comparing the scans before and after exposures of CO_2 and /or UV light, the differences could be observed as to whether there were any reactions of CO_2 with both single crystal surfaces.

2.5.1 AES analysis of single crystal surfaces

2.5.1.1 Data collection

AES scans were performed using a 3 keV electron beam. A kinetic energy range of 50-650 eV for TiO_2 and 50-1250 eV for MgO was used. The spectra were measured in 1 eV intervals with a dwell time of 25 milliseconds and were averaged over 5 scans. The differentiated AES spectrum of MgO or TiO_2 versus kinetic energy was saved by AugerScan data acquisition software.

2.5.1.2 Qualitative analysis of spectrum

Each element has its unique AES transition energy. AES can be used to identify elements in the surface region as long as the atom has three or more electrons. The correct identification of major Auger peaks can be accomplished by referring to standard Auger spectra[1]. There might be some peak shifts of a few eV due to the chemical bonding. Only the prominent peaks of these elements will be observed in the spectrum.

Figure 2.9 is an Auger spectrum of the MgO (100) surface. The derivative of the signal intensity with respect to the energy is plotted versus kinetic energy. This is done as the Auger signal is slowing changing on a broad background. The carbon transition is observed about 270 eV, the oxygen transition can be detected around 503 eV, and the Mg transition can be measured near 1174 eV.

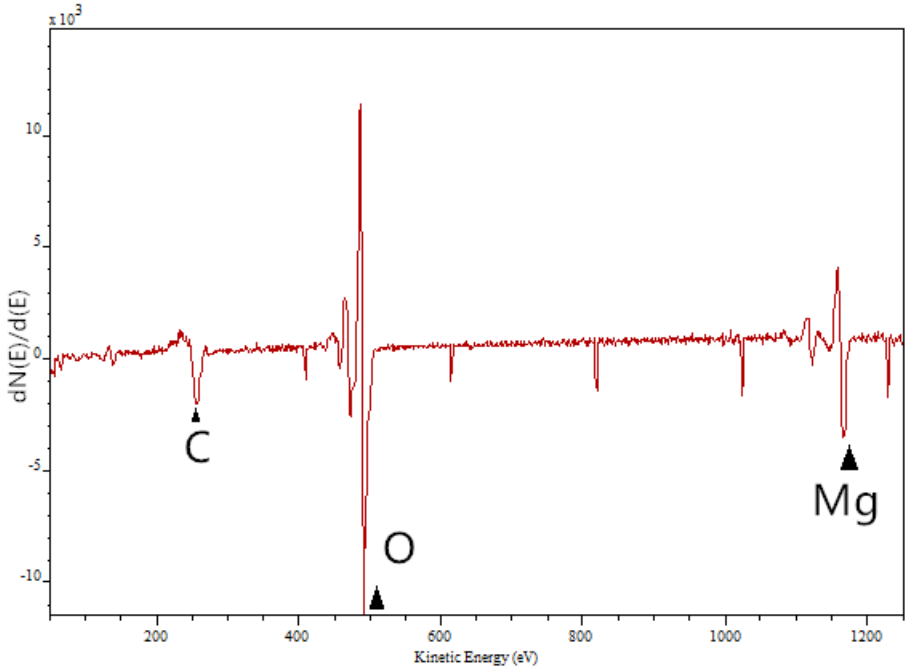

Figure 2. 9. Auger spectrum of the MgO (100) surface.

2.5.1.3 Quantitative analysis of spectrum

The peak-to-peak height of an Auger transition can be used to determine the relative atomic concentration of a given element. The Auger peak intensity of an element can be correlated to its atomic concentration using the equation 2.1

$$x_A\% = \frac{I_A/S_A}{\sum_i^n I_i/S_i} \times 100 \quad (2.1)$$

Where x_A is atomic percentage of element A,

I_i is the peak to peak intensity of a given element, and

S_i is the respective sensitivity factors for an element.

2.5.2 XPS analysis of single crystal surfaces

2.5.2.1 Data collection

XPS scans were performed using a VSW TA-10 X-ray source with a twin anode (Mg/Al). The Al K_α photon energy was 1486.6 eV. A wide scan which concluding photoemission features from all components and detailed scans of each individual elemental regions were collected with pass energies of 100 eV and 50 eV, respectively. For the wide scan, the spectra were measured using 1 eV intervals with a dwell time of 75 milliseconds and were averaged over 20 scans. These settings result in adequate resolution (ΔE= 2eV) for elemental identification and produce very high signal intensities, minimizing data acquisition time and maximizing elemental detectability[2]. For detailed scans, the spectra were measured in 0.05 eV intervals with a dwell time of 75 milliseconds and were averaged for 50 scans for each elemental region.

2.5.2.2 Qualitative analysis of a spectrum

The data was saved in a binary format by the AugerScan data acquisition software and then processed in Casa XPS software[3]. Wide scan spectra can be used to identify all

of elements present in the sample surface. Detailed spectra can be used to show the information of each element, including its energy position, area, and peak FWHM (full width at half maximum) for each XPS transition. Peaks were fit using a GL30 (Gaussian 70%-Lorentzian 30%) line shape. An XPS spectrum is obtained by measuring the kinetic energy of the ejected photoelectrons versus intensity.

2.5.2.3 Quantitative analysis of spectra

Quantitative analysis of the spectra was also carried out. A complete XPS spectrum of a material includes peaks that can be associated with different elements except H and He present in the outer 10 nm of this material. The area under these peaks is proportional to the amount of each element present. Therefore, the atomic percentage of each element detected by the XPS could be calculated by the peak areas and correcting them for the appropriated instrumental factors. The common equation used for this calculation is shown in equation 2.2:

$$\%n_i = \left(\frac{I_{ij}}{\sigma_{ij} KE^{0.7}}\right) / \sum \left(\frac{I_{ij}}{\sigma_{ij} KE^{0.7}}\right) \quad (2.2)$$

Where n_i is the atomic percentage of element I,

I_{ij} is the area of peak j from element I,

σ_{ij} is the photoionization cross-section of peak j from element i, and

KE is the kinetic energy of peak j from element i.

The main elements studied included carbon, oxygen, and magnesium for MgO (100). Carbon, oxygen, and titanium are the main elements examined for TiO_2 (110). By measuring the change in elemental concentration, we can determine the extent of adsorption of CO_2 on the surfaces.

2.6 References

1. Davis, L. E.; MacDonald, N. C.; Palmberg, P. W.; Ricach, G. E.; Weber, R. E., Handbook of Aguer Electron Spectroscopoy. **1976**.
2. Wagner, C. D.; Riggs, W. M.; Davis, L. E.; Muilenberg, G. E., Handbook of X-ray photoelectron spectroscopy. **1979**.
3. Fairley, N., CasaXPS Version 2.3.14. **1999**.

Chapter 3 Results

3.1 Thermal reactions of CO_2 on MgO (100) single crystal surface

Auger electron spectroscopy and X-ray photoelectron spectroscopy are used to examine the clean surface and modified surface. Details of methods were introduced in Chapter 2. All of analysis in this chapter are based on AES and XPS results.

3.1.1 AES spectra of MgO (100) single crystal surfaces

Figure 3.1 shows respective AES results for exposing MgO (100) to CO_2 (500-5000 L) at different substrate temperatures. The MgO (100) substrate is held at a constant temperature during each exposure. In each set of spectra, the very bottom line is a clean surface spectrum. Then after exposures, any carbon deposited on the surface was detected by AES at a kinetic energy around 270 eV. However, some carbon may be present on the clean surface of MgO (100) before a CO_2 exposure since we used a 1% cut off for carbon cleanliness. The amount of carbon deposited changed from 0.8% to 2.4% as the temperature changed from 550 to 650 ^{0}C and exposure changed from 500 to 5000 L.

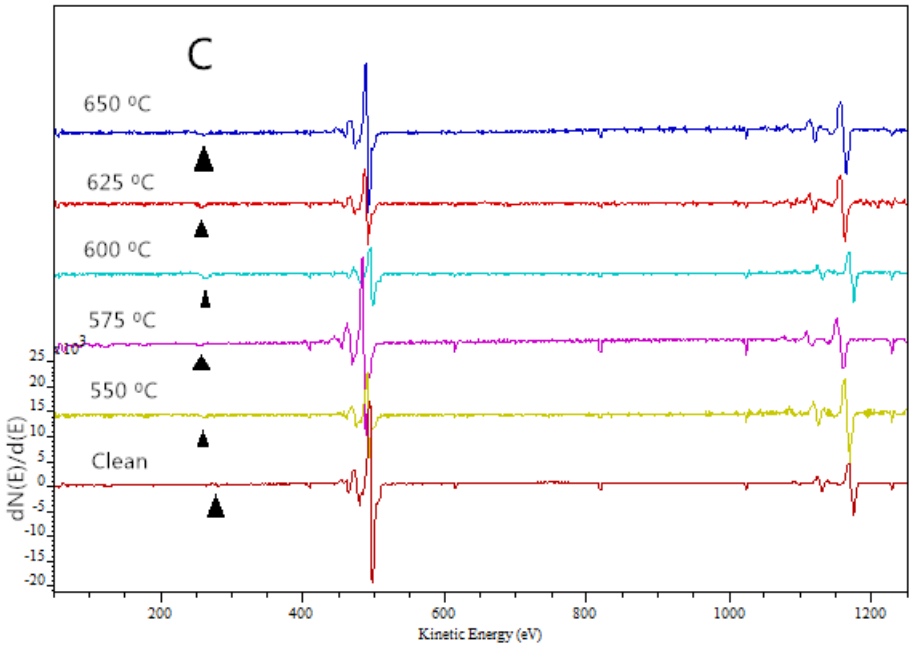

(a) 500 L CO_2

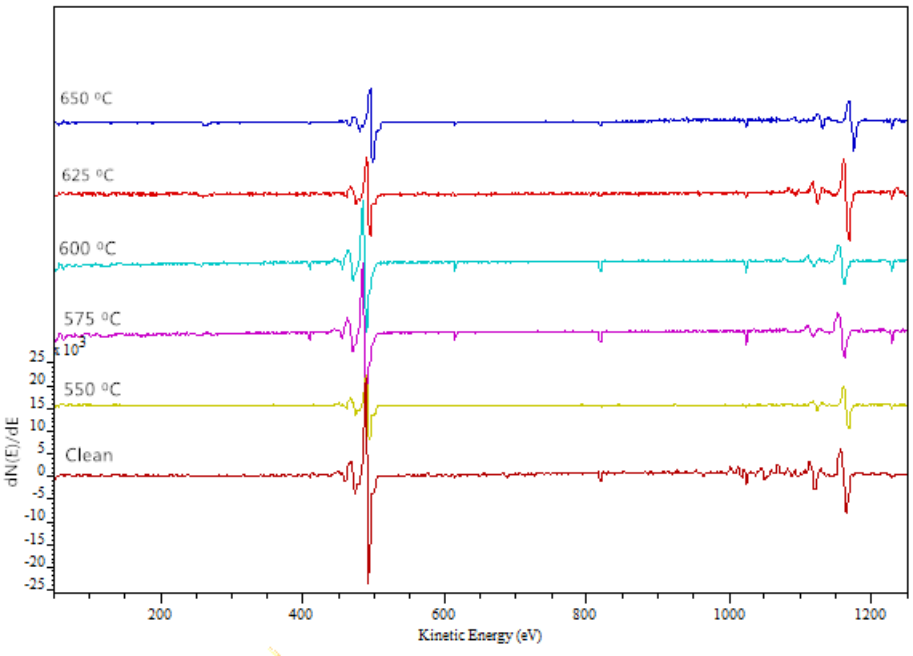

(b) 1000 L CO_2

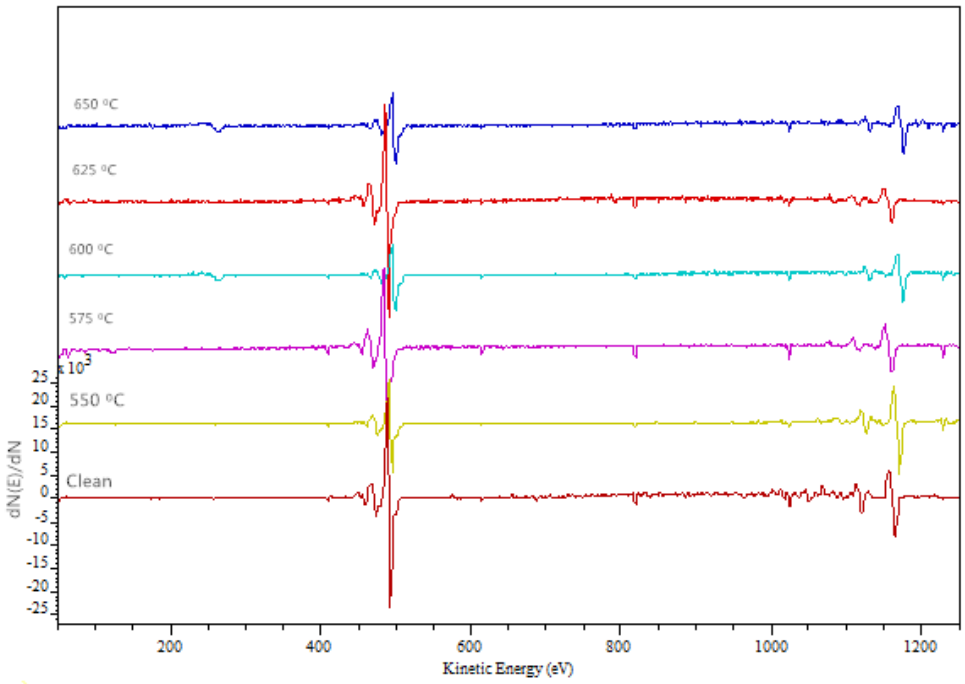

(c) 5000 L CO_2

Figure 3. 1. AES spectra obtained after exposing MgO to 500-5000L CO_2 at various surface temperatures. (a) 500 L; (b) 1000 L; (c) 5000L.

Table 3.1 summarizes a series of experiments examining the influence of MgO surface temperatures and CO_2 exposures. After each exposure, the sample was cooled to room temperature and the Auger spectrum was taken. The amount of carbon at the surface is determined from the peak-to-peak intensities of a given elemental transition in the spectrum, along with the appropriate sensitivity factors. Details of the quantitative calculations were illustrated in Chapter 2. If any carbon was present on the surface before the exposure, then its concentration is subtracted from the amount present after exposure.

These results are shown in Table 3.1. And the atomic percentages are averages of at least triplicate measurements on different MgO (100) crystal surfaces.

Table 3. 1. Change in the atomic surface concentration of carbon in thermal reactions of CO_2 with MgO (100) single crystal surfaces measured by AES.

Temperature (^{0}C)	AES		
	500L	1000L	5000L
550	0.8±0.1%	1.6±0.2%	0.8±0.1%
575	1.4±0.6%	1.4±0.7%	1.4±0.7%
600	0.5±0.1%	0.9±0.1%	1.7±0.6%
625	0.8±0.5%	1.4±0.5%	1.0±0.2%
650	1.8±0.5%	1.6±0.7%	2.4±0.9%

In order to see the changes of carbon percentage with substrate temperatures and exposures more clearly, the data in Table 3.1 are presented as Figure 3.2.

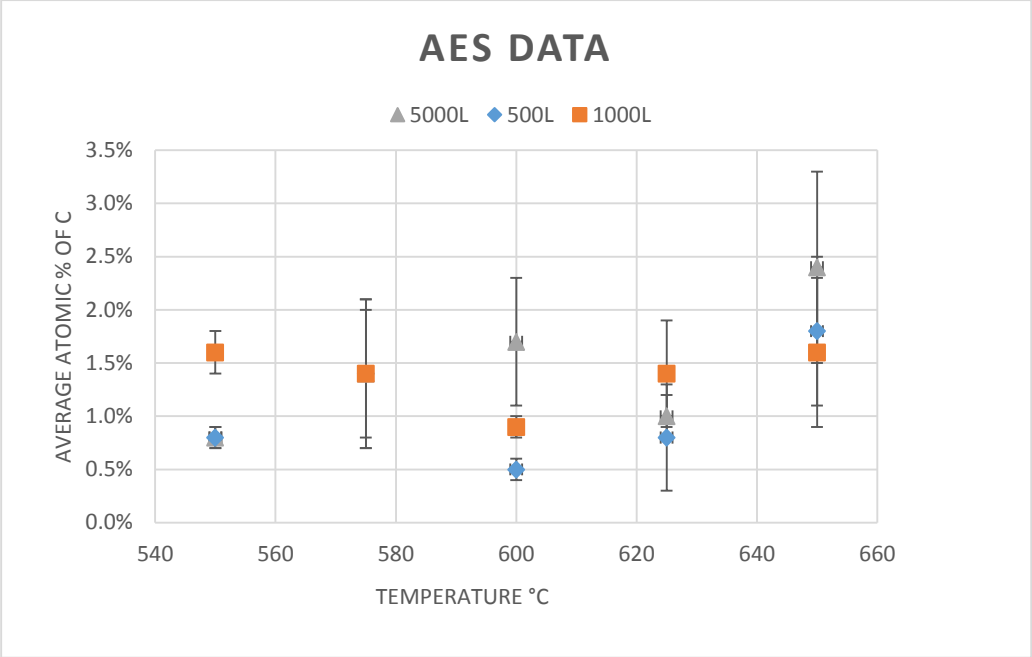

Figure 3. 2. Change in the atomic surface concentrations of carbon on MgO (100) in thermal reactions.

3.1.2 Analysis of wide XPS spectrum

X-ray photoelectron spectroscopy can present complete information about bound electron states in the material by measuring the kinetic energy distribution of photoelectrons emitted from the specimen material excited by an X-ray source.

An XPS full spectrum of MgO (100) surface is shown in Figure 3.3. Intense and sharp Mg peaks can be observed, as well as smaller carbon and oxygen peaks. The weak carbon peak (binding energy (B.E) of ~284 eV) corresponds to the C (1s) transition and indicates that a low amount of amorphous carbon is adsorbed on the surface. The carbon can be removed by O_2 heating at 973 K[1]. Except for this peak, no other impurities are observed, proving that the sample is composed of magnesium and oxygen. In the range of 304.4-308.8 eV are the Mg KLL Auger emission peaks which are attributed to the +2

oxidation state magnesium. And also, O KLL Auger emission peaks at a binding energy range of 992-1102 eV are obtained as well.

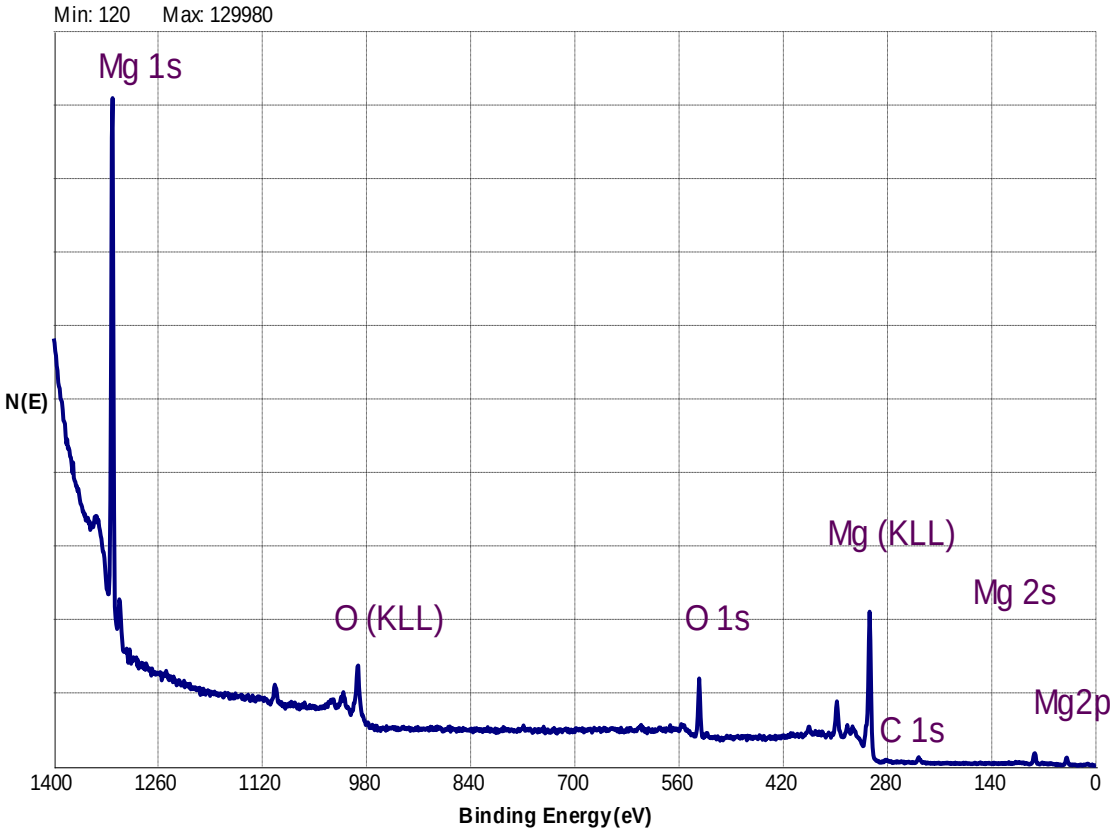

Figure 3. 3. A full XPS spectrum of MgO (100) surface.

3.1.3 Analysis of detailed XPS spectra

Detail spectra are used for chemical state identification, and quantitative analysis of minor components. Peak deconvolution and other mathematical manipulations of the data is most often performed with detailed scans. Peaks from any species thought to be radiation-sensitive or transient should be run first, such as C (1s). An analyzer pass energy of 50 eV (ΔE=0.5 eV) is adequate for routine detail scans.

3.1.3.1 C (1s)

Detailed C (1s) spectra of MgO surface before (red) and after (green) 5000 L CO_2 exposure at 650 ^{0}C are shown in Figure 3.4. After the exposure, the carbon peak area increased slightly (see also Table 3.3). AES data also proved an increase carbon concentration in Section 3.1.1. One broad peak is observed with a binding energy of 286.6 eV matching literature values for carbonates, refer to Table 3.2. However, most previous studies were performed at room temperature or lower. Our results show that with higher surfaces temperatures and "high" exposures, carbon can still be adsorbed on the MgO surface, although the exact structure of carbon is still unclear. The XPS line width is rather broad and might be due to overlapping structures related to chemical shifts or different adsorption sites on the surface.

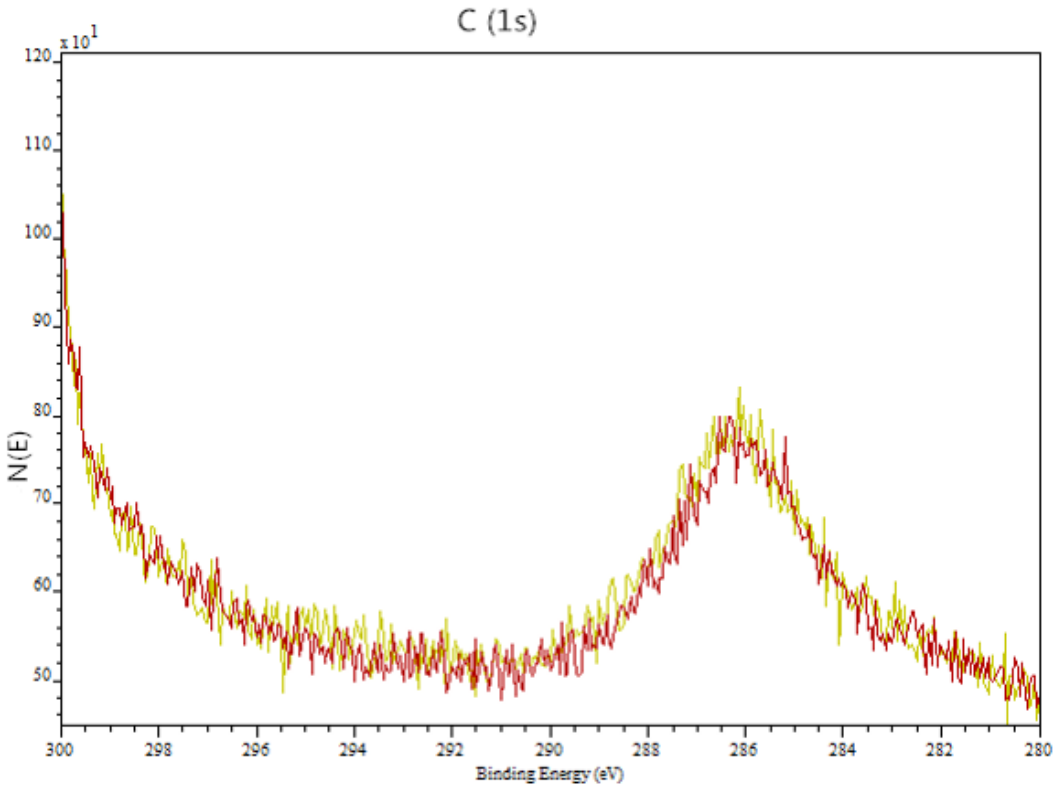

Figure 3. 4. C (1s) spectra of MgO (100) surface before exposure (red) and after a 5000 L CO_2 exposure (green) at a surface temperature of 650 ^{0}C.

Table 3. 2. XPS C (1s) lines seen for adsorbed CO_2.

System	C (1s)-XPS line position (eV)	Carbonate	Ref.
CO_2-MgO (001)	290.0	×	[2]
CO_2-MgO (111)	290.0	×	[2]
CO_2-MgO (001)	286.6	×	This work

With increasing exposures of CO_2 (500-5000L) to the surface at a constant temperature (650 ^{0}C), the C (1s) peak area changed as observed in Figure 3.5. The red line is MgO surface after exposure to 500 L CO_2, the green line is after a 1000 L CO_2 exposure, and the purple line is obtained after a 5000 L CO_2. The atomic percentages of carbon changed along with the changing conditions are summarized in Table 3.3. At lower exposures, the carbon concentration did not change much. However, at the highest exposures of CO_2 (5000L), the amount of carbon deposited increased by 1.2%.

Table 3.4 lists the changes in carbon concentration on MgO (100) surfaces with different CO_2 exposures (500-5000L) and temperatures (550-650 ^{0}C). The reported values are averages of at least triplicate measurements on different MgO (100) single crystal surfaces.

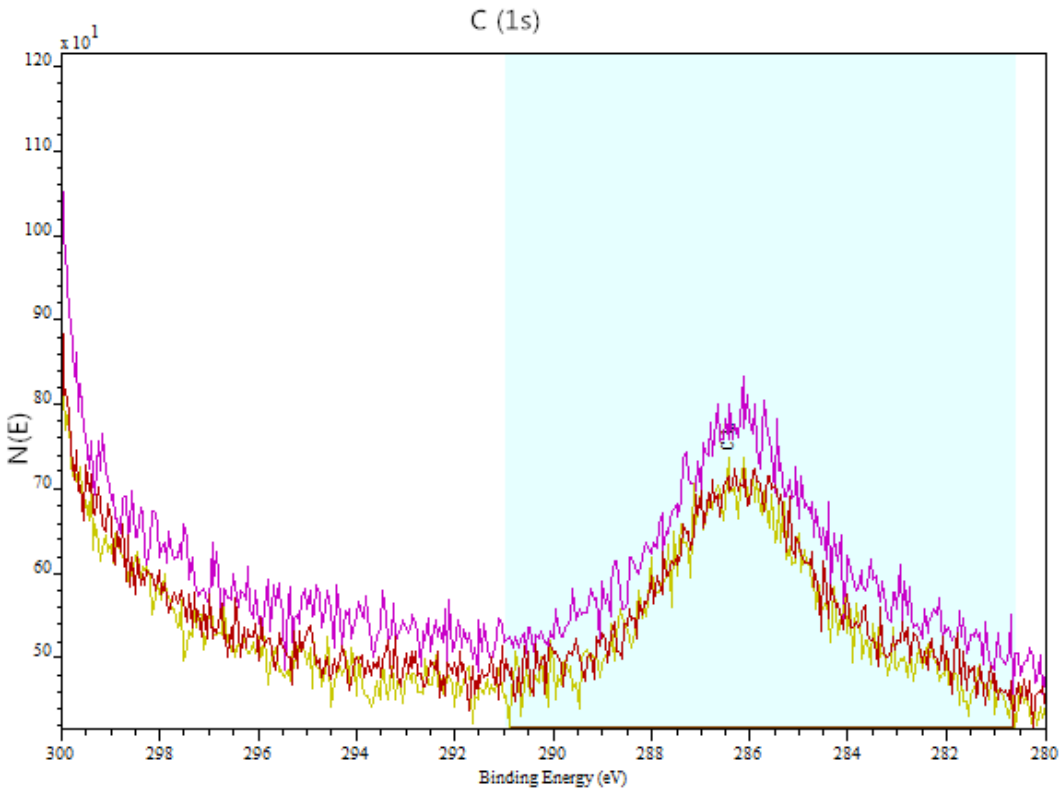

Figure 3. 5. C (1s) region of MgO (100) surface with different CO_2 exposures at 650 ^{0}C. The CO_2 exposures are 500 L (red), 1000 L (green), and 5000 L (purple).

Table 3. 3. Carbon concentration on MgO (100) after CO_2 exposures as measured by XPS

System	Temp. (^{0}C)	CO_2 Exposure (L)	Peak position (eV)	Peak area	Atomic percentage
"clean" surface			286.6	1079.3	7.0%
1	650	500	286.6	1012.8	7.6%
2	650	1000	286.6	1096.8	7.9%
3	650	5000	286.6	1169.7	8.2%

Table 3. 4. Average carbon surface concentrations on MgO (100) single crystal surfaces resulting from thermal reactions with CO_2 as measured by XPS

Temp. (^{0}C)	XPS		
	500L	1000L	5000L
550	1.0±0.5%	0.6±0.1%	0.5±0.3%
575	0.5±0.3%	0.3±0.1%	0.4±0.1%
600	0.8±0.3%	0.7±0.1%	0.7±0.1%
625	0.6±0.2%	0.5±0.1%	0.7±0.1%
650	1.0±0.4%	0.8±0.3%	1.3±0.3%

In order to see the change in carbon concentration with substrate temperature and exposure more clearly, the data in Table 3.4 are presented in Figure 3.6. There is a

general trend that with increasing temperature and exposure, the carbon concentration increases. The temperature /exposure pair of 650 ^{0}C and 5000 L of CO_2 yielded the highest concentration of carbon. Little change in surface carbon concentrations is observed between 500 L and 1000 L exposures.

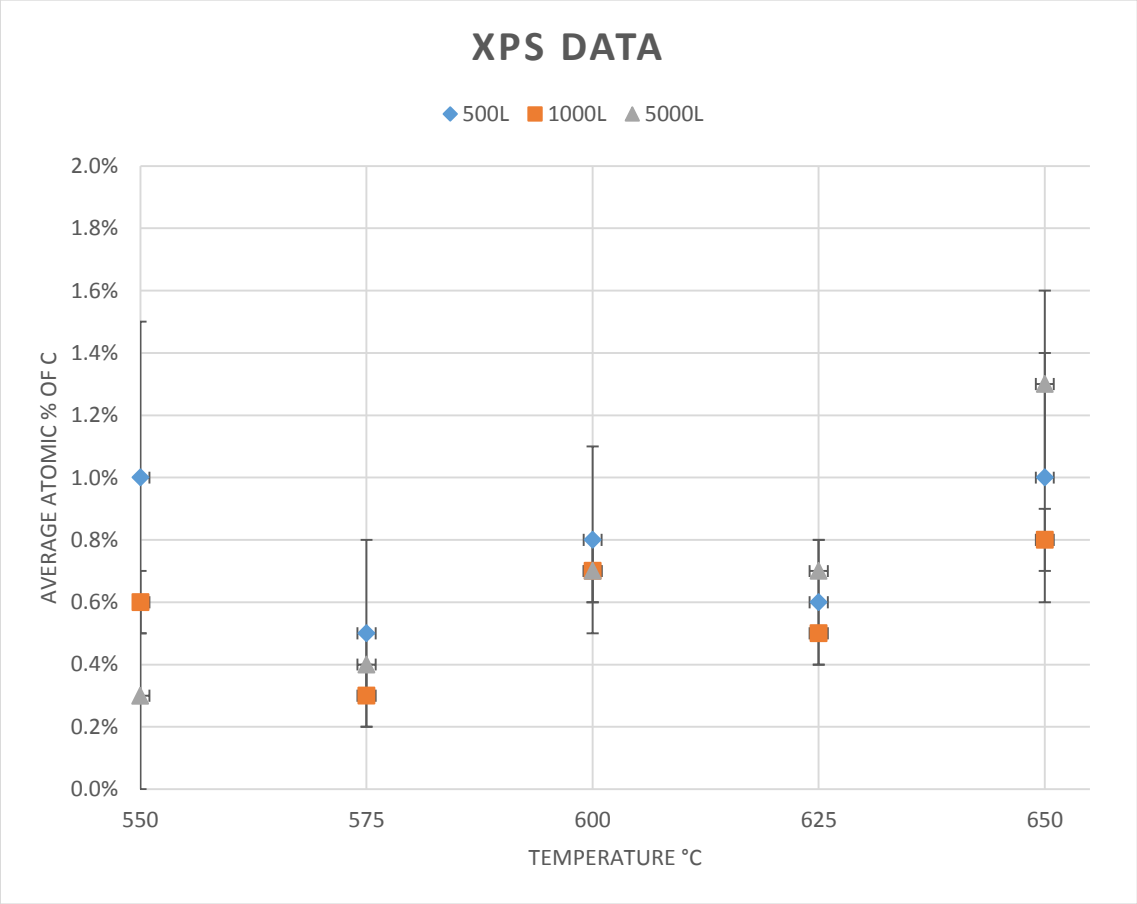

Figure 3. 6. Change in the atomic surface concentrations of carbon on MgO (100).

3.1.3.2 O (1s)

Detailed spectra of the O (1s) region of MgO (100) surfaces are shown in Figure 3.7. At 534 eV binding energy, there is only single peak. The red line is before exposure,

and the green line is after a 5000 L CO_2 exposure at 650 ^{0}C. The two spectra are essentially the same.

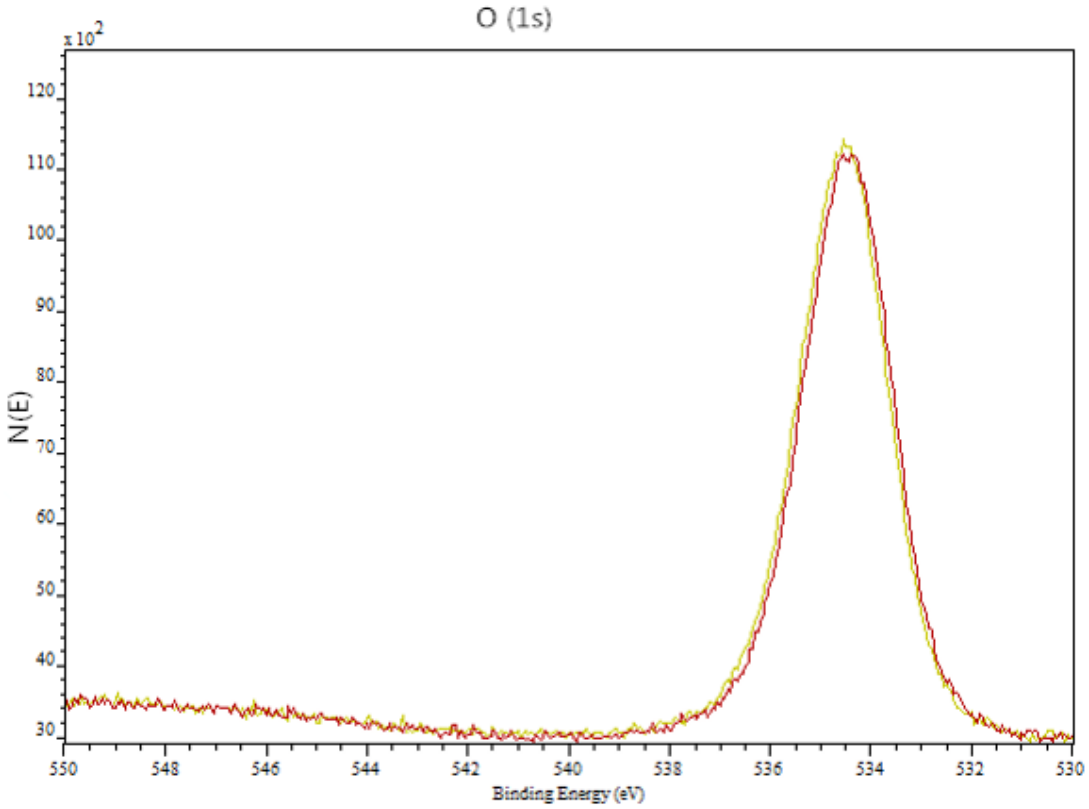

Figure 3. 7. O (1s) XPS spectra of MgO (100) surface before (red) and after a 5000 L (green) exposure of CO_2 at a surface temperature of 650 ^{0}C.

Different exposures of CO_2 at 650 ^{0}C temperature results in little change to the O (1s) peak area. Figure 3. shows the O (1s) region after three different exposures. The red line is the O (1s) spectrum taken after a 500 L CO_2 exposure, the green line is from a 1000 L CO_2 exposure, and the purple line is after a 5000 L CO_2 exposure. The O (1s) spectra for the 500 L and 1000 L exposures almost the same. However, there is an

increase in the O (1s) area after the 5000 L exposure. The quantitative results for these exposures are summarized in Table 3.5. The concentration of oxygen on the surface increased from 45.6% to 49.2% when increasing the exposure to 5000 L.

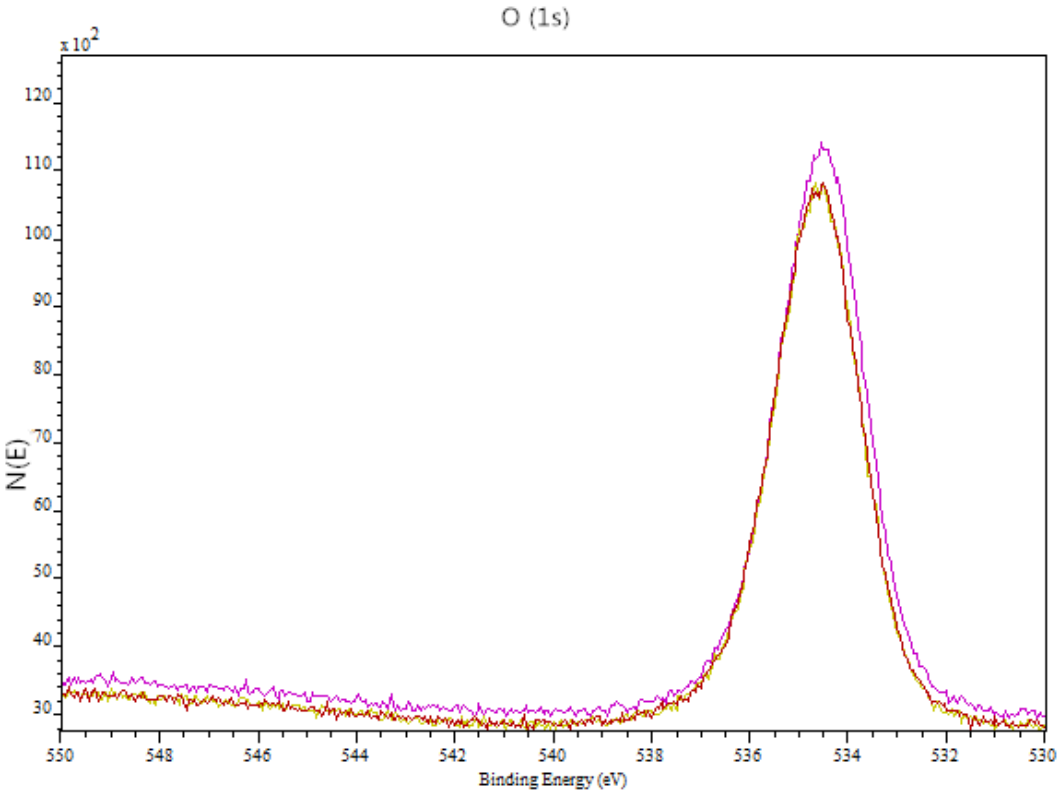

Figure 3. 8. O (1s) region of MgO (100) with different CO_2 exposures at 650 ^{0}C. The exposures are 500 L (red), 1000 L (green) and 5000 L (purple).

Table 3. 5. O (1s) atomic percentage on MgO (100) as a function of CO_2 exposure at a surface temperature of 650 ^{0}C.

System	Temp. (^{0}C)	CO_2 Exposure (L)	Peak position (eV)	Peak area	Atomic percentage
1	650	500	534.5	16313	45.6%
2	650	1000	534.5	16373	45.8%
3	650	5000	534.5	17596	49.2%

The probe depths of XPS and AES are different, even though both are surface-sensitive techniques. AES measures its signal over a greater depth as shown schematically in Figure 3.9. The atomic concentration of oxygen measured by both techniques is listed in Table 3.6.

Figure 3. 9. Schematic of AES and XPS measurement depth.

The oxygen atomic concentration of CO_2-exposed surface is decreased in XPS data compared to that of clean surface which can be seen in Table 3.6. This shows that

after the exposure and higher temperatures, there is some oxygen decomposed from the very near surface region compared to deeper layers.

3.1.3.3 Mg (2p)

Detailed spectra of Mg (2p) regions are shown in Figure 3.11. The red line is Mg (2p) XPS spectrum of the MgO (100) surface before exposure and the green line is after a 5000 L CO_2 exposure at 650 ^{0}C. The spectra in this figure show that a chemical shift of the 2p level occurs at higher B.E (54.3 eV) due to Mg^{2+}, leading to broadening of linewidth[3]. The literature value of Mg (2p) level for metallic Mg is 49.75 eV. The shift to 54.3 eV binding energy is consistent with a 2+ oxidation state for Mg.

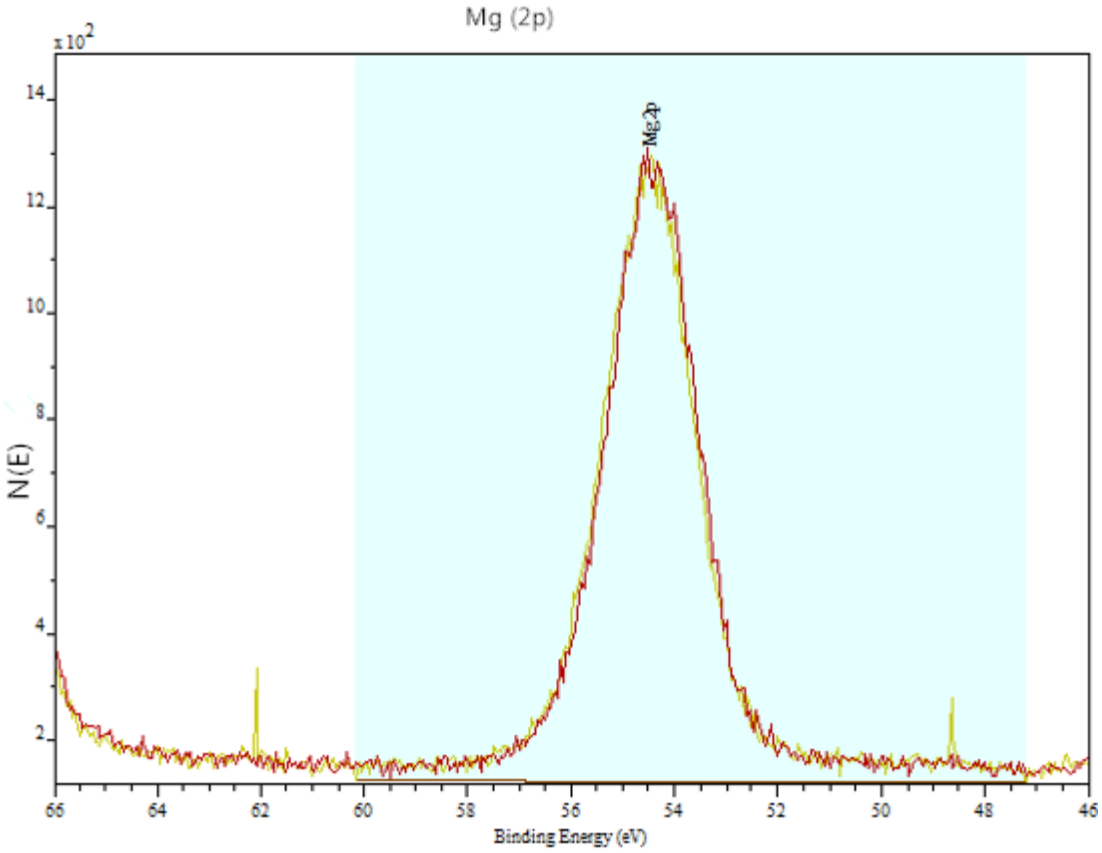

Figure 3. 10. Mg (2p) region before exposure to CO_2 (red) and after a 5000 L CO_2 exposure (green) at a surface temperature of 650 ^{0}C.

The atomic concentrations of C (1s), O (1s) and Mg (2p) of MgO surface before and after each exposure at 550 ^{0}C are listed in Table 3.7. For each temperature and exposure, there is a small increase in carbon. The ratio between oxygen and magnesium is near 1:1 for both measurements in XPS and AES. These results indicate that after exposures, the surface is still stoichiometric.

Table 3. 6. Elemental concentrations on MgO (100) as measured by XPS and AES after exposure to CO_2 at a surface temperature of 550 ^{0}C.

			XPS			AES		
	Temp. (^{0}C)	CO2(L)	C%	O%	Mg%	C%	O%	Mg%
"clean"			5.8	52.5	41.7	0.8	42.9	56.3
1	550	500	7.4	49.7	42.9	0.8	43.5	55.7
2	550	1000	7.0	49.9	43.1	0.0	43.2	56.8
3	550	5000	6.1	50.2	43.8	0.8	43.5	55.7

3.2 Photocatalytic reactions of CO_2 on MgO (100) single crystal surfaces

Due to the wide band gap of magnesium oxide (7.8 eV[4]), UV light (λ~290 nm, 4.3 eV) will not have sufficient energy to photo-excite electrons across the band gap in MgO. However, the UV light might be able to alter the structure of MgO to create a Mg-rich surface which could supply more adsorption sites for CO_2.

3.2.1 Analysis of AES spectra

AES spectra are shown in Figure 3.12. The red spectrum was taken from clean surface, and at 273 eV kinetic energy, there is no carbon present. The green spectrum was taken after a 1000 L CO_2 exposure at room temperature. After the exposure, carbon was observed, and the atomic percentage is 1.7%. The purple spectrum was taken after a 10 minutes UV irradiation, and the green spectrum was obtained after another 10 minutes of UV irradiation. After UV irradiation, the concentration of carbon did not change. All the carbon concentrations are listed in Table 3.8. Supplementary information about the detailed data is shown in Appendix B.

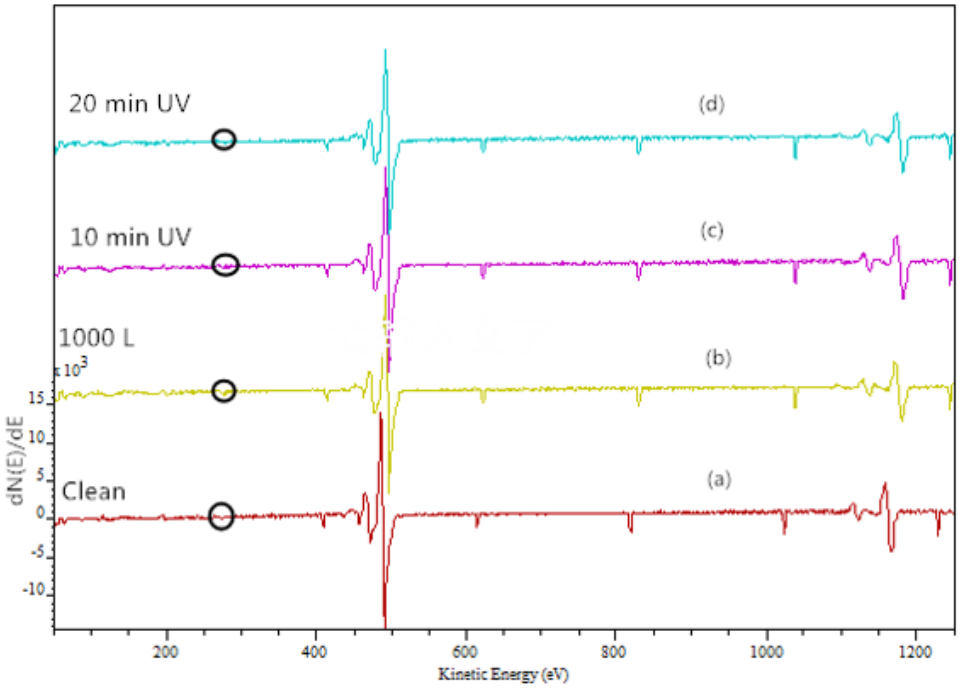

Figure 3. 11. AES spectra of MgO (100). Spectra (a) is of the clean surface, (b) spectrum after a 1000 L CO_2 exposure at room temperature. (c) spectrum after a 10 min UV exposure, and (d) spectrum after 20 min of UV exposure.

Table 3. 7. Atomic percentage of elements from MgO (100) as measured by AES

Experiment	AES		
	C%	O%	Mg%
Clean	0.0	43.2	56.8
1000 L CO_2	1.7	42.8	55.5
10 min UV	1.7	42.5	55.8
20 min UV	1.7	41.9	56.4

3.2.2 Analysis of detailed XPS spectra

3.2.2.1 C (1s)

Detailed spectra of the C (1s) region from MgO (100) are shown in Figure 3.13 a. The red spectrum was taken from the clean surface. There was some carbon on the "clean" surface which was not detected by AES. The green spectrum was taken after a 1000 L CO_2 exposure at room temperature. There is a small increase in the peak intensity. In Figure 3.13 b, the red spectrum is the same one shown in Figure 3.13 a for the 1000 L CO_2 exposure, and the green spectrum is the spectrum obtained after a 10 minutes UV irradiation. The peak shape and intensity did not change at all. The calculated atomic percentages of carbon are listed in Table 3.9.

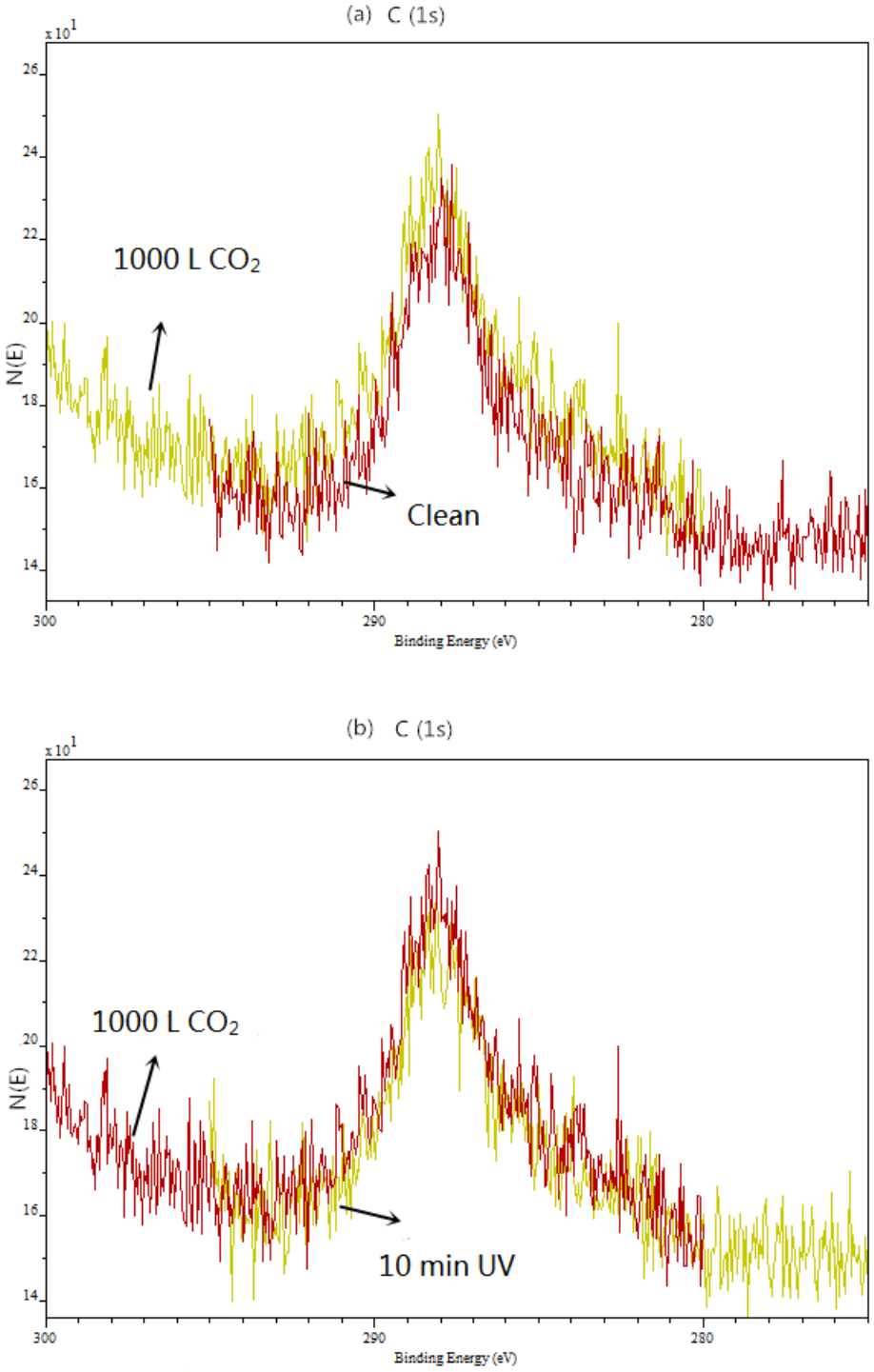

Figure 3. 12. C (1s) spectra of MgO (100) in photocatalytic reactions. (a) Clean surface (red) vs. 1000 L CO_2 exposed surface (green) at room temperature; (b) 1000 L CO_2 exposed surface (red) vs. 10 min UV irradiation (green).

3.2.2.2 Mg (2p) and O (1s)

Detailed spectra of the O (1s) and Mg (2p) regions are shown in Figure 3.14. In each part of the figure, there are three different colored lines. The red line is the spectrum taken from the surface after a 1000 L CO_2 exposure at room temperature, the green line is the spectrum taken after 10 minutes of UV irradiation, and the purple line is the spectrum taken after another 10 minutes of UV irradiation. All of three spectra matched with each other well. There is no big change in surface concentrations between each experiment. The concentrations of O and Mg were presented in Table 3.10.

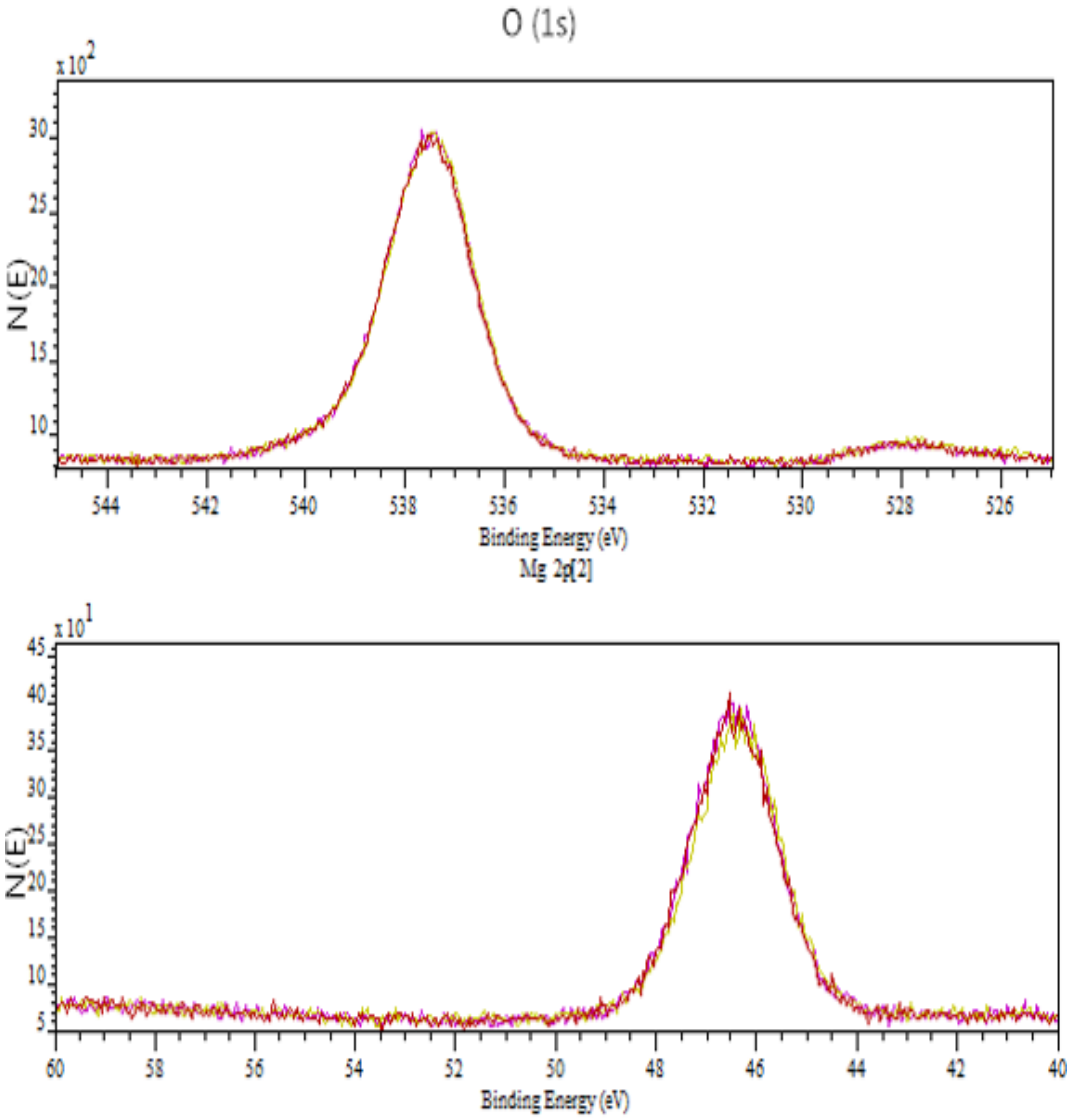

Figure 3. 13. O (1s) and Mg (2p) regions of MgO (100) single crystal surface in photocatalytic reactions. Spectrum taken from the surface after a 1000 L CO_2 exposure at room temperature (red), spectrum taken after 10 minutes UV irradiation (green) and the spectrum taken after another 10 minutes UV irradiation (purple).

Table 3. 8. Atomic percentage of all elements on MgO (100) single crystal surface measured by XPS in photocatalytic reactions.

Experiment	XPS		
	C%	O%	Mg%
Clean	6.7	47.1	46.2
5000 L	7.4	47.5	45.1
10 min UV	7.4	48.2	44.4
20 min UV	7.4	48.8	44.8

3.3 Thermal reactions of CO_2 with TiO_2 at room temperature

3.3.1 Analysis of AES spectra

AES spectra of TiO_2 (110) single crystal surface are shown in Figure 3.15. The surface was exposed to a 5000 L CO_2 with different surface temperatures from (200-700 ºC). The Ti peak is measured at 418 eV kinetic energy and oxygen peak is located at 503 eV. The carbon peak, if present, would be observed at 272 eV. However, no carbon deposition is observed. When all seven spectra are overlaid with one another (shown in Figure 3.15b), it was more obvious that no carbon is deposited. These results demonstrate that there is no thermal reaction of CO_2 with the TiO_2 surface. The XPS data presented in Section 3.3.3 are also consistent with this point.

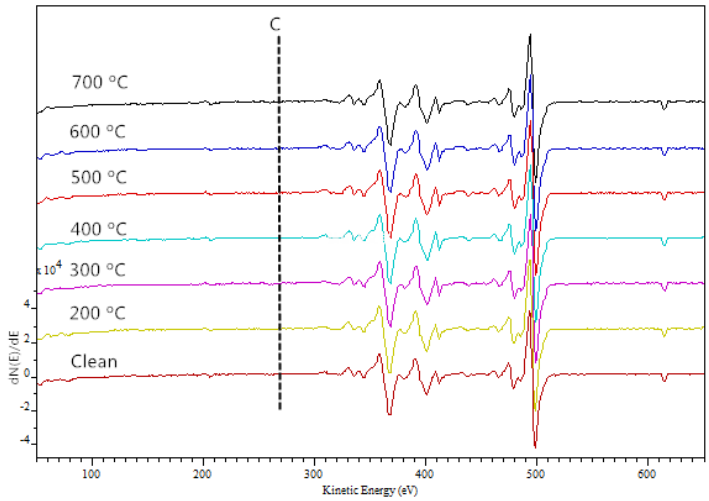

(a)

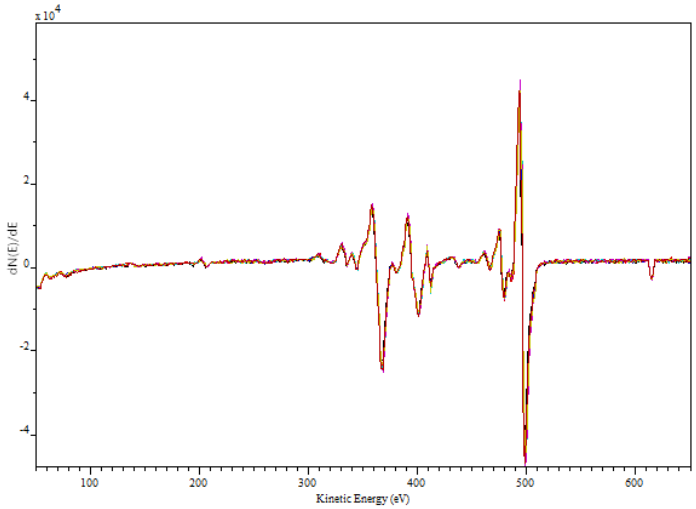

(b)

Figure 3. 14. AES spectra of TiO2 (110). (a) Seven colored AES spectra: clean spectrum (dark red), spectrum taken after given the surface a 5000 L CO_2 exposure at a constant surface temperature of 200 °C (yellow), 300 °C (purple), 400 °C (blue), 500 °C (red), 600 °C (dark blue) and 700 °C (black). (b) Overlap of all seven colored spectra.

The TiO_2 (110) single crystal surface was exposed to various exposure of CO_2 (500-5000) and different surface temperatures. The carbon concentration measured by AES for these reactions are summarized in Table 3.10. If any carbon was present on the surface before the exposure (<1%), then its concentration was subtracted from the amount present after an exposure. These results are shown in Table and the percentages are averages of at least triplicate measurements on the same TiO_2 (110) single crystal surface. The surface concentrations of carbon are essentially unchanged with exposure indicating that there is thermal reaction of CO_2 with TiO_2 (110).

Table 3. 9. C atomic concentrations on TiO_2 (110) measured by AES for different CO_2 exposures and surface temperatures.

Temp./Exposures	Atomic %		
	500 L	1000 L	5000 L
200 °C	0.8 ± 0.9	0.2 ± 0.4	1.5 ± 1.6
250 °C	n. d.*	0.1 ± 0.1	-0.3 ± 0.5
300 °C	0.7 ± 1.3	-0.5 ± 0.8	n. d.
350 °C	0.7 ± 1.2	0.2 ± 0.4	0.5 ± 0.9
400 °C	0.6 ± 1.0	-0.4 ± 0.5	0.2 ± 0.4
450 °C	0.7 ± 1.3	0.5 ± 0.7	-0.7 ± 1.8
500 °C	0.2 ± 0.4	-0.3 ± 1.2	0.2 ± 0.4
550 °C	1.6 ± 1.6	0.6 ± 0.6	1.6 ± 1.6
600 °C	n. d.	0.7 ± 1.3	0.5 ± 0.8
650 °C	0.4 ± 0.8	-0.2 ± 1.0	0.4 ± 0.7
700 °C	n. d.	-0.4 ± 0.8	0.2 ± 0.4

*n. d.: not detected.

3.3.2 Analysis of wide XPS spectrum

An XPS wide spectrum of TiO_2 surface is shown in Figure 3.16. The sharp O (1s) peak is observed at 503 eV binding energy (B.E.), the Ti ($2p_{1/2}$) and ($2p_{3/2}$) are seen at 464.2 eV and 458.5 eV B.E., respectively. At 284 eV B.E, there is a very weak peak due to carbon contamination. The carbon could be eliminated by cycles of sputtering and annealing. Also, O the KVV Auger electron transition is observed. Only titanium, oxygen, argon and carbon are observed in this wide spectrum.

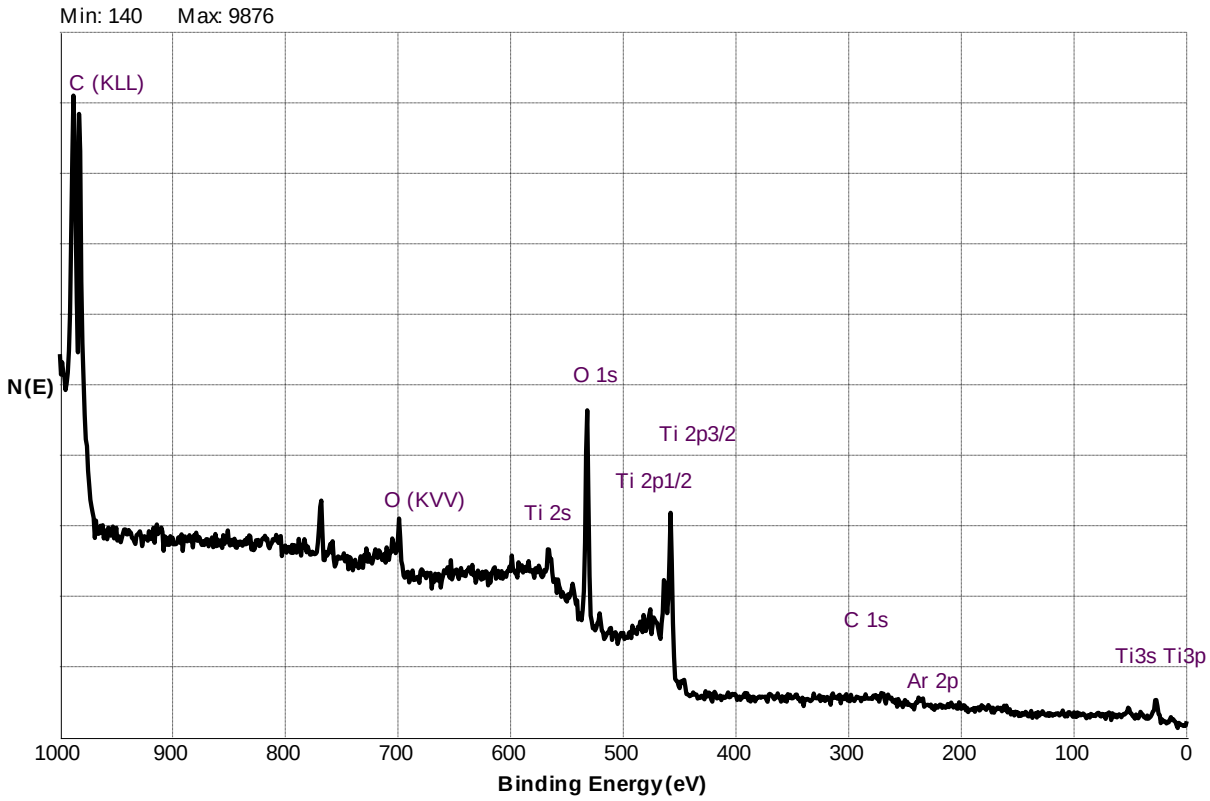

Figure 3. 15. A wide spectrum of TiO_2 (110) surface.

3.3.3 Analysis of detailed XPS spectra

3.3.3.1 C (1s)

C (1s) XPS spectra are shown in Figure 3.17. The red line is clean surface spectrum. The TiO_2 (110) single crystal surface was exposed to different amounts of CO_2 (green - 500 L and purple - 5000 L) at a surface temperature of 200 ^{0}C. This result shows that after the CO_2 exposures, there is no carbon adsorbed on the surface under these conditions.

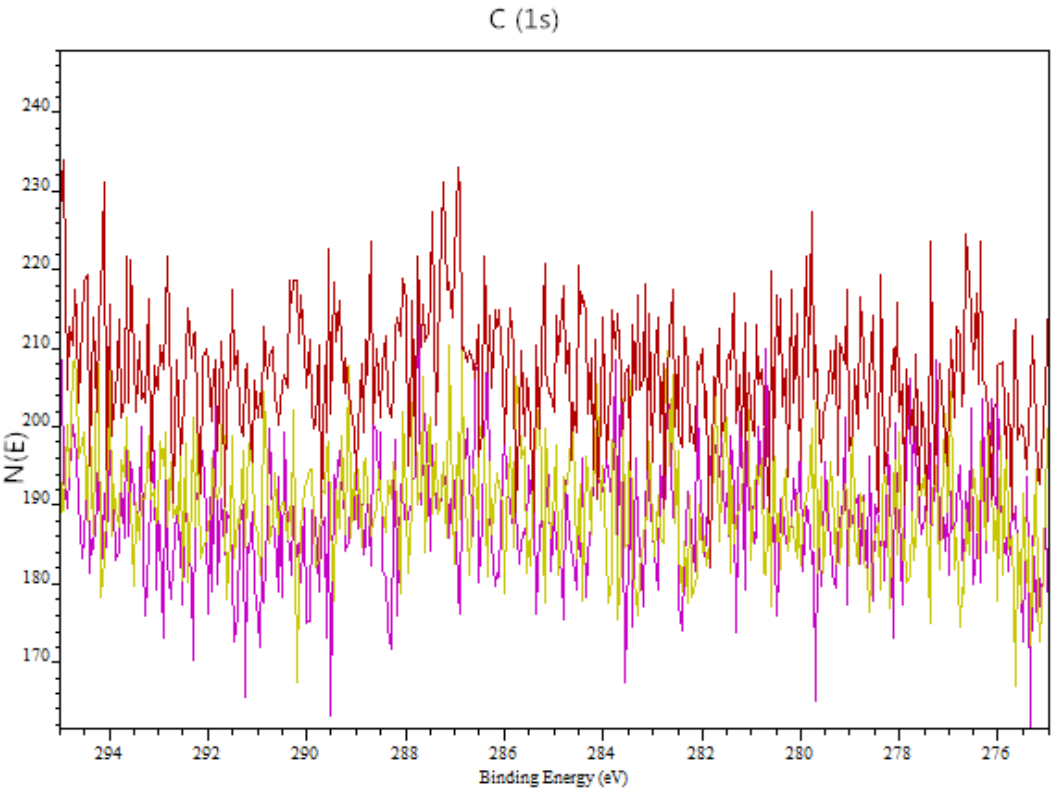

Figure 3. 16. C (1s) spectra of TiO_2 (110) single crystal surface in thermal reaction. Clean surface spectrum (red), spectrum was taken after a 500 L CO_2 (green) and 5000 L CO_2 (purple) exposure at a constant surface temperature of 200 ^{0}C.

Quantitative determination of carbon concentrations from all the CO_2 exposure and surface temperature experiments are listed in Table 3.11. If any carbon was present on the surface before the exposure (<1%), then its concentration is subtracted from the amount present after a given exposure. The results show that after each pair of exposure and temperature, there is no carbon left on the surface which is consistent with the data results from AES.

Table 3. 10. C (1s) atomic concentrations on TiO_2 (110) measured by XPS as a function of CO_2 exposure and surface temperature.

Temp./Exposures	Atomic % of carbon		
	500 L	1000 L	5000 L
200 °C	-0.1 ± 0.2	-0.1 ± 1.1	0.9 ± 0.8
250 °C	n.d.*	-0.2 ± 0.6	-0.7 ± 0.6
300 °C	0.1 ± 0.1	n.d	0.6 ±1.7
350 °C	0.1 ± 0.3	-0.7 ± 1.2	n.d.
400 °C	0.1 ± 0.3	1.1 ± 3.0	-0.1 ± 0.7
450 °C	n.d.	-0.1 ± 1.1	0.4 ± 1.5
500 °C	-0.2 ± 0.4	1.3 ± 0.9	0.2 ± 0.8
550 °C	0.1 ± 0.1	0.6 ± 1.6	1.2 ± 1.2
600 °C	-0.3 ± 0.4	-0.3 ± 1.2	1.0 ± 2.1
650 °C	-0.1 ± 0.3	1.1 ± 2.8	-0.3 ± 0.5
700 °C	0.1 ± 0.3	-0.6 ± 1.1	n.d.

*n.d.: not detected.

3.3.3.2 O (1s)

O (1s) XPS spectra are shown in Figure 3.18. At 531 eV binding energy, there is a single peak due to oxygen. In Figure 3.18, the red line is O (1s) spectrum of the clean surface. The green line is the spectrum obtained after a 5000 L CO_2 exposure at a surface

temperature of 200 ^{0}C. No change is observed in the O (1s) region with the CO_2 exposure.

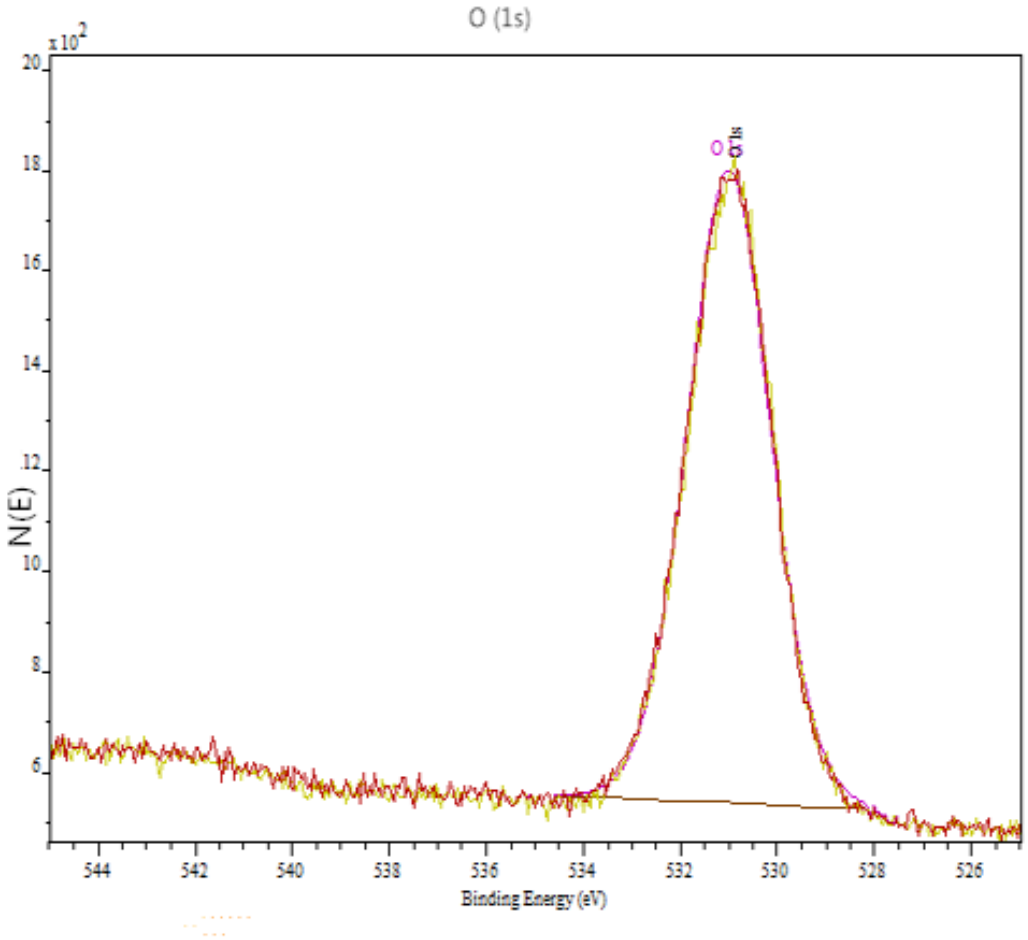

Figure 3. 17. O (1s) spectra of TiO_2 (110) single crystal surface in thermal reactions. Spectrum of clean surface (red), and spectrum taken after a 5000 L CO_2 exposure at a surface temperature of 200 ^{0}C.

3.3.3.3 Ti (2p)

Ti (2p) spectra are shown in Figure 3.19. The Ti $2p_{3/2}$ peak is measured at 463 eV B.E. and 5.7 eV higher B.E. is the Ti $2p_{1/2}$ peak. The clean surface Ti (2p) XPS is the red line in Figure 3.19 and the green line is the spectrum obtained after a 5000 L CO_2 exposure at a surface temperature of 200 ^{0}C. No evidence of a reaction with CO_2 is observed.

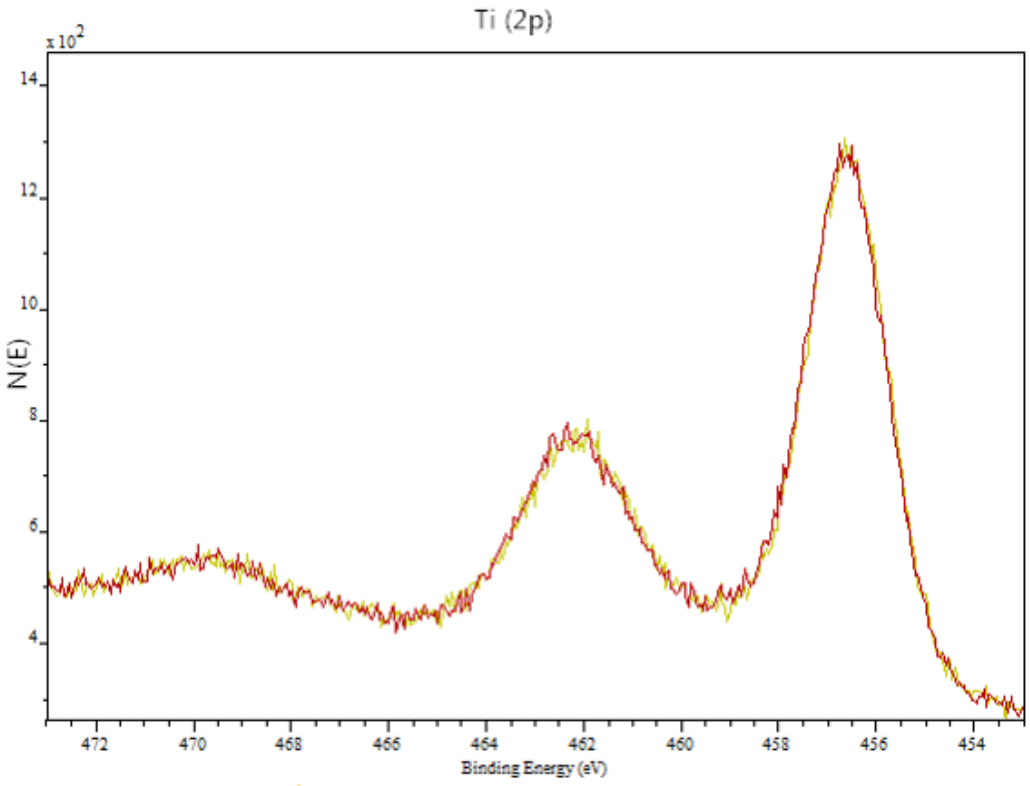

Figure 3. 18. Ti (2p) spectra of TiO_2 (110) single crystal surface in thermal reactions. Before exposure (red line), 5000 L CO_2 exposure at a surface temperature of 200 ^{0}C (green line.)

3.4 Photocatalytic reactions of CO_2 with TiO_2 at room temperature

The thermal reactions of CO_2 with the TiO_2 (110) single crystal surface within a temperature range of 200-700 ^{0}C shows no carbon adsorption in Section 3.3. TiO_2 has a narrow band gap (3.0-3.3 eV), and therefore the Hg UV light (wavelength is lower than 290 nm) can be used in the photocatalytic reaction to illustrate the mechanism of possible CO_2 reaction with the TiO_2 (110) single crystal surface.

3.4.1 Analysis of AES spectra

AES spectra of TiO_2 (110) surface are shown in Figure 3.20. There are five different colored lines. The bottom dark red line is the AES spectrum of the clean surface. The yellow line is the AES spectrum taken after a 500 L CO_2 exposure. There is an increase in the carbon concentration. The purple line is the AES spectrum taken after illuminating the surface with UV light during the 500 L CO_2 exposure. The carbon concentration decreased by 0.8%. The blue line is the AES spectrum taken after the surface exposed to 500 L CO_2, followed by 10 minutes of UV irradiation. The top red line is the AES spectrum taken after a 500 L CO_2 exposure, followed by 20 minutes of UV irradiation. The average carbon concentration measured by AES after each exposure and UV irradiation are listed in Table 3.12. The concentration are the average of at least three replicate trials. If any carbon was present on the surface before the exposure (<1%), then its concentration is subtracted from the amount present after exposure. The results indicate that at room temperature, some CO_2 will adsorb on the TiO_2 surface and the average atomic percentage is 1.9 ± 1.2%. However, when the CO_2-exposed surface was illuminated with UV light, there is a decrease in carbon concentration.

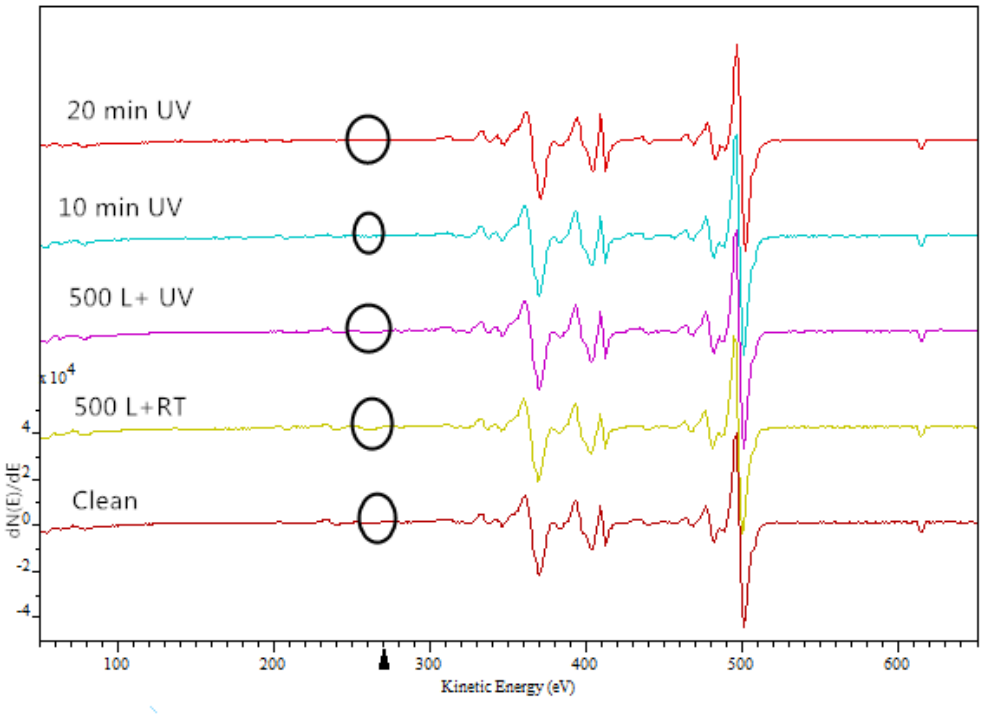

Figure 3. 19. AES spectra of TiO_2 (110) single crystal surface in photocatalytic reactions.Clean surface (dark red), surface exposed to a 500 L CO_2 exposure (yellow), surface exposed to a 500 L CO_2 and UV irradiation (purple), 500 L CO_2-exposed surface with 10 min UV irradiation (blue), and 500 L CO_2 exposed-surface with 20 min UV irradiation (red).

Table 3. 11. Average of C concentrations on TiO_2 (110) measured by AES with CO_2 exposure and UV irradiation at room temperature.

Experiments	Atomic % of carbon		
	500 L	1000 L	5000 L
R. T	1.9 ± 1.2	2.2 ± 1.0	1.4 ± 0.4
UV irradiation	n.d.	n. d.*	n.d.
10 min UV irradiation	1.3 ± 2.3	-0.6 ± 1.0	-0.3 ± 0.5
20 min UV irradiation	0.3 ± 1.2	n. d.	-0.6 ± 1.0

*n. d.: not detected.

3.4.2 Analysis of detailed XPS spectra

3.4.2.1 C (1s)

Detailed XPS spectra of C (1s) region of TiO_2 are shown in Figure 3.21. In Figure 3.21 a, the red spectrum was taken from the clean surface and the green spectrum was taken after the surface was exposed to 500 L CO_2 at room temperature. It is an increase in the C (1s) intensity compared to clean surface. In Figure 3.21 b, the red spectrum was taken from the 500 L CO_2 exposed surface, and the green spectrum was taken after 20 minutes UV irradiation on the surface. There is a small decrease in the carbon intensity after the UV irradiation. The average carbon concentration change of each trial are summarized in Table 3.13. The reported values are averages of at least three replicate measurements. These data were converted to Figure 3.22 to visualize these comparisons more clearly. First, when TiO_2 is exposed to CO_2 at room temperature, there is some

carbon present on the surface (0.8 ± 0.2% for 500 L, 0.4 ± 0.3% for 1000 L and 0.3 ± 0.2% for 5000 L CO_2 exposure). After UV irradiation of the CO_2-exposed surface, the concentration of carbon decreased. These results indicate that after UV irradiation, carbon is removed as a gaseous product into the vacuum chamber.

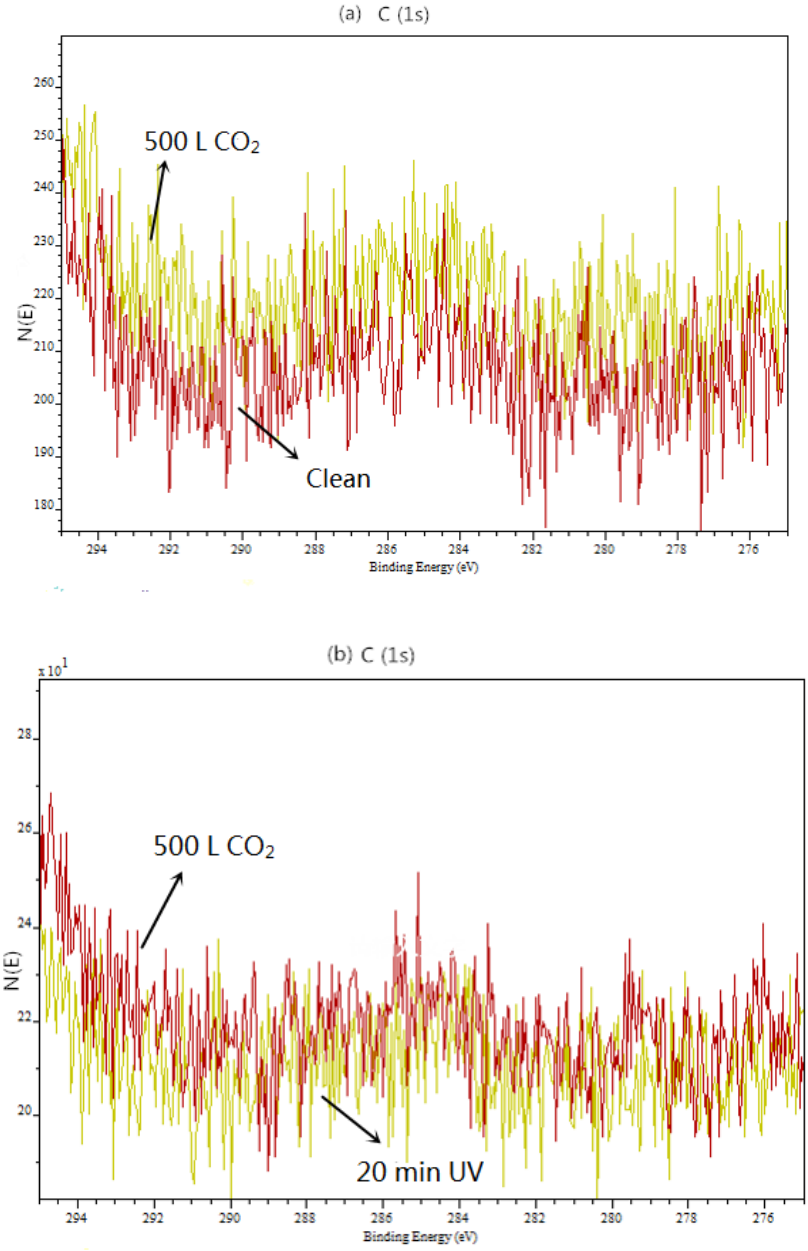

Figure 3. 20. C (1s) spectra of TiO_2 in photocatalytic reaction. (a) Red line is clean surface, green line is surface exposed to 500 L CO_2; (b) Red line is surface exposed to 500 L CO_2, and green line is after a 500 L CO_2 exposure followed by 20 min UV irradiation.

Table 3. 12. Averages of C concentrations on TiO_2 measured by XPS.

Experiments	Atomic % of carbon		
	500 L	1000 L	5000 L
R. T	0.8 ± 0.2	0.4 ± 0.3	0.3 ± 0.2
UV irradiation	-0.2 ± 0.4	-0.3 ± 0.3	-0.1 ± 0.1
10 min UV irradiation	-0.4 ± 0.3	-0.1 ± 0.2	-1.3 ± 0.6
20 min UV irradiation	-0.3 ± 0.2	n.d.*	-0.3 ± 0.2

*n.d.: not detected

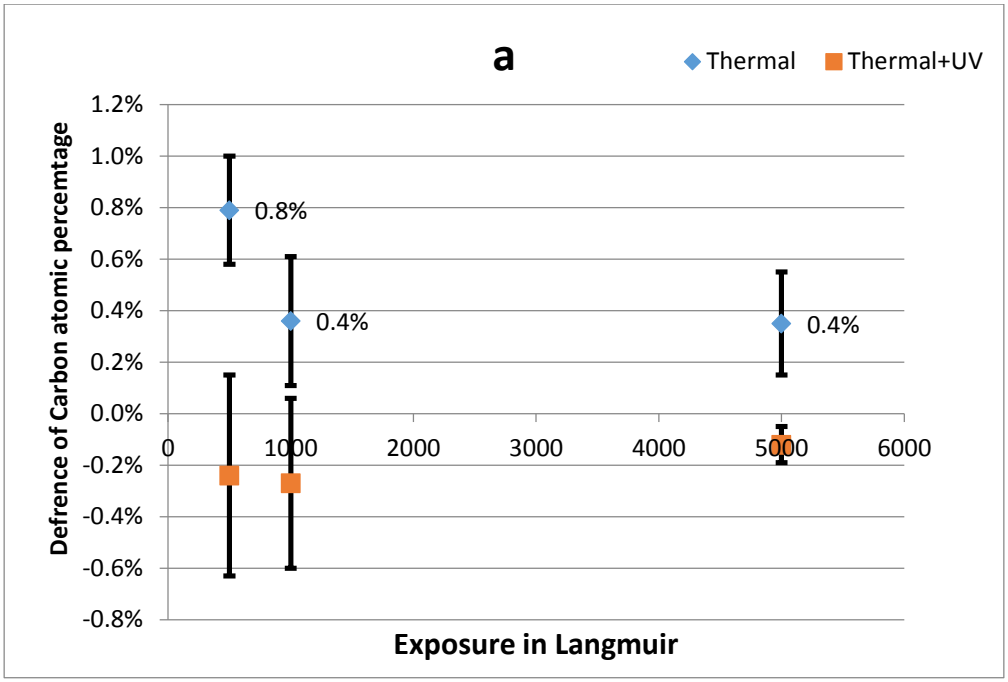
a
Thermal
Thermal+UV
1.2%
1.0%
0.8%
0.6%
0.4%
0.2%
0.0%
-0.2%
-0.4%
-0.6%
-0.8%
0.8%
0.4%
0.4%
0
1000
2000
3000
4000
5000
6000
Defrence of Carbon atomic percemtage
Exposure in Langmuir

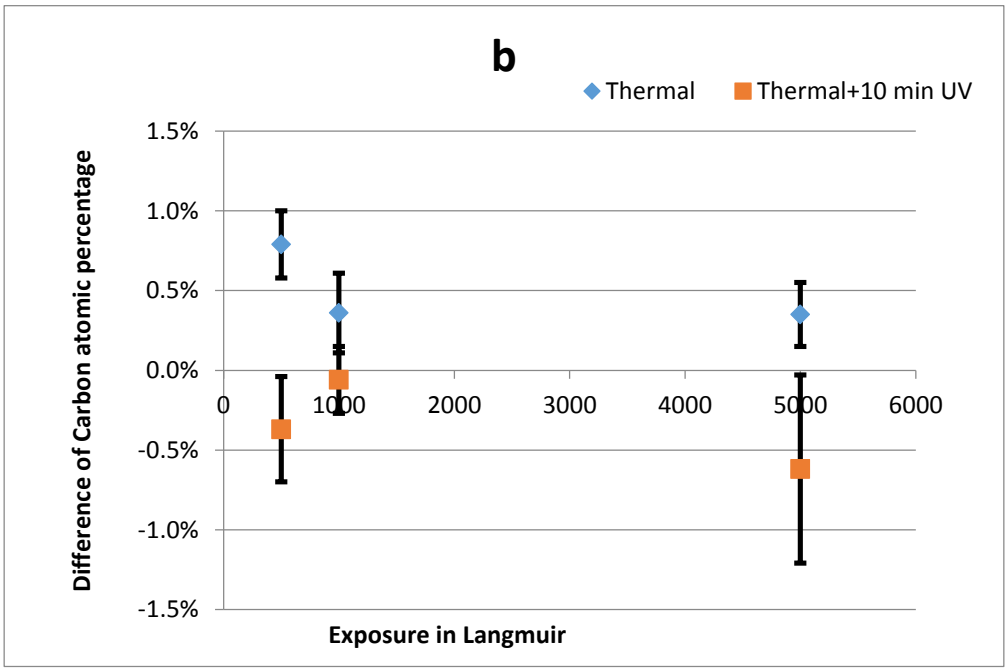
b
Thermal
Thermal+10 min UV
1.5%
1.0%
0.5%
0.0%
-0.5%
-1.0%
-1.5%
0
1000
2000
3000
4000
5000
6000
Difference of Carbon atomic percentage
Exposure in Langmuir

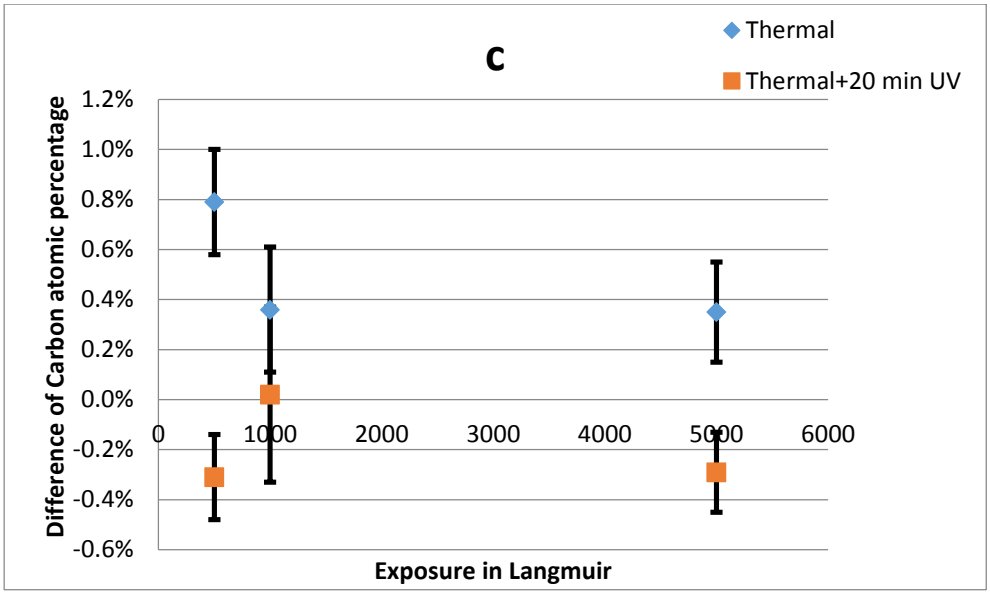

Figure 3. 21. Carbon concentrations on TiO_2. a) Thermal reactions (surface exposed to 500-5000 L CO_2 at room temperature) vs. Photocatalytic reactions (500-5000 L CO_2-exposed surface with UV irradiation); b) Thermal reactions (surface exposed to 500-5000 L CO_2 at room temperature) vs. 500-5000 L CO_2-exposed surface and followed by 10 min UV irradiation; c) Thermal reactions (500-5000 L CO_2-exposed surface) vs. 500-5000 L CO_2-exposed surface and followed by 20 min UV irradiation.

3.4.2.2 O (1s)

O (1s) XPS spectra are shown in Figure 3.23. The red spectrum was taken after a 500 L CO_2 exposure at room temperature and the green spectrum was taken 10 min UV irradiation to the CO_2-exposed surface. There is an increase in the O intensity after UV irradiation. All of the O (1s) atomic concentrations from the different CO_2 exposures and irradiation times are summarized in Appendix D. Under the conditions the oxygen concentration increased when the CO_2-exposed surfaces are illumnation with UV light.

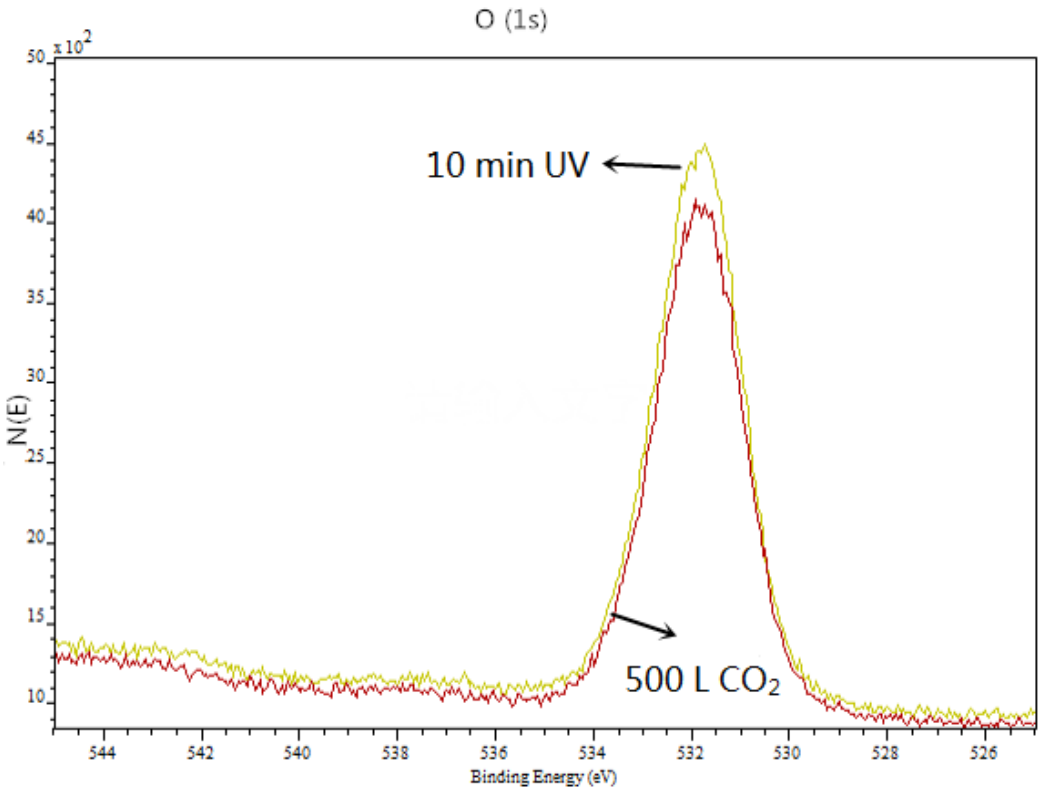

Figure 3. 22. O (1s) XPS spectra of TiO_2 (110) single crystal surface after a 500 L CO_2 (red) at room temperature followed by a 10 min UV irradiation (green).

3.4.2.3 Ti (2p)

Detailed XPS spectra of the Ti (2p) region are shown Figure 3.24. The red spectrum was taken after a 500 L CO_2 exposure at room temperature. The green spectrum was taken after a 500 L CO_2 exposure along with UV irradiation. After the irradiation, the intensity of titanium decreased. The concentrations of oxygen and titanium are listed in Table 3.14.

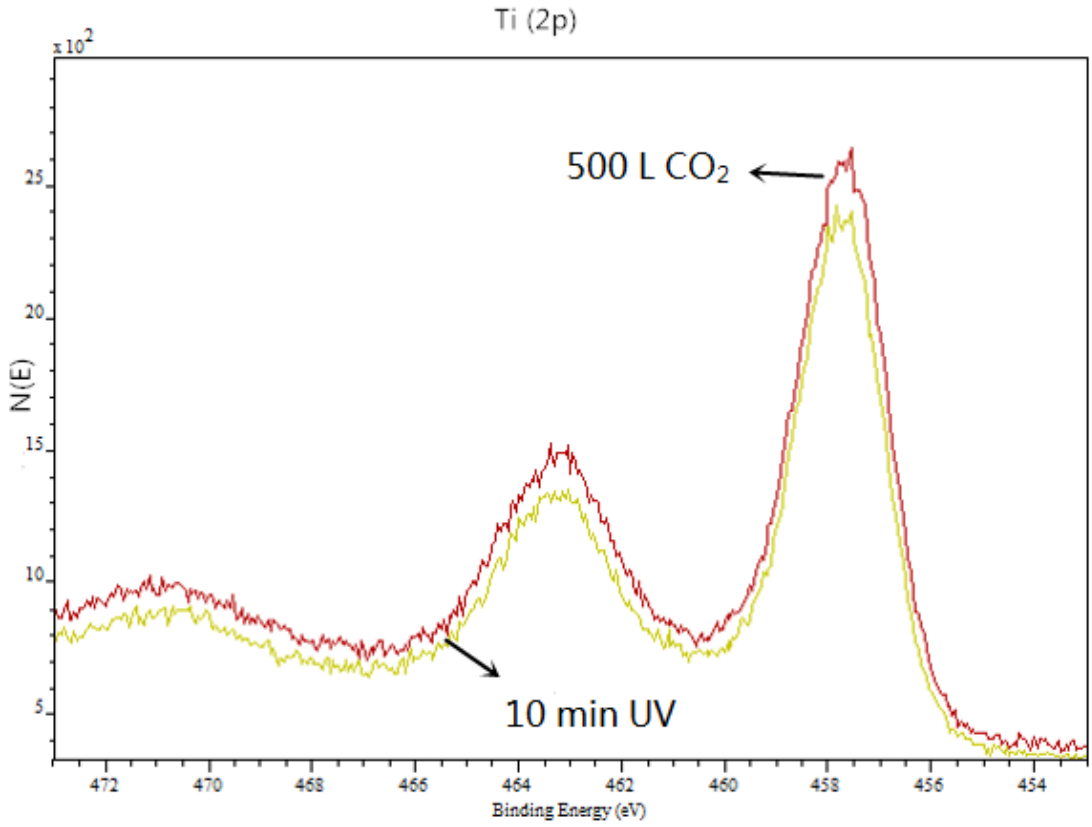

Figure 3. 23. Ti (2p) spectra of TiO_2 (110) single crystal surface in photocatalytic reactions. The red line is surface after a 500 L CO_2 exposure. The green line XPS spectrum after a 500 L CO_2 exposure during UV irradiation.

Table 3. 13. Atomic percentage changes of oxygen and titanium in photocatalytic reactions of CO_2 with TiO_2 (110).

Experiment	Atomic % of O and Ti	
	O	Ti
500 L	-1.7 ± 0.8	0.9 ± 0.6
500 L+UV	1.1 ± 0.3	-0.4 ± 0.4
500L+10 miin UV	0.8 ± 1.1	-0.6 ± 1.1
500 L+20 min UV	-0.1 ± 1.2	0.4 ± 1.0
1000 L	-2.4 ± 0.3	2.1 ± 0.5
1000 L+UV	n.d.*	0.4 ± 1.0
1000L+10 min UV	-0.9 ± 1.4	0.7 ± 1.8
1000 L+20 min UV	-0.7 ± 1.8	0.7 ± 1.9
5000 L	-1.4 ± 1.0	1.1 ± 0.7
5000 L+UV	-0.5 ± 1.1	0.8 ± 2.0
5000L+10 miin UV	0.5 ± 1.1	-0.4 ± 1.1
5000 L+20 min UV	0.1 ± 1.2	-0.5 ± 1.3

*n.d.: not detected.

3.5 References

1. Ochs, D.; Maus-Friedrichs, W.; Brause, M.; Günster, J.; Kempter, V.; Puchin, V.; Shluger, A.; Kantorovich, L., Study of the surface electronic structure of MgO bulk crystals and thin films. Surface Science **1996,** 365 (2), 557-571.
2. Onishi, H.; Egawa, C.; Aruga, T.; Iwasawa, Y., Adsorption of Na atoms and oxygen-containing molecules on MgO (100) and (111) surfaces. Surface Science **1987,** 191 (3), 479-491.
3. (a) Müller, M.; Matthes, F.; Schneider, C. M., Photoemission study of the Fe(001)/MgO interface for varying oxidation conditions of magnesium oxide. Journal of Applied Physics **2007,** 101 (9), 09G519; (b) Corneille, J. S.; He, J.-W.; Goodman, D. W., XPS characterization of ultra-thin MgO films on a Mo(100) surface. Surface Science **1994,** 306 (3), 269-278.
4. Taurian, O. E.; Springborg, M.; Christensen, N. E., Self-consistent electronic structures of MgO and SrO. Solid State Communications **1985,** 55 (4), 351-355.

Chapter 4 Discussion

4.1 Thermal reactions of CO_2 on MgO (100) single crystal surfaces

The wide XPS spectrum of the clean MgO surface (Figure 3.3) can give us a general picture of the surface. It is very clear to see the O (KLL) Auger electron transition, Mg (KLL) Auger electron transition, O (1s), Mg (2s) and Mg (2p) peaks. There is a small peak of C (1s) around 283 eV binding energy which is due to the carbon contamination. There are no other impurities.

When the clean MgO (100) surface was exposed to CO_2 (500-5000 Langmiur) at different surface temperatures (550-650 °C), Auger electron and X-ray photoelectron spectroscopy results indicated the presence of carbon adsorbed on the surface. In Table 3.1 and Table 3.4, it is obvious that after each exposures with a certain surface temperature, the atomic concentration of carbon on the surface increased in both AES and XPS compared to the clean surface. However, a general relationship between the CO_2 exposure and surface temperature was not observed. Most previous studies examined CO_2 adsorption at room temperature or lower and used relatively low CO_2 exposures compared to the studies described here. Our results show that with higher surfaces temperatures and "larger" CO_2 exposures, there is CO_2 decomposition on the MgO surface. However, the exact structure of carbon formed on the surface is still unclear.

The probe depths of XPS and AES are different. The AES signal can go over a greater depth (1-25 atomic layers) than XPS (1-9 atomic layers). The oxygen atomic concentration, with different (500-5000 L) CO_2 exposure at a surface temperature of 550 °C, increased from 49.7 % to 50.2 % (Table 3.6, XPS data). However, the AES data

showed that the atomic concentration of oxygen stayed around 43.5%. This means that "larger" exposure of CO_2 can increase the atomic concentration of the very near surface region compared to deeper layers after CO_2 exposure. However, when compared with clean surface, the oxygen atomic concentration is decreased. This result indicated that there is some oxygen depletion from the surface in some gaseous formation such as O_2 which was proposed in Sabatier[1] reaction shown in equation 4.1[2]. Even though, the elemental concentrations (C : O : Mg) on MgO (100) as measured by XPS (7.4 % : 49.7 % : 42.9 %) and AES (0.8 % : 43.5 % : 55.7 %) after exposure to 500 L CO_2 at a surface temperature of 550 ^{0}C show that the ratio between Mg and O is around 1:1, therefore, the surface is still stoichiometric after CO_2 exposure.

A possible mechanism for the reaction of CO_2 with MgO (100) is shown in equation 4.1. When the clean surface of MgO (100) exposed to CO_2, some carbonate can form on the surface as a carbonate-intermediate. It is very unstable and decomposed to other products, such as C and O_2 as proposed by Sabatier[1]. This predicts the carbon adsorption on the surface with an increase of atomic concentration. And it also accounts for the oxygen atomic concentration decrease because of its decomposition from the surface.

$$\mathrm{MgO} + \mathrm{CO_2} \leftrightarrows \mathrm{MgCO_3} \qquad (4.1)$$

$$\mathrm{MgCO_3} \rightarrow \mathrm{MgO} + \mathrm{C} + \mathrm{O_2}$$

At the same time, the efficiency of carbon dioxide decomposition can be estimated. From the kinetic theory of gasses, the collisional rate of CO_2 molecules (z) is given by equation 4.2.

$$z = \frac{P}{\sqrt{2\pi mkT}}\ cm^{-2} \cdot s^{-1} \qquad 4.2$$

P is the ambient pressure in $N \cdot cm^{-2}$;

M is the molecular weight of gas in kg/molecule;

k is Boltzman constant in $J \cdot K^{-1}$; and

T is the gas absolute temperature in Kelvin.

Assuming the sticking probability is 1, we can estimate z for CO_2. Using a 5000 Langmiur (5×10^{-6} torr · 1000 sec) exposure with a surface temperature 650 °C, the amount of carbon measured by AES was 2.5% (Table 3.1).

The gas source is at room temperature (298 K), so

$z = 5\times10^{-6}\times 0.0133322/\sqrt{2 \times \pi \times (44) \times 1.66 \times 10^{-27} \times 1.38 \times 10^{-23} \times 298}$

$= 1.53 \times10^{15}\ cm^{-2} \cdot s^{-1}$.

In 1000 seconds duration, the total number of CO_2 molecule is 1.53×10^{18}. However, the AES results show that the carbon atomic concentration increased by about 2.5 % on the surface. The dimension of MgO crystal surface is 1 cm×1 cm, and the lattice constant is 4.212 Å. Therefore, the total atoms number on the MgO (100) surface can be calculated at about 1.70×10^{14}. The number of carbon atoms at the surface is 1.70×10^{14} ×2.5 % = 4.25×10^{12}. Therefore, the efficiency of the reaction is 2.8×10^{-4} % /cm^{-2}.

4.2 Photocatalytic reactions of CO_2 on MgO (100) single crystal surfaces

MgO has a wide band gap of 7.7 eV[3]. So the UV light (ΔE = 4.3 eV, λ = 290 nm) can not excite the electrons across the band gap in MgO. When the clean MgO (100) surface is exposed to different CO_2 exposures (500-5000 Langmuir) at room temperature, there is some carbon adsorbed on the surface as observed with both AES spectra (Figure 3.11) and XPS spectra (Figure 3.12). When the CO_2-exposed surface was illuminated with UV light for 10-20 min, neither AES nor XPS showed a change in the atomic concentration of C, Mg or O. Therefore, there is no change in atomic concentrations of elements on the surface. On the contrary, TiO_2 has a narrow band gap (3.0-3.3 eV[4]). So the UV light can lead to the atomic concentration change on the surface and the details will be addressed in Section 4.4. However, after UV irradiation on the MgO surface, the atomic percentage of all elements on MgO (100) single crystal remains unchanged and the Mg:O atomic ratio is still 1:1 or stoichiometric.

4.3 Thermal reactions of CO_2 with TiO_2

The wide XPS spectrum of TiO_2 (110) surface also can show all the elements on the surface. The O (KVV) Auger electron transition, O (1s), Ti ($2p_{3/2}$), Ti ($2p_{1/3}$), and C (1s), which is due to the contamination, and Ar (2p) which is due to the Ar sputtering are all observed on the surface.

When the clean TiO_2 (110) surface was exposed to different CO_2 exposures (500-5000 Langmuir) with different surface temperatures (200-700 ºC), neither AES nor XPS results show carbon deposition on the surface. These results demonstrate that there is no thermal reaction between CO_2 and TiO_2 surface over this surface temperature range and CO_2 exposure.

4.4 Photocatalytic reactions of CO_2 with TiO_2 at room temperature

Compared to the wide band gap of MgO, TiO_2 has a narrow band gap (3.0-3.3 eV[4]), and therefore the Hg UV light (ΔE = 4.3 eV, λ = 290 nm) can be used in the photocatalytic reaction to illustrate the mechanism of possible CO_2 reaction with the TiO_2 (110) single crystal surface.

When the clean surface exposed to different CO_2 exposures (500-5000 Langmiur) at room temperature, there is some carbon adsorption observed on AES. In Table 3.11, the average atomic percentage of carbon is 1.9 ± 1.2% for 500 L, 2.2 ± 1.0% for 1000 L and 1.4 ± 0.4 for 5000L CO_2 exposure.

Once the surface is explosed to 10-min UV light, the atomic concentration of carbon decreased (Table 3.11).

In the XPS results, when TiO_2 is exposed to CO_2 at room temperature, there is some carbon present on the surface and the average carbon concentration is shown in Table 3.12.

After UV irradiation on the CO_2-exposed surface, the concentration of carbon decreased in Table 3.12 which is consistent with the results of AES. These results indicated that after UV irradiation, some carbon is removed from the surface. At the same time, when we compared the UV-irradiated surface with the CO_2-exposed surface, the oxygen concentration increased in both AES and XPS spectra results. The titanium atomic concentration decreased which can be seen in Figure 3.23 and Table 3.13. A possible mechanism that can explain these results is shown 4.3[5]

$$TiO_2 + hv \rightarrow h^+ + e^- \quad (4.3)$$

$$O_V + h^+ \rightarrow O_V^+$$

$$CO_2 + e^- \rightarrow CO_2^{\cdot-}$$

$$CO_2^{\cdot-} \rightarrow CO + O^{\cdot-}$$

$$O^{\cdot-} + O_V^+ \rightarrow O_{surf.}$$

In the first step of this mechanism, when the CO_2-exposed TiO_2 surface was irradiated by the UV light (ΔE = 4.3 eV, λ = 290 nm) which is larger than the band gap of TiO_2, the electron in valance band can be excited to conduction band and an electron-hole pair (e^--h^+) is generated. This electron-hole pair can migrate to the surface. The hole combines with an oxygen vacancy (O_V) to form O_V^+. CO_2 can be the acceptor molecule to accept the e^- and form $CO_2^{\cdot-}$. $CO_2^{\cdot-}$ decomposes to CO and desorbs from the surface. This can explain why the atomic concentration of carbon is decreased on TiO_2 with UV light exposure. And $O^{\cdot-}$ is the other product that can combine with O_V^+ to create a surface oxygen atom. This reaction accounts for the addition of oxygen on the surface as observed.

4.5 References

1. Armstrong, E. F.; Hilditch, T. P., A Study of Catalytic Actions at Solid Surfaces. X. The Interaction of Carbon Monoxide and Hydrogen as Conditioned by Nickel at Relatively Low Temperatures. A Practical Synthesis of Methane. Proceedings of the Royal Society of London. Series A, Containing Papers of a Mathematical and Physical Character **1923,** 103 (720), 25-34.
2. Carrier, X.; Doyle, C. S.; Kendelewicz, T.; Brown, G. E., Reaction Of CO_2 With MgO(100) Surfaces. Surface Review and Letters **1999,** 06 (06), 1237-1245.
3. Taurian, O. E.; Springborg, M.; Christensen, N. E., Self-consistent electronic structures of MgO and SrO. Solid State Communications **1985,** 55 (4), 351-355.
4. Dette, C.; Pérez-Osorio, M. A.; Kley, C. S.; Punke, P.; Patrick, C. E.; Jacobson, P.; Giustino, F.; Jung, S. J.; Kern, K., TiO_2 Anatase with a Bandgap in the Visible Region. Nano Letters **2014,** 14 (11), 6533-6538.
5. Pipornpong, W.; Wanbayor, R.; Ruangpornvisuti, V., Adsorption CO_2 on the perfect and oxygen vacancy defect surfaces of anatase TiO_2 and its photocatalytic mechanism of conversion to CO. Applied Surface Science **2011,** 257 (24), 10322-10328.

Chapter 5 Summary and Implications for Future Work

The conversion of CO_2 to useful products has significant meaning for mitigating CO_2 emission compared to CO_2 sequestration. The conversion of CO_2 to useful fuels, such as CO and CH_4, will bring both economic and environmental benefits. However, the conversion of CO_2 is still challenging and many scientists are exploring options. In order to achieve these conversions, a better understanding of how CO_2 reacts on catalysts is essential. In this dissertation, we used MgO (100) and TiO_2 (110) as catalytic models to further our understanding of the mechanisms for the thermal decomposition of CO_2. Photocatalytic reactions of CO_2 were also explored on both crystal surfaces.

There is an increasing number of studies examining the interactions between CO_2 and metal surfaces. According to the results of these studies, the key species in the reactions are: physisorbed CO_2; chemisorbed $CO_2^{\cdot-}$; carbon dissociation, carbonate and oxalate formation. Table 5.1 summarizes some of these studies. The interaction between CO_2 and MgO has two common species; physisorbed CO_2 and carbonate. In Chapter 1, Figure 1.3 indicated five possible carbonate structures on MgO surface[1]. Compared to other oxide single crystals, MgO is widely available in nature and easy to be regenerated in its bulk form at low cost. It is a refractory metal oxide with a NaCl crystal structure.

In this dissertation, our results showed that the clean MgO surface exposed to different CO_2 (500-5000 Langmiur) exposure with a surface temperature (550-650 °C) can adsorb carbon on the surface. However, the exact structure of carbon is still unknown now. And the atomic concentration of oxygen on the very near surface decreased after exposure. Therefore, we can assume that the CO_2 adsorbs on the surface and forms some carbonate which then decomposes to other products, such as C and O_2 as we discussed in

Chapter 4. For the future experiments, we can use mass spectrometry to examine the gaseous products. Some studies have also shown that the interaction between CO_2 and MgO surface has an exchange of oxygen between the CO_2 and surface oxygen. We can use $C^{18}O_2$ instead of $C^{16}O_2$ and use mass spectrometry to verify what kind of gaseous products are generated; O_2, $^{18}O_2$, or $O^{18}O$.

Table 5. 1. CO_2 interactions with single crystal surfaces.

	CO_2 (Phys.)	Carbonate	Ref.
Barium Oxide			
BaO (Poly)	×	×	2, 3
Calcium Oxide			
CaO (100)	×	×	4
Chromium Oxide			
Cr_2O_3 (111)	×	×	5
Manganese Oxide			
MnO (100)			6
Magnesium Oxide			
MgO (100)	×		4, 7
MgO (100)	×	×	8
MgO (111)			8a
Sodium Oxide			
Na_2O (100)	×	×	9
Na_2O (110)			9
Nickle Oxide			
NiO (100)	×		10
Titanium Dioxide			
TiO_2 (110)	×	×	11
Zinc Oxide			
ZnO	×		12

At the same time, surface studies of TiO_2 are quickly growing in recent years. One reason is its wide range of possible applications, which were introduced in Chapter 1. The photocatalytic reduction of CO_2 with TiO_2 is an active area of research due to its potential to contribute to environmental protection and energy saving areas. Compared to

other transition metal oxides, TiO_2 has these three distinct characteristics: 1) high oxidizing ability; Some studies have shown the presence of some oxidative radicals such as ·OH are produced when H_2O and CO_2 are exposed to Uv light over TiO_2[13]; 2) good chemical stability; TiO_2 does not dissolve in water which is a common solvent for photocatalytic studies. TiO_2 does not dissolve in most acidic, basic and organic solvents. 3) safety; TiO_2 is relatively nontoxic.

In photocatalytic reactions of CO_2 with TiO_2, when the clean surface exposed to different (CO_2) exposures at room temperature, there is an increasing atomic concentration of carbon on the surface. However, once the surface was under UV irradiation, the atomic concentration of carbon is decreased. At the same time, the oxygen concentration at the outermost surface layers increased. All of results indicated that the CO_2-exposed surface after UV light irradiation, resulted in some carbon leaving the surface as gaseous product, such as CO. Mass spectrometry can be used to identify the gaseous products. In order to prove whether there is an exchange of oxygen between CO_2 and the surface, we can use $C^{18}O_2$ to perform the experiments instead of $C^{16}O_2$, and then follow the mass spectrometry to determine the gaseous products, such as CO, $C^{18}O$ or some other products.

The study of the catalytic reaction of CO_2 over metal oxides is a promising research area. All the methods discussed in this dissertation indicate that a metal oxide with a wide band gap, for example, MgO, can supply the CO_2 activation sites. However, due to its wide band gap, it makes a poor photocatalyst. Using a metal oxide with a band gap small enough for UV light to create electron-hole pairs, could be an active catalyst

for the reaction with CO_2 and should be examined. Potential metal oxides with small band gap include TiO_2 (3.0 eV), WO_3 (2.8 eV), and Fe_2O_3 (2.3 eV)[14].

Future studies of metal oxide assisted catalytic reactions should also be extended to high surface area powdered surfaces. These high surface area powders can supply more sites for CO_2 activation. Modification to powdered samples by cation/anion doping or metal impregnation will serve as sites for CO_2 activation, and could lead to changes in the band gap. Alteration the band gap and increasing the number of active sites with powdered samples should help the development of processes that produce fuels and valued chemicals from CO_2 in the future.

References

1. Little, L. H., Infrared spectra of adsorbed species. Academic Press: 1966.
2. Freund, H. J.; Roberts, M. W., Surface chemistry of carbon dioxide. Surface Science Reports **1996,** 25 (8), 225-273.
3. Mueller, D.; Shih, A.; Roman, E.; Madey, T.; Kurtz, R.; Stockbauer, R., A synchrotron radiation study of BaO films on W (001) and their interaction with H_2O, CO_2, and O_2. Journal of Vacuum Science & Technology A **1988,** 6 (3), 1067-1071.
4. Pacchioni, G.; Ricart, J. M.; Illas, F., Ab Initio Cluster Model Calculations on the Chemisorption of CO_2 and SO_2 Probe Molecules on MgO and CaO (100) Surfaces. A Theoretical Measure of Oxide Basicity. Journal of the American Chemical Society **1994,** 116 (22), 10152-10158.
5. Cappus, D.; Menges, M.; Xu, C.; Ehrlich, D.; Dillmann, B.; Ventrice Jr, C. A.; Libuda, J.; Bäumer, M.; Wohlrab, S.; Winkelmann, F.; Kuhlenbeck, H.; Freund, H. J., Electronic and geometric structure of adsorbates on oxide surfaces. Journal of Electron Spectroscopy and Related Phenomena **1994,** 68, 347-355.
6. Allen, V. M.; Jones, W. E.; Pacey, P. D., A molecular orbital study of carbon monoxide adsorption on a MnO surface. Surface Science **1988,** 199 (1), 309-319.
7. (a) Heidberg, J.; Meine, D., Polarized infrared spectra of CO_2 adsorbed on the MgO(100) single crystal surface. Surface Science **1992,** 279 (1–2), L175-L179; (b) Heidberg, J.; Meine, D.; Redlich, B., CO_2 adsorption on the MgO (100) single crystal surface detected by polarization FTIR spectroscopy and SPA-LEED. Journal of Electron Spectroscopy and Related Phenomena **1993,** 64–65 (0), 599-608; (c) Meixner, D. L.; Arthur, D. A.; George, S. M., Kinetics of desorption, adsorption, and surface diffusion of CO_2 on MgO(100). Surface Science **1992,** 261 (1–3), 141-154.
8. (a) Pacchioni, G., Physisorbed and chemisorbed CO_2 at surface and step sites of the MgO(100) surface. Surface Science **1993,** 281 (1-2), 207-219; (b) Suzanne, J.; Panella, V.; Ferry, D.; Sidoumou, M., The structure of CO_2 monolayers on MgO (100) single crystal surfaces. Surface Science Letters **1993,** 293 (3), L912-L916.
9. Onishi, H.; Egawa, C.; Aruga, T.; Iwasawa, Y., Adsorption of Na atoms and oxygen-containing molecules on MgO(100) and (111) surfaces. Surface Science **1987,** 191 (3), 479-491.
10. Onishi, H.; Aruga, T.; Iwasawa, Y., Na_2O overlayers epitaxially prepared on Pd (100) and structure-sensitive CO_2 adsorption. Surface Science **1994,** 310 (1–3), 135-146.
11. Göpel, W.; Rocker, G.; Feierabend, R., Intrinsic defects of TiO_2 (110): Interaction with chemisorbed O_2, H_2, CO, and CO_2. Physical Review B **1983,** 28 (6), 3427-3438.
12. Watanabe, M., Photosynthesis of methanol and methane from CO_2 and H_2O molecules on a ZnO surface. Surface Science **1992,** 279 (3), L236-L242.
13. Yates Jr, J. T., Photochemistry on TiO_2: Mechanisms behind the surface chemistry. Surface Science **2009,** 603 (10-12), 1605-1612.
14. Kasap, S., Kapper, Peter, Springer Handbook of Electronic and Photonic Materials
2007, 54327.

APPENDICES

Appendix A

Supplementary Information for Section 3.1

Thermal reaction of CO_2 with MgO (100) single crystal surfaces.

			XPS			AES		
	Temp. (^{0}C)	CO_2 (L)	C%	O%	Mg%	C%	O%	Mg%
SAMPLE A								
Clean			7.8	50.7	41.5	0.9	44.1	55.0
1	650	5000	8.2	49.4	42.4	12.6	40.1	47.3
Difference			0.5	-1.3	0.9	11.7	-4.0	-7.7
Clean			7.1	49.8	43.1	1.1	37.9	61.0
2	650	1000	7.9	47.1	45.0	1.9	23.8	74.3
Difference			0.8	-2.7	1.9	0.8	-14.1	13.3
Clean			6.9	47.5	45.6	1.4	23.2	75.4
3	650	500	7.6	48.9	43.5	1.4	23.7	74.9
Difference			0.7	1.4	-2.1	0.0	0.5	-0.5
Clean			6.9	49.4	43.7	1.0	24.3	74.8
4	650	5000	7.1	46.2	46.7	3.3	41.8	54.9
Difference			0.2	-3.2	3.0	2.3	17.6	-19.9
Clean			6.2	50.3	43.4	1.0	51.6	47.4
5	650	1000	6.9	48.5	44.6	3.4	25.0	71.6
Difference			0.7	-1.8	1.1	2.4	-26.6	24.2
Clean			6.7	49.5	43.8	0.8	42.9	56.3
6	600	500	6.9	49.8	43.4	6.4	20.2	73.5

Difference			0.2	0.2	-0.4	5.5	-22.7	17.2
Clean			6.4	48.9	44.7	0.0	44.5	55.5
7	600	5000	7.2	46.5	46.4	7.3	21.8	70.9
Difference			0.7	-2.4	1.7	7.3	-22.7	15.4
Clean			5.8	44.7	49.5	1.1	57.4	41.4
8	650	500	6.8	49.8	43.3	3.1	22.6	74.3
Difference			1.1	5.1	-6.2	2.0	-34.8	32.8
SAMPLE B								
Clean			7.5	48.3	44.3	0.0	34.1	65.9
9	650	1000	8.8	46.3	45.0	2.3	23.2	74.5
DIFFERENCE			1.3	-2.0	0.7	2.3	-10.9	8.6
CLEAN			7.7	47.8	44.5	0.0	33.3	66.7
10	650	5000	8.9	45.7	45.4	4.1	25.8	70.2
Difference			1.2	-2.1	0.9	4.1	-7.5	3.5
Clean			8.4	47.9	43.7	0.0	33.3	66.7
11	650	500	8.5	48.1	43.4	2.2	22.2	75.6
Difference			0.1	0.2	-0.3	2.2	-11.1	9.0
Clean			7.2	48.0	44.9	0.9	23.1	75.9
12	625	500	8.0	46.8	45.2	2.1	21.2	76.7
Difference			0.8	-1.2	0.4	1.2	-1.9	0.7
Clean			8.1	46.9	45.0	0.0	33.3	66.7
13	625	1000	8.7	45.0	46.3	1.9	18.7	79.3
Difference			0.6	-1.9	1.3	1.9	-14.6	12.7
Clean			8.5	48.1	43.4	0.9	22.6	76.5
14	625	1000	9.0	46.1	45.0	2.4	24.3	73.3
Difference			0.4	-2.0	1.6	1.5	1.7	-3.2
Clean			6.7	44.7	48.6	0.0	33.3	66.7

15	550	500	6.8	46.9	46.2	1.6	19.7	78.7
Difference			0.1	2.3	-2.4	1.6	-13.6	12.0
Clean			7.3	43.5	49.2	0.0	44.5	55.5
16	550	1000	7.9	46.6	45.4	1.6	26.4	72.0
Difference			0.6	3.1	-3.8	1.6	-18.1	16.5
Clean			7.2	44.0	48.8	0.0	33.3	66.7
17	550	1000	8.0	47.2	44.8	1.4	23.2	75.4
Difference			0.7	3.2	-3.9	1.4	-10.1	8.7
Clean			6.5	45.2	48.4	0.0	33.3	66.7
18	550	500	7.1	47.3	45.5	0.6	21.7	77.6
Difference			0.7	2.2	-2.8	0.6	-11.6	11.0
Clean			6.9	44.7	48.5	0.0	33.3	66.7
19	550	1000	7.4	48.0	44.6	0.5	27.7	71.8
Difference			0.5	3.4	-3.9	0.5	-5.6	5.1
Clean			6.7	44.6	48.7	0.0	33.3	66.7
20	550	5000	6.9	48.5	44.5	0.8	19.8	79.4
Difference			0.3	3.9	-4.1	0.8	-13.5	12.7
Clean			6.0	49.0	45.0	0.0	33.3	66.7
21	600	500	7.0	45.9	47.1	0.0	27.7	71.8
Difference			0.9	-3.1	2.1	0.0	-5.6	5.1
Clean			7.3	43.4	49.4	0.0	33.3	66.7
22	650	5000	8.1	47.3	44.6	0.8	21.2	78.0
Difference			0.9	3.9	-4.8	0.8	-12.1	11.3
Clean			6.8	49.0	44.2	0.0	33.3	66.7
23	600	500	7.3	46.1	46.5	0.5	27.7	71.8
Difference			0.6	-2.9	2.3	0.5	-5.6	5.1
SAMPLE C								
Clean			6.9	47.9	45.2	0.0	42.1	57.9

24	650	500	8.3	47.2	44.5	3.4	43.6	52.9
Difference			1.5	-0.7	-0.8	3.4	1.6	-5.0
Clean			7.3	44.6	48.2	0.6	65.2	34.2
25	650	1000	9.6	48.5	41.9	2.2	54.7	43.1
Difference			2.3	3.9	-6.2	1.5	-10.4	8.9
Clean			7.8	49.1	43.1	0.0	42.1	57.9
26	650	5000	7.9	47.9	44.2	3.4	43.0	53.6
Difference			0.1	-1.2	1.1	3.4	0.9	-4.3
Clean			9.2	44.5	46.4	1.0	49.1	49.9
27	625	500	9.3	46.6	44.2	1.4	70.8	27.9
Difference			0.1	2.1	-2.2	0.4	21.7	-22.1
Clean			7.8	45.2	47.0	0.0	68.5	31.5
28	625	5000	8.4	48.3	43.3	1.2	60.9	37.9
Difference			0.6	3.2	-3.7	1.2	-7.7	6.5
Clean			8.5	48.1	43.3	0.0	54.9	45.1
29	625	1000	8.9	45.7	45.4	1.8	46.4	51.8
Difference			0.4	-2.5	2.1	1.8	-8.5	6.7
Clean			8.0	47.3	44.7	0.0	54.9	45.1
30	650	5000	9.4	45.9	44.6	1.5	50.5	48.0
Difference			1.4	-1.4	0.0	1.5	-4.5	3.0
Clean			7.0	42.8	50.3	0.0	49.6	50.4
31	650	500	7.3	48.9	43.7	1.2	60.9	37.9
Difference			0.4	6.1	-6.5	1.2	11.3	-12.5
SAMPLE D								
Clean			7.1	48.0	44.9	0.0	60.9	39.1
32	650	500	7.6	47.4	45.0	3.7	61.9	34.5
Difference			0.5	-0.5	0.1	3.7	1.0	-4.6
Clean			7.4	46.2	46.4	0.6	65.2	34.2

33	650	1000	8.2	47.1	44.7	2.5	63.9	33.6
Difference			0.8	0.9	-1.7	1.9	-1.2	-0.6
Clean			6.9	45.0	48.0	1.3	66.9	31.8
34	650	5000	8.4	48.8	42.8	1.3	66.1	32.6
Difference			1.5	3.7	-5.2	0.0	-0.7	0.7
Clean			6.6	47.2	46.3	0.0	60.9	39.1
35	600	500	7.8	48.0	44.2	1.4	69.1	29.5
Difference			1.2	0.8	-2.1	1.4	8.2	-9.6
Clean			7.4	48.3	44.3	0.0	60.9	39.1
37	600	5000	8.2	47.5	44.3	1.3	66.1	32.6
Difference			0.7	-0.8%	0.0	1.3	5.2	-6.5
Clean			6.0	45.8	48.3	0.6	61.2	38.2
38	600	500	6.6	49.2	44.2	1.2	58.5	40.3
Difference			0.6	3.5	-4.1	0.5	-2.7	2.2
Clean			7.0	47.9	45.1	0.0	60.9	39.1
39	600	5000	7.6	45.5	46.9	2.1	52.8	45.1
Difference			0.6	-2.4	1.8	2.1	-8.1	6.0
Clean			5.8	48.5	45.7	0.7	71.2	28.1
40	650	500	6.5	48.2	45.3	1.1	57.4	41.4
Difference			0.7	-0.3	-0.4	0.4	-13.8	13.4
Clean			6.5	48.2	45.3	0.0	54.0	46.0
41	650	1000	6.6	45.0	48.5	1.0	51.6	47.4
Difference			0.1	-3.2	3.1	1.0	-2.4	1.4
Clean			6.8	47.2	46.0	0.8	39.5	59.7
42	650	5000	7.2	47.4	45.4	1.1	55.3	43.6
Difference			0.4	0.2	-0.5	0.3	15.8	-16.1
Clean			5.9	47.0	47.1	1.0	49.1	49.9
43	650	1000	6.3	48.0	45.7	1.2	63.4	35.4
Difference			0.4	1.0	-1.4	0.3	14.3	-14.6
Clean			6.2	47.1	46.7	0.7	73.0	26.3

44	650	5000	7.8	48.7	43.5	1.1	53.4	45.6
Difference			1.6	1.7%	-3.3	0.3	-19.6	19.2
SAMPLE E								
Clean			6.4	50.0	43.6	0.0	45.8	54.2
45	575	500	1.6	53.2	45.2	0.9	45.4	53.7
Difference			-4.8	3.2	1.6	0.9	-0.4	-0.5
Clean			6.7	51.5	41.8	0.0	45.2	54.8
46	550	500	7.4	49.7	42.9	0.9	43.5	55.7
Difference			0.7	-1.9	1.1	0.9	-1.7	0.8
Clean			7.0	49.9	43.1	0.0	43.2	56.8
47	550	1000	7.4	52.4	40.2	1.7	44.4	53.9
Difference			0.4	2.5	-2.9	1.7	1.1	-2.9
Clean			6.6	50.5	42.9	0.9	44.1	55.0
48	575	1000	6.8	50.0	43.2	0.9	43.5	55.7
Difference			0.2	-0.5	0.2	0.0	-0.6	0.6
Clean			6.6	50.5	42.9	0.0	45.2	54.8
49	600	1000	6.6	50.7	42.8	1.7	43.1	55.2
Difference			0.0	0.2	-0.2	1.7	-2.0	0.3
Clean			1.5	53.6	44.9	0.0	45.2	54.8
50	625	1000	6.5	50.7	42.9	0.9	45.4	53.7
Difference			5.0	-2.9	-2.0	0.9	0.3	-1.2
Clean			6.0	50.3	43.7	1.7	44.4	53.9
51	600	5000	6.0	51.7	42.3	8.7	40.1	51.3
Difference			0.0	1.4	-1.4	6.9	-4.3	-2.6
SAMPLE F								
Clean			5.2	49.4	45.4	0.8	42.9	56.3

52	550	5000	6.1	50.2	43.8	0.9	43.5	55.7
Difference			0.8	0.8	-1.7	0.0	0.6	-0.6
Clean			5.8	52.5	41.7	0.8	42.9	56.3
53	575	5000	6.3	50.9	42.8	0.9	43.5	55.7
Difference			0.4	-1.6	1.1	0.0	0.6	-0.6
Clean			5.8	52.5	41.7	1.6	40.8	57.6
54	575	1000	6.6	50.0	43.3	3.4	58.3	38.3
Difference			0.8	-2.5	1.7	1.8	17.5	-19.3
Clean			4.8	50.7	44.5	2.1	52.8	45.1
55	575	500	7.7	48.8	43.6	2.1	53.8	44.1
Difference			2.9	-2.0	-0.9	0.0	0.9	-1.0
Clean			6.2	49.6	44.2	2.0	51.9	46.0
56	575	1000	6.4	51.2	42.4	1.7	42.5	55.8
Difference			0.2	1.6	-1.8	-0.4	-9.4	9.8
Clean			5.7	53.3	41.0	0.0	42.6	57.4
57	575	500	6.4	50.6	43.0	1.7	42.5	55.8
Difference			0.7	-2.6	2.0	1.7	-0.1	-1.6
Clean			6.8	48.4	44.8	1.6	41.4	57.0
58	575	5000	7.8	49.9	42.3	1.7	42.5	55.8
Difference			1.0	1.5	-2.5	0.0	1.2	-1.2
SAMPLE G								
Clean			4.3	48.7	47.0	0.9	45.4	53.7
59	550	500	6.0	50.5	43.5	1.7	44.4	53.9
Difference			1.7	1.8	-3.5	0.9	-1.1	0.2
Clean			6.6	50.4	43.0	0.0	44.5	55.5
60	575	500	6.9	47.6	45.4	0.9	44.1	55.0
Difference			0.3	-2.7	2.4	0.9	-0.4	-0.5
Clean			5.9	50.8	43.3	0.0	46.5	53.5

61	575	1000	6.4	47.2	46.4	0.9	45.4	53.7
Difference			0.4	-3.6	3.1	0.9	-1.1	0.2
Clean			5.6	46.6	47.8	0.0	45.2	54.8
62	575	1000	6.7	49.0	44.3	0.0	45.2	54.8
Difference			1.0	2.4	-3.5	0.0	0.0	0.0
Clean			5.6	46.6	47.8	0.0	45.2	54.8
63	575	5000	5.6	45.1	49.3	0.0	44.5	55.5
Difference			-0.1	-1.5	1.6	0.0	-0.7	0.7
Clean			5.5	49.8	44.8	0.0	46.5	53.5
64	575	5000	5.8	50.6	43.6	0.0	45.2	54.8
Difference			0.4	0.8	-1.2	0.0	-1.4	1.4
65	550	5000	6.0	50.2	43.8	0.0	45.2	54.8
Difference			0.2	-0.4	0.2	0.0	0.0	0.0
Clean			5.6	43.0	51.4	0.0	43.9	56.1
66	575	5000	6.0	50.0	44.0	0.9	44.8	54.3
Difference			0.4	7.0	-7.4	0.9	0.9	-1.8
Clean			6.0	51.0	43.0	0.0	45.8	54.2
67	550	5000	6.6	49.7	43.7	0.0	45.8	54.2
Difference			0.6	-1.3	0.7	0.0	0.0	0.0
Clean			6.3	52.4	41.3	0.0	45.8	54.2
68	550	5000	6.6	46.0	47.4	0.9	44.1	55.0
Difference			0.3	-6.4	6.2	0.9	-1.7	0.9
69	600	1000	7.4	50.2	42.4	0.9	44.1	55.0
Difference			1.1	-2.2	1.2	0.9	-1.7	0.9
Clean			6.3	45.0	48.7	0.9	44.1	55.0
70	600	1000	6.8	48.1	45.0	0.0	45.2	54.8
Difference			0.5	3.1	-3.7	-0.9	1.0	-0.2
Clean			5.4	46.8	47.8	0.0	43.9	56.1
71	600	1000	6.2	50.4	43.3	0.0	45.2	54.8
Difference			0.8	3.7	-4.5	0.0	1.3	-1.3

72	625	500	6.6	45.9	47.4	0.0	45.2	54.8
Difference			0.4	-4.5	4.1	0.0	0.0	0.0
73	625	1000	7.0	49.2	43.7	0.9	44.1	55.0
Difference			0.4	3.3	-3.7	0.9	-1.0	0.2
Clean			5.9	44.2	49.9	0.0	44.5	55.5
74	625	500	6.4	49.6	44.0	0.0	44.5	55.5
Difference			0.5	5.4	-6.0	0.0	0.0	0.0
75	625	5000	7.0	46.7	46.4	0.9	43.5	55.7
Difference			0.6	-3.0	2.4	0.9	-1.0	0.2
Clean			5.1	44.5	50.4	0.0	43.9	56.1
76	625	5000	6.1	47.1	46.8	0.0	43.9	56.1
Difference			1.0	2.6	-3.6	0.0	0.0	0.0
77	625	5000	6.8	50.3	42.9	0.0	45.2	54.8
Difference			0.7	5.8	-7.5	0.0	1.3	-1.3
78	625	5000	7.8	48.5	43.7	0.0	45.2	54.8
Difference			0.9	-1.8	0.8	0.0	0.0	0.0

Appendix B

Supplementary Information for Section 3.2

Photocatalytic reactions of CO_2 with MgO (100) single crystal surfaces.

B-1. 500 L CO_2 exposure with MgO (100) at room temperature.

		XPS			AES		
EXP.	CO_2 (L)	C%	O%	Ti%	C%	O%	Ti%
Trial 1							
1	N/A	7.3	44.8	47.8	2.5	42.2	55.3
2	500	7.8	48.5	43.7	3.3	41.8	54.9
Difference		0.5	3.7	-4.2	0.8	-0.3	-0.5
3	10 min UV	7.6	48.6	43.8	2.4	40.5	57.1
Difference		-0.2	0.1	0.1	-0.9	-1.3	2.2
Trial 2							
1	N/A	6.0	52.1	41.9	0.8	42.9	56.3
2	500	6.3	48.6	45.1	2.5	42.2	55.3
Difference		0.3	-3.5	3.2	1.6	-0.7	-0.9
3	10 min UV	6.4	49.3	44.3	1.7	43.7	54.5
Difference		0.1	0.7	-0.8	-0.8	1.6	-0.8
Trial 3							
1	N/A	6.5	50.9	42.7	0.8	42.9	56.3
2	500	6.9	51.2	41.9	2.5	41.6	55.9
Difference		0.4	0.4	-0.8	1.6	-1.3	-0.3
3	10 min UV	6.9	51.3	41.8	1.6	41.6	55.9
Difference		0.0	0.1	-0.1	0.0	0.0	0.0

B-2. 1000 L CO_2 exposure with MgO (100) at room temperature.

		XPS			AES		
EXP.	CO_2 (L)	C%	O%	Ti%	C%	O%	Ti%
Trial 1							
1	N/A	5.5	49.1	45.4	0.0	43.2	56.8
2	1000	7.1	48.4	44.5	2.5	42.8	54.7
Difference		1.6	-0.7	-0.9	2.5	-0.5	-2.0
3	10 min UV	7.1	48.2	44.7	2.5	42.5	55.0
Difference		0.0	-0.2	0.2	0.0	-0.3	0.3
Trial 2							
1	N/A	5.5	49.1	45.4	0.0	43.2	56.8
2	1000	7.1	48.4	44.5	2.5	42.8	54.7
Difference		1.6	-0.7	-0.9	2.5	-0.5	-2.0
3	10 min UV	7.3	47.7	45.0	1.7	41.9	56.4
Difference		0.1	-0.6	0.5	-0.9	-0.8	1.7
Trial 3							
1	N/A	5.5	49.1	45.4	0.0	43.2	56.8
2	1000	7.1	48.4	44.5	2.5	42.8	54.7
Difference		1.6	-0.7	-0.9	2.5	-0.5	-2.0
3	10 min UV	7.3	48.7	44.0	0.0	43.2	56.8
Difference		0.2	0.3	-0.5	-2.5	0.5	2.0

B-3. 5000 L CO_2 exposure with MgO (100) at room temperature.

		XPS			AES		
EXP.	CO_2 (L)	C%	O%	Ti%	C%	O%	Ti%
Trial 1							
1	N/A	6.7	47.2	46.1	0.0	42.6	57.4
2	5000	7.4	47.6	45.0	0.0	43.9	56.1
Difference		0.7	0.4	-1.1	0.0	1.3	-1.3
3	10 min UV	7.4	48.2	44.4	0.0	43.9	56.1
Difference		0.0	0.6	-0.6	0.0	0.0	0.0
Trial 2							
1	N/A	5.5	47.7	46.8	0.0	43.2	56.8
2	5000	6.4	49.4	44.2	0.8	42.9	56.3
Difference		0.9	1.7	-2.6	0.8	-0.3	-0.5
3	10 min UV	6.0	48.9	45.1	0.8	42.1	57.1
Difference		-0.4	-0.5	0.9	0.0	-0.8	0.8
Trial 3							
1	N/A	7.8	46.4	45.8	0.0	44.5	55.5
2		8.9	46.6	44.5	0.0	42.6	57.4
Difference		1.1	0.2	-1.3	0.0	-1.9	1.9
3	10 min UV	7.4	48.6	44.0	0.0	42.1	57.9
Difference		-1.5	2.0	-0.5	0.0	-0.5	0.5

Appendix C

Supplementary Information for Section 3.3

Thermal reaction of CO_2 with TiO_2 at different surface temperatures (200-700 °C)

			XPS			AES		
EXP.	Temp. (°C)	CO_2 (L)	C%	O%	Ti%	C%	O%	Ti%
Clean			1.8	72.4	25.7	0.0	74.8	25.2
1	200	500	1.7	73.4	24.9	1.4	20.1	78.5
Difference			-0.2	0.9	-0.8	1.4	-54.6	53.3
Clean			1.0	73.4	25.6	0.0	73.6	26.4
2	250	500	1.4	72.6	26.0	0.0	73.6	26.4
Difference			0.3	-0.8	0.4	0.0	0.0	0.0
3	300	500	1.5	73.4	25.2	2.2	74.5	23.3
Difference			0.1	0.0	-0.1	2.2	0.8	-3.0
Clean			0.8	73.3	25.9	0.0	73.2	26.8
4	350	500	1.2	73.1	25.7	2.1	72.5	25.3
Difference			0.4	-0.2	-0.2	2.1	-0.6	-1.5
5	450	500	0.9	73.1	26.0	2.2	74.0	23.8
Difference			-0.2	0.0	0.3	0.0	1.4	-1.5
6	500	500	1.1	73.0	25.9	0.7	75.1	24.2
Difference			0.1	-0.1	-0.1	-1.4	1.1	0.4
Clean			1.3	73.1	25.7	0.0	70.0	30.0
7	550	500	1.2	74.1	24.7	2.7	68.5	28.8
Difference			0.0	1.0	-1.0	2.7	-1.5	-1.2
8	600	500	0.8	73.2	26.0	0.0	75.6	24.4

Difference			-0.4	-0.9	1.3	-2.7	7.1	-4.4
9	650	500	1.3	73.5	25.2	1.5	74.0	24.5
Difference			0.5	0.3	-0.8	1.5	-1.6	0.1
Clean			1.0	75.5	23.5	0.0	75.1	24.9
10	700	500	1.5	72.6	25.9	0.0	74.6	25.4
Difference			0.5	-2.9	2.4	0.0	-0.5	0.5
11	200	1000	1.6	72.8	25.6	0.0	76.2	23.8
Difference			0.1	0.2	-0.3	0.0	1.5	-1.5
12	250	1000	1.5	73.5	25.0	1.5	74.5	24.0
Difference			-0.1	0.7	-0.6	1.5	-1.6	0.2
Clean			2.7	80.3	17.0	1.6	81.6	16.8
13	200	1000	3.2	79.7	17.0	6.3	79.5	14.2
Difference			0.5	-0.6	0.0	4.7	-2.1	-2.6
14	250	1000	2.2	79.9	17.9	1.6	82.8	15.6
Difference			-1.0	0.1	0.9	-4.6	3.3	1.3
Clean			2.5	81.1	16.4	3.2	81.5	15.3
15	300	1000	3.2	80.5	16.3	1.7	84.1	14.3
Difference			0.7	-0.6	-0.1	-1.6	2.6	-1.0
16	350	1000	1.9	80.6	17.6	0.8	83.5	15.7
Difference			-1.3	0.1	1.2	-0.8	-0.6	1.4
Clean			1.5	80.9	17.6	1.6	82.8	15.6
17	400	1000	1.6	81.4	17.0	0.8	84.1	15.1
Difference			0.1	0.5	-0.6	-0.8	1.3	-0.5
18	450	1000	1.4	81.3	17.4	0.0	84.8	15.2
Difference			-0.3	-0.1	0.4	-0.8	0.7	0.1
Clean			2.7	82.6	14.7	1.6	81.6	16.8
19	500	1000	4.7	81.8	13.5	0.8	86.1	13.1
Difference			2.0	-0.8	-1.2	-0.8	4.5	-3.7
20	550	1000	2.6	82.0	15.4	0.8	84.8	14.4
Difference			-2.0	0.1	1.9	0.0	-1.3	1.3

Clean			2.6	82.0	15.4	0.0	83.6	16.4
21	600	1000	1.8	81.7	16.5	0.0	84.2	15.8
Difference			-0.8	-0.3	1.1	0.0	0.6	-0.6
Clean			1.8	81.7	16.5	0.0	84.8	15.2
22	650	1000	1.1	96.3	2.5	0.8	84.1	15.1
Difference			-0.7	14.6	-13.9	0.8	-0.7	-0.1
Clean			2.3	81.3	16.4	1.6	83.4	14.9
23	700	1000	1.3	81.7	16.9	0.0	85.5	14.5
Difference			-1.0	0.4	0.6	-1.6	2.0	-0.4
Clean			1.3	81.7	16.9	0.0	84.8	15.2
23	200	5000	1.9	82.5	15.6	3.1	78.6	18.3
Difference			0.6	0.8	-1.4	3.1	-6.2	3.1
24	250	5000	1.5	82.6	15.9	0.0	84.8	15.2
Difference			-0.5	0.1	0.4	-3.1	6.2	-3.1
Clean			1.9	82.7	15.4	0.0	86.1	13.9
25	300	5000	1.3	82.4	16.3	0.0	84.8	15.2
Difference			-0.6	-0.3	0.9	0.0	-1.3	1.3
26	350	5000	1.6	82.8	15.5	1.6	82.8	15.6
Difference			0.3	0.4	-0.7	1.6	-2.0	0.4
Clean			1.6	82.8	15.5	1.6	83.4	14.9
27	400	5000	2.1	82.4	15.5	2.3	78.7	19.0
Difference			0.5	-0.4	0.0	0.7	-4.8	4.1
Clean			5.3	89.8	4.9	2.7	93.1	4.2
28	450	5000	7.3	89.0	3.7	0.0	98.2	1.8
Difference			2.0	-0.8	-1.2	-2.7	5.2	-2.4
Clean			7.3	89.0	3.7	0.0	95.7	4.3
29	500	5000	6.4	89.6	4.0	0.0	98.0	2.0
Difference			-0.9	0.6	0.3	0.0	2.3	-2.3
Clean			6.4	89.6	4.0	0.0	95.7	4.3
30	550	5000	6.1	88.8	5.1	2.8	93.9	3.4

Difference			-0.3	-0.8	1.1	2.8	-1.8	-0.9
Clean			16.6	70.0	13.4	1.4	73.1	25.5
31	550	1000	15.3	70.3	14.3	0.7	72.6	26.6
Difference			-1.2	0.3%	0.9	-0.7	-0.4	1.2
Clean			20.9	69.7	9.4	0.7	72.6	26.6
32	500	1000	21.2	70.3	8.5	0.8	77.7	21.5
Difference			0.3	0.6	-0.9	0.0	5.0	-5.1
33	450	1000	22.7	69.4	7.9	1.5	74.5	24.0
Difference			1.6	-1.0	-0.6	0.7	-3.2	2.5
34	400	1000	27.6	88.6	-16.3	0.7	75.1	24.2
Difference			4.9	19.3	-24.2	-0.7	0.6	0.2
35	350	1000	23.9	69.7	6.5	0.7	75.6	23.7
Difference			-3.8	-19.0	22.7	0.0	0.5	-0.5
Clean			21.7	70.3	8.0	1.4	72.6	26.0
36	300	1000	11.5	71.4	17.1	1.3	63.9	34.9
Difference			-10.2	1.1	9.1	-0.2	-8.7	8.9
37	250	1000	22.4	70.0	7.7	1.4	73.1	25.5
Difference			0.7	-0.3	-0.3	1.6	81.8	16.6
38	200	1000	24.0	70.1	5.9	1.4	72.6	26.0
Difference			1.6	0.1	-1.7	0.0	-0.5	0.5
39	200	1000	23.4	69.8	6.8	1.4	72.6	26.0
Difference			-0.5	-0.3	0.8	0.0	0.0	0.0
Clean			20.1	69.5	10.5	1.5	75.0	23.5
40	250	1000	23.2	69.1	7.7	1.5	74.0	24.5
Difference			3.2	-0.4	-2.8	0.0	-1.0	1.0
41	300	1000	22.0	70.0	8.0	1.4	69.9	28.8
Difference			-1.2	0.9	0.3	-0.1	-4.2	4.2
42	350	1000	18.5	71.2	10.3	1.5	74.5	24.0
Difference			-4.7	2.1	2.6	0.0	0.5	-0.5

43	400	1000	24.6	69.0	6.4	1.5	74.0	24.5
Difference			6.1	-2.2	-3.9	0.0	-0.5	0.5
Clean			24.7	71.0	4.4	1.5	75.5	23.0
44	450	1000	23.7	69.9	6.4	2.1	71.2	26.7
Difference			-1.0	-1.1	2.1	0.6	-4.4	3.8
45	500	1000	25.2	68.8	6.0	2.6	65.7	31.7
Difference			1.5	-1.1	-0.5	0.5	-5.5	5.0
Clean			25.2	68.8	6.0	0.0	73.6	26.4
46	550	1000	20.4	69.9	9.7	0.0	72.7	27.3
Difference			-4.8	1.1	3.7	0.0	-1.0	1.0
Clean			25.2	68.8	6.0	0.0	72.7	27.3
47	600	1000	25.0	69.5	5.5	2.7	69.3	27.9
Difference			-0.2	0.7	-0.5	2.7	-3.3	0.6
Clean			21.8	70.8	7.3	0.0	72.2	27.8
48	650	1000	26.0	70.1	3.9	0.0%	73.6	26.4
Difference			4.1	-0.7	-3.4	0.0	1.4	-1.4
49	700	1000	20.4	70.8	8.8	0.0	77.2	22.8
Difference			-5.6	0.7	4.9	0.0	3.6	-3.6
Clean			26.0	70.1	3.9	0.0	73.6	26.4
50	700	1000	26.9	69.7	3.4	0.0	73.6	26.4
Difference			0.9	-1.1	-1.6	-1.6	-1.6	-1.6
Clean			24.9	69.6	5.5	0.0	76.7	23.3
51	650	1000	23.0	69.6	7.4	0.0	73.6	26.4
Difference			-1.9	0.0	1.9	0.0	-3.0	3.0
52	600	1000	23.5	69.2	7.3	0.0	74.1	25.9
Difference			0.5	-0.4	-0.1	0.0	0.5	-0.5
Clean			20.2	70.3	9.5	0.0	72.7	27.3
53	700	5000	23.5	68.2	15.6	0.7	72.2	27.1
Difference			3.3	-2.2	-1.2	0.7	-0.5	-0.2
53	650	5000	24.1	70.0	5.9	0.7	73.1	26.2

Difference			0.6	1.8	11.8	0.0	0.9	-1.0
Clean			24.1	70.0	5.9	0.0	72.2	27.8
54	600	5000	23.5	70.6	5.9	1.4	70.8	27.9
Difference			-0.5	0.6	-0.1	1.4	-1.5	0.1
55	550	5000	25.1	70.1	4.8	0.0	74.6	25.4
Difference			1.5	-0.5	-1.0	-1.4	3.9	-2.5
Clean			22.9	69.8	7.4	0.0	77.2	22.8
56	500	5000	23.3	69.7	7.0	0.7	73.1	26.2
Difference			0.5	-0.1	-0.4	0.7	-4.1	3.4
57	450	5000	21.8	70.4	7.8	1.4	69.9	28.8
Difference			-1.5	0.7	0.8	0.7	-3.2	2.6
Clean			24.2	69.7	6.1	0.0	72.7	27.3
58	400	5000	23.5	70.2	6.3	0.0	67.4	32.6
Difference			-0.8	0.5	0.2	0.0	-5.3	5.3
Clean			21.8	69.9	8.3	0.0	72.7	27.3
59	650	5000	21.0	69.5	9.4	1.4	68.6	30.1
Difference			-0.7	-0.4	1.1	1.4	-4.1	2.8
Clean			21.0	69.5	9.4	0.0	75.6	24.4
60	300	5000	24.4	69.1	6.5	0.0	73.6	26.4
Difference			3.3	-0.5	-2.9	0.0	-2.0	2.0
Clean			22.2	69.3	8.5	0.0	75.1	24.9
61	250	5000	20.8	69.4	9.8	0.0	74.6	25.4
Difference			-1.4	0.1	1.3	0.0	-0.5	0.5
62	200	5000	24.0	69.7	6.3	1.4	72.6	26.0
Difference			1.8	0.4	-2.2	1.4	-2.5	1.1
Clean			23.1	70.7	6.2	1.7	86.0	12.3
63	200	1000	21.9	69.6	8.5	2.4	82.1	15.4
Difference			-1.2	-1.1	2.3	0.7	-3.9	3.1
Clean			21.9	69.6	8.5	0.0	87.5	12.5
64	250	1000	21.5	70.7	7.7	0.0	88.2	11.8

Difference			-0.4	1.1	-0.7	0.0	0.7	-0.7
65	300	1000	22.2	69.5	8.3	0.0	89.6	10.4
Difference			0.6	-1.2	0.6	0.0	1.4	-1.4
Clean			22.2	69.5	8.3	1.6	81.6	16.8
66	350	1000	23.7	70.1	6.2	1.6	81.0	17.4
Difference			1.6	0.6	-2.1	0.0	-0.6	0.6
67	400	1000	22.6	70.2	7.2	1.7	86.0	12.3
Difference			-1.1	0.2	0.9	0.1	5.0	-5.1
68	450	1000	23.0	69.7	7.3	0.0	89.6	10.4
Difference			0.4	-0.5	0.1	-1.7	3.6	-1.9
Clean			21.7	70.2	8.1	1.5	76.0	22.5
69	500	1000	24.1	70.3	5.6	0.0	86.1	13.9
Difference			-21.7	-70.2	-8.1	-1.5	-76.0	-22.5
Clean			19.3	70.0	10.7	1.6	83.4	14.9
70	550	1000	25.0	69.6	5.4	1.5	77.6	20.8
Difference			5.7	-0.4	-5.3	-0.1	-5.8	5.9
Clean			18.6	70.8	10.6	1.6	83.4	14.9
71	600	1000	20.0	69.9	10.1	1.7	84.1	14.3
Difference			1.4	-0.9	-0.5	0.0	0.6	-0.6
Clean			20.0	71.1	8.9	3.3	83.3	13.4
72	650	1000	22.6	70.4	7.0	1.7	86.0	12.3
Difference			2.7	-0.8	-1.9	-1.6	2.7	-1.1
73	700	1000	21.8	70.0	8.2	1.7	85.3	13.0
Difference			-0.9	-0.4	1.3	0.0	-0.7	0.7
Clean			1.2	73.1	25.7	0.0	89.6	10.4
74	700	500	1.2	72.7	26.1	0.0	87.5	12.5
Difference			0.0	-0.4	0.4	0.0	-2.1	2.1
Clean			1.2	73.1	25.8	0.0	88.9	11.1
75	600	500	1.2	72.7	26.1	0.0	88.9	11.1

Difference			0.0	-0.4	0.4	0.0	0.0	0.0
Clean			1.2	72.7	26.1	0.0	88.9	11.1
76	600	500	1.3	72.6	26.0	0.0	89.6	10.4
Difference			0.1	-0.1	-0.1	0.0	0.7	-0.7
Clean			1.3	71.1	27.6	0.0	89.6	10.4
77	550	500	1.3	72.3	26.4	0.0	88.9	11.1
Difference			0.0	1.2	-1.2	0.0	-0.7	0.7
Clean			1.3	72.3	26.4	0.0	88.9	11.1
78	500	500	0.9	71.5	27.6	0.0	88.2	11.8
Difference			-0.5	-0.8	1.2	0.0	-0.7	0.7
79	450	500	1.1	72.3	26.6	0.0	87.5	12.5
Difference			1.1	0.8	-1.0	0.0	-0.7	0.7
80	400	500	1.5	71.4	27.2	0.0	87.5	12.5
Difference			0.4	-1.0	0.6	0.0	0.0	0.0
81	350	500	1.4	72.4	26.3	0.0	87.5	12.5
Difference			-0.1	1.0	-0.9	0.0	0.0	0.0
Clean			1.0	72.3	26.7	0.0	87.5	12.5
82	300	500	1.0	72.6	26.3	0.0	86.8	13.2
Difference			0.0	0.4	-0.4	0.0	-0.7	0.7
Clean			0.0	0.4	26.7	0.0	-0.7	0.7
83	250	500	1.2	1.2	97.7	0.0	87.5	12.5
Difference			1.2	-0.1	0.0	0.0	0.7	-0.7
84	200	500	1.3	72.7	26.1	0.0	88.2	11.8
Difference			0.1	0.1	-0.1	0.0	0.7	-0.7
Clean			1.0	71.2	27.9	0.0	88.2	11.8
85	200	500	0.9	73.1	26.0	0.0	88.2	11.8
Difference			-0.1	1.9	-1.8	0.0	0.0	0.0
Clean			0.9	73.1	26.0	0.0	88.2	11.8
86	250	500	0.6	72.5	26.9	0.0	88.2	11.8
Difference			-0.3	-0.6	0.9	0.0	0.0%	0.0

87	300	500	0.8	72.8	26.4	0.0	87.5	12.5
Difference			0.2	0.3	-0.6	0.0	-0.7	0.7
88	350	500	0.8	72.1	27.1	0.0	88.2	11.8
Difference			0.0	-0.7	0.7	0.0	0.7	-0.7
89	400	500	1.0	72.3	26.7	0.0	84.8	15.2
Difference			0.2	0.3	-0.4	0.0	-3.3	3.3
90	450	500	1.0	72.4	26.6	0.0	87.5	12.5
Difference			0.0	0.1	0.0	0.0	2.7	-2.7
Clean			1.7	72.8	25.5	0.0	88.2	11.8
91	500	500	1.5	72.9	25.6	0.0	88.2	11.8
Difference			-0.2	0.1	0.1	0.0	0.0	0.0
92	550	500	1.5	72.4	26.1	0.0	86.8	13.2
Difference			0.0	-0.5	0.5	0.0	-1.4	1.4
Clean			1.3	71.1	27.5	0.0	89.6	10.4
93	600	500	0.6	86.4	12.9	0.0	89.6	10.4
Difference			-0.7	15.3	-14.6	0.0	0.0	0.0
94	650	500	1.1	72.0	26.9	0.0	88.9	11.1
Difference			0.4	-14.4	14.0	0.0	-0.7	0.7
95	700	500	1.0	72.4	26.6	0.0	89.6	10.4
Difference			-0.1	0.4	-0.3	0.0	0.7	-0.7
96	700	5000	1.1	72.0	26.9	0.0	86.8	13.2
Difference			0.1	-0.4	0.3	0.0	-2.8	2.8
Clean			1.1	72.4	26.6	0.0	89.6	10.4
97	700	5000	1.0	73.2	25.8	0.0	89.6	10.4
Difference			-0.1	0.8	-0.8	0.0	0.0	0.0
Clean			1.3	71.8	26.9	0.0	90.3	9.7
98	650	5000	1.4	72.3	26.3	0.0	90.7	9.3
Difference			0.1	0.5	-0.6	0.0	0.4	-0.4
99	650	5000	1.5	72.6	26.0	0.0	87.5	12.5
Difference			0.1	0.3	-0.3	0.0	-3.2	3.2

Clean			1.6	70.2	28.2	0.0	89.6	10.4
100	600	5000	1.4	73.4	25.2	0.0	88.9	11.1
Difference			-0.3	3.2	-2.9	0.0	-0.7	0.7
101	600	5000	1.3	72.9	25.8	0.0	88.2	11.8
Difference			-0.1	-0.5	0.5	0.0	-0.7	0.7
Clean			1.7	71.5	26.8	0.0	89.6	10.4
102	550	5000	1.3	72.4	26.4	0.0	87.5	12.5
Difference			-0.4	0.9	-0.5	0.0	-2.1	2.1
103	500	5000	1.3	72.5	26.2	0.0	87.5	12.5
Difference			0.0	0.2	-0.2	0.0	0.0	0.0
Clean			1.4	71.1	27.5	0.0	87.5	12.5
104	450	5000	1.4	73.0	25.6	0.0	88.9	11.1
Difference			0.0	1.9	-1.9	0.0	1.4	-1.4
105	400	5000	1.3	72.0	26.7	0.0	87.5	12.5
Difference			0.0	-1.0	1.0	0.0	-1.4	1.4
Clean			1.5	71.9	26.6	0.0	88.9	11.1
106	350	5000	1.4	72.6	26.0	0.0	88.9	11.1
Difference			-0.1	0.7	-0.6	0.0	0.0	0.0
107	300	5000	1.2	72.8	26.0	0.0	87.5	12.5
Difference			-0.1	0.2	0.0	0.0	-1.4	1.4
Clean			1.3	72.6	26.0	0.0	88.2	11.8
108	250	5000	1.1	72.6	26.3	0.0	89.6	10.4
Difference			-0.2	0.0	0.3	0.0	1.4	-1.4
Clean			0.8	72.6	26.5	0.0	90.3	9.7
109	200	5000	1.1	72.8	26.1	0.0	89.6	10.4
Difference			0.2	0.2	-0.4	0.0	-0.7	0.7
Clean			1.8	72.7	25.5	0.0	87.5	12.5
110	200	500	1.5	73.3	25.2	1.7	88.0	10.2
Difference			-0.3	0.6	-0.3	1.7	0.6	-2.3
111	650	500	1.6	71.7	26.7	0.0	85.5	14.5

Difference			0.1	-1.5	1.5	-1.7	-2.6	4.3
Clean			1.9	71.9	26.3	0.0	89.6	10.4
112	400	500	1.7	72.5	25.8	1.7	87.3	10.9
Difference			-0.2	0.6	-0.6	1.7	-2.2	0.5

Appendix D

Supplementary Information for Section 3.4

Photocatalytic reactions of CO_2 with TiO_2 at room temperature

D.1 Photocatalytic reaction of 500 L CO_2 with TiO_2 at room temperature.

	XPS			AES		
	C%	O%	Ti%	C%	O%	Ti%
Trial 1						
Clean	1.4	74.2	24.4	0.8	84.8	14.4
500 L CO_2	2.0	73.4	24.6	1.7	88.0	10.2
Difference	0.6	-0.8	0.2	0.9	3.3	-4.2
500 L +UV	1.0	74.4	24.6	0.0	81.7	18.3
Difference	-1.0	1.0	0.0	-1.7	-6.3	8.0
500 L +10minUV	0.7	76.5	22.8	4.0	82.0	13.9
Difference	-0.3	2.1	-1.8	4.0	0.3	-4.3
Clean	1.5	74.7	23.8	0.7	75.6	23.7
500 L +20minUV	1.1	75.0	23.8	0.0	75.6	24.4
Difference	-0.4	0.3	0.1	-0.7	0.1	0.7
Trial 2						
Clean	1.1	75.0	23.8	0.0	75.6	24.4
500 L CO_2	2.1	72.8	25.1	1.5	78.7	19.7
Difference	1.0	-2.3	1.3	1.5	3.1	-4.6
500 L +UV	2.0	73.7	24.3	1.5	78.7	19.7

Difference	-0.1	1.0	-0.8	0.0	0.0	0.0
Clean	1.3	75.3	23.	0.0	80.5	19.5
500 L +10min UV	1.0	75.2	23.8	0.0	81.1	18.9
Difference	-0.2	-0.1	0.3	0.0	0.6	-0.6
Clean	1.4	74.6	24.0	0.0	80.5	19.5
500 L+20 min UV	1.0	75.4	23.6	0.0	84.2	15.8
Difference	-0.4	0.8	-0.4	0.0	84.2	15.8
TRIAL 3						
Clean	1.0	75.4	23.6	0.0	84.2	15.8
500 L CO_2	1.8	73.5	24.6	3.2	80.9	15.9
Difference	0.8	-1.9	1.1	3.2	-3.3	0.1
500 L +UV	0.9	75.0	24.2	3.5	87.9	8.7
Difference	-0.9	1.4	-0.5	0.3	7.0	-7.3
Clean	1.2	74.3	24.5	0.0	86.1	13.9
500 L +10minUV	1.1	74.8	24.2	0.0	88.2	11.8
Difference	-0.1	0.5	-0.4	0.0	2.0	-2.0
500 L +20minUV	1.	73.3	25.7	1.7	84.1	14.3
Difference	-0.1%	-1.4	1.5	1.7	-4.1	2.5

D.2 Photocatalytic reaction of 1000 L CO_2 with TiO_2 at room temperature.

	XPS			AES		
	C%	O%	Ti%	C%	O%	Ti%
TRIAL 1						
Clean	1.3	75.9	22.8	0.0%	80.5	19.5
1000 L CO_2	1.8	73.8	24.3	1.7%	84.7	13.6
Difference	0.6	-2.1	1.5	1.7%	4.2	-5.8
Clean	0.9	75.3	23.8	0.0%	82.6	17.4
1000 L +UV	0.3	75.9	23.8	0.0%	85.5	14.5
Difference	-0.5	0.5	0.0	0.0%	2.8	-2.8
1000 L +10min UV	1.1	76.4	22.5	0.0%	82.3	17.7
Difference	-0.2	0.5	-0.3	0.0%	1.8	-1.8
Clean	1.2	73.9	24.9	0.8%	85.4	13.8
1000 L +20min UV	1.2	75.0	23.7	0.9%	89.5	9.6
Difference	0.1	1.1	-1.2	0.0	4.1	-4.1
TRIAL 2						
Clean	1.1	75.6	23.4	0.0	84.8	15.2
1000 L CO_2	1.2	72.9	25.9	1.7	87.3	10.9
Difference	0.1	-2.6	2.5	1.7	2.5	-4.2
Clean	1.1	72.7	26.2	0.0	84.8	15.2
1000 L +UV	0.7	73.4	25.9	0.0	84.2	15.8
Difference	-0.4	0.7	-0.3	0.0	-0.6	0.6
Clean	1.2	74.9	23.9	0.0	85.5	14.5
1000 L +10min UV	1.1	73.8	25.1	0.0	88.9	11.1
Difference	-0.1	-1.1	1.2	0.0	3.4	-3.4
Clean	1.0	74.5	24.6	0.0	88.2	11.8
1000 L +20min UV	1.0	73.6	25.3	0.0	88.2	11.8
Difference	0.0	-0.8	0.8	0.0	0.0	0.0

TRIAL 3						
Clean	1.2	75.4	23.3	0.0	88.9	11.1
1000 L CO_2	1.7	72.8	25.5	3.4	85.2	11.4
Difference	0.4	-2.6	2.2	3.4	-3.7	0.3
Clean	1.1	75.1	23.8	0.0	86.8	13.2
1000 L +10min UV	0.9	73.8	25.3	0.0	91.0	9.0
Difference	-0.2	-1.3	1.5	0.0	4.2	-4.2
Clean	1.2	75.7	23.1	1.7	84.1	14.3
1000 L +10min UV	1.2	73.5	25.3	0.0	93.3	6.7
Difference	0.0	-2.2	2.2	-1.7	9.3	-7.6
Clean	1.2	75.8	23.0	0.0	84.2	15.8
1000 L +20min UV	1.2	73.3	25.5	0.0	92.5	7.5
Difference	0.0	-2.5	2.5	0.0	8.4	-8.4

D.3 Photocatalytic reaction of 5000 L CO_2 with TiO_2 at room temperature.

	XPS			AES		
	C%	O%	Ti%	C%	O%	Ti%
Clean	1.3	74.8	23.9	0.0	89.6	10.4
5000 L CO_2	1.2	74.4	24.4	0.0	88.2	11.8
Difference	-0.1	-0.3	0.4	0.0	-1.4	1.4
Clean	1.2	52.1	46.7	0.0	87.5	12.5
5000 L +UV	1.1	75.1	23.8	1.8	90.2	8.1
Difference	-0.1	23.0	-22.9	1.8	2.7	-4.5
Clean	1.2	74.4	24.4	0.0	88.2	11.8
5000 L+10min UV	1.3	74.7	24.0	0.0	87.5	12.5
Difference	0.1	0.4	-0.4	0.0	-0.7	0.7
Clean	1.2	74.8	24.0	0.0	84.2	15.8
5000 L+ 20 min UV	1.1	75.4	23.5	0.0	87.5	12.5
Difference	-0.1	0.6	-0.5	0.0	3.3	-3.3
TRIAL 2						
Clean	1.0	74.6	24.4	0.0	84.8	15.2
5000 L CO_2	1.6	73.1	25.3	0.0	86.1	13.9
Difference	0.6	-1.5	0.9	0.0	1.3	-1.3
Clean	0.5	75.3	24.2	0.0	82.3	17.7
5000 L +UV	0.5	73.1	26.4	0.0	86.8	13.2
Difference	0.0	-2.2	2.2	0.0	4.5	-4.5
5000 L+10min UV	0.4	74.7	24.9	0.0	86.1	13.9
Difference	-0.1	1.6	-1.5	0.0	-0.7	0.7
5000 L+ 20 min UV	0.9	73.4	25.7	0.0	82.9	17.1
Difference	0.5	-1.3	0.8	0.0	-3.2	3.2
TRIAL 3						
Clean	0.9	75.5	23.7	0.0	87.6	12.4
5000 L CO_2	1.4	73.1	25.5	0.0	87.0	13.0
Difference	0.5	-2.4	1.8	0.0	-0.7	0.7

5000 L +UV	0.8	74.3	24.9	0.0	89.7	10.3
Difference	-0.6	1.2	-0.7	0.0	2.7	-2.7
5000 L+10min UV	0.6	73.8	25.6	0.0	87.5	12.5
Difference	-0.2	-0.5	0.7	0.0	-2.2	2.2
5000 L+ 20 min UV	1.4	74.7	23.8	0.0	87.6	12.4
Difference	0.8	0.9	-1.7	0.0	0.2	-0.2

Vita

Juan Wang was born in March, 1987 in Binzhou, Shandong Province, P. R. China, where she finished her elementary, middle school and high school studies. She received her Bachelor of Science (B. S) in Pharmacy from Shandong University of Traditional Chinese Medicine, Shandong Providence, 2010.

Since 2010, she studied analytical chemistry in University of Missouri-Columbia. Her research focused on surface chemistry studies of carbon dioxide with MgO (100) and TiO_2 (110). She obtained a Ph. D. degree in chemistry from University of Missouri-Columbia in 2016.